17618-H179-RO-00

PROJECT TECHNICAL REPORT

CHARACTERIZATION OF ATTITUDE CONTROL PROPULSION SYSTEMS

MSC/TRW TASK 705-1

NAS 9-8166

June, 1971

Prepared for
NATIONAL AERONAUTICS AND SPACE ADMINISTRATION
MANNED SPACECRAFT CENTER
HOUSTON, TEXAS

FACILITY FORM 602
N71-37375 (ACCESSION NUMBER)
157 (PAGES)
CR-115183 (NASA CR OR TMX OR AD NUMBER)
(THRU) G3
(CODE) 28
(CATEGORY)

OFFICE OF PRIME RESPONSIBILITY

EP4

TRW SYSTEMS GROUP

CR-115183

17618-H179-RO-00

PROJECT TECHNICAL REPORT

CHARACTERIZATION OF ATTITUDE CONTROL PROPULSION SYSTEMS

MSC/TRW TASK 705-1

NAS 9-8166

June, 1971

Prepared for
NATIONAL AERONAUTICS AND SPACE ADMINISTRATION
MANNED SPACECRAFT CENTER
HOUSTON, TEXAS

Prepared by
P. F. Thompson
T. J. Walsh
Propulsion Systems Section
Chemical and Mechanical Systems Department

Approved by: _____
P. F. Thompson, Task Manager
MSC/TRW Task 705-1

Approved by: _____
J. M. Richardson, Head
Propulsion Systems Section

Approved by: _____
D. W. Vernon, Manager
Chemical and Mechanical
Systems Department

TRW SYSTEMS GROUP

PRECEDING PAGE BLANK NOT FILMED

CONTENTS

		Page No.
1.0	PURPOSE AND CONCLUSIONS	1
1.1	Purpose	1
1.2	Conclusions and Recommendations	1
2.0	INTRODUCTION	3
3.0	CHARACTERIZATION AND EVALUATION	7
3.1	Literature/Computer Simulation Search (Phase I)	8
3.2	Comparison Review (Phase II)	9
3.3	Technique Evaluation (Phase III)	10
3.4	ACPS Transient and Steady-State Characterizations	15
3.4.1	Supply Lines Steady-State	17
3.4.1.1	Gas Lines with Friction and Heat Transfer	17
3.4.1.2	Liquid Line	20
3.4.1.3	Isothermal Lines	21
3.4.1.4	Adiabatic Lines	22
3.4.2	Supply Line Transients	25
3.4.3	Accumulators and Pressure Vessels Steady-State	32
3.4.3.1	Accumulator/Storage Tank	32
3.4.3.2	Pressure Boundary	36
3.4.4	Accumulator, Pressures and Flowrate Boundaries for Transient Program	39
3.4.4.1	Pressure and Flowrate Boundaries	39
3.4.4.2	Pressure Boundary with Variable Resistance	40
3.4.4.3	Accumulator and Pressure Vessel Transients	42
3.4.5	Manifolds, Injectors, Orifices, Valves and Pipebends	44
3.4.6	Orifices, Valves, and Linebends Transients	46
3.4.7	Line Junction Subroutine (JUNCL)	49
3.4.8	Junction Transients	52
3.4.9	Pressure Regulator Steady-State	54
3.4.10	Pressure Regulator Transients	56

CONTENTS (continued)

		Page No.
3.4.11	Combustors Steady-State	61
3.4.11.1	Bi-Propellant Combustor Steady-State	61
3.4.11.2	Monopropellant Combustor	62
3.4.12	Combustor Transients	66
3.4.13	Turbopumps Steady-State	72
3.4.14	Turbopump and Gas Generator Transients	79
3.4.15	Steady-State Heat Exchanger Model	86
3.4.16	Transient Heat Exchanger Model	93
3.4.17	Steady-State Modeling - Gas Generator (high and low pressure)	106
3.4.18	Feedback Constraint Steady-State	109
3.4.19	Solution of a System of Implicit Equations . . .	110
3.4.20	Integration Subroutine	111
3.4.21	Thermodynamic Property Subroutines	112
4.0	ACPS SYSTEM SIMULATION RESULTS CASES	115
5.0	REFERENCES	147
6.0	BIBLIOGRAPHY	151

LIST OF TABLES

		Page No.
1.	COMPUTER PROGRAM CAPABILITY REQUIREMENTS	5
2.	TYPICAL ACPS COMPONENTS/SUBASSEMBLIES	7
3.	HEAT EXCHANGER RESPONSE TIME COMPARISON	92
4.	NON-DIMENSIONALIZED PARAMETERS, ε-NTU APPROACH	97
5.	INPUTS TO THE TRANSIENT MODEL FROM THE STEADY-STATE PROGRAM	99

PRECEDING PAGE BLANK NOT FILMED

LIST OF ILLUSTRATIONS

		Page No.
1.	ACPS HIGH PRESSURE TURBOPUMP CYCLE	10
2.	LOW PRESSURE ACPS	11
3.	CONSTANT HEAT FLUX INTO LINE ELEMENT	16
4.	DEFINITION OF ADIABATIC WALL TEMPERATURE	17
5.	COMPUTATIONAL GRID FOR INTERIOR POINTS	27
6.	TANK COMPONENT SCHEMATIC	31
7.	COMPUTATIONAL GRID FOR END POINTS	38
8.	PRESSURE BOUNDARY WITH VARIABLE RESISTANCE	39
9.	ACCUMULATOR	41
10.	SIMPLIFIED MANIFOLD ORIFICE	43
11.	ORIFICE OR VALVE IN A LINE	45
12.	JUNCTION	57
13.	PRESSURE REGULATOR	55
14.	COMBUSTOR	65
15.	TURBOPUMP AND GAS GENERATOR	78
16.	IDEALIZED HEAT EXCHANGER	93
17.	ε-NTU EFFECT FOR COUNTERFLOW AND PARALLEL FLOW HEAT EXCHANGE	94
18.	GAS/GAS HEAT EXCHANGE $C_{MIN}/C_{MAX} \geq 0.8$	98
19.	ACPS-TYPE CRYOGENIC EXCHANGER $C_{MIN}/C_{MAX} \leq 0.2$	99
20.	REGULA FALSI METHOD	110
21.	HYDROGEN PROPERTY DATA RANGE	113
22.	OXYGEN PROPERTY DATA RANGE	113
23.	ACPS STEADY-STATE DEMONSTRATION SCHEMATIC	115
24.	COMBUSTION CHAMBER GAS PROPERTIES AND PERFORMANCE FOR OXYGEN AND HYDROGEN (ISP, TC, CP)	116
25.	COMBUSTION CHAMBER GAS PROPERTIES AND PERFORMANCE FOR OXYGEN AND HYDROGEN (C*, MW)	117
26.	HYDROGEN PUMP CHARACTERISTICS, 50,000 RPM	118
27.	TURBINE EFFICIENCY CURVE FOR HYDROGEN TURBOPUMP	119
28.	TEST CASE FOR LINE MODEL	120
29.	PRESSURE AT VALVE	122
30.	FLOW RATE OF UPSTREAM END	123

LIST OF ILLUSTRATIONS (continued)

Page No.

31. PRESSURE AT THE VALVE 124
32. FLOW RATE AT UPSTREAM END 125
33. PRESSURE AT VALVE 126
34. FLOW RATE AT UPSTREAM END 127
35. PRESSURE AT THE VALVE 128
36. FLOW RATE AT UPSTREAM END 129
37. COMBUSTOR TRANSIENT MODEL STUDY 133
38. ACPS TRANSIENT TEST CASE SCHEMATIC 134
39. ACPS TRANSIENT TEST CASE 135

1.0 PURPOSE AND CONCLUSIONS

1.1 Purpose

The purpose of this report is to present the results of an effort to develop generalized, transient and steady-state simulation models for the oxygen and hydrogen attitude control propulsion systems (ACPS) for the space shuttle. The document presents: (1) the results of a literature and computer survey of methods and models currently used by industry, NASA centers and other government agencies to simulate the steady-state and dynamic operation of ACPS and/or individual components; (2) a comparison and evaluation of various simulation techniques obtained from the survey; and (3) the techniques selected or developed for use in this program to develop generalized and flexible steady-state and dynamic simulations models to characterize ACPS. The transient and steady-state computer programs resulting from this effort can be used to characterize the operation of a wide variety of ACPS configurations. Oxygen (O_2) and hydrogen (H_2) data have been incorporated into the programs to allow ease in evaluation of O_2 - H_2 ACPS shuttle configurations. Propellant data must be incorporated into the programs in order to simulate ACPS using different liquid or gaseous propellants.

This program was conducted under the TRW-Houston Support Contract NAS 9-8166, and this effort was identified as Task 705-1. Effort was initiated in September 1970 and completed in June 1971.

1.2 Conclusions and Recommendations

The effort under MSC/TRW Task 705-1, Characterization of the Attitude Control Propulsion Systems, has resulted in the development of generalized steady-state and transient models for simulating the operation of a variety of ACPS configurations. Both programs were developed in modular form (each module representing a system component) and provide the user with the flexibility to model many different ACPS concepts through the use of input data. The models were developed in sufficient detail to characterize the thermo-

dynamic and fluid mechanics performance of each component and their effects on overall system performance. ACPS transients can be analyzed for pressure and flow rate variation and both programs are capable of performing parameter studies. The fluid pressure and temperature profiles resulting from operating the ACPS during a particular mission duty cycle can be determined. In addition, alternative control modes and system operational sequences compatible with a given mission duty cycle can be determined by the programs. The programs are also capable of determining ACPS performance and behavior while simulating critical system component malfunctions and alternate modes of operation.

Due to the limited resources and time available to Task 705-1, both models contain simplifications. There are several candidate areas for program expansion which would result in greater program capability. For example, the current steady-state program contains a simplified combustor model in which the specific impulse and the properties of the combustion products are modeled as functions of mixture ratio only. In order to simulate in more detail the effects of combustor performance on overall system performance, the combustor model should be expanded to include the effects of the nozzle expansion area ratio, inlet temperature, and variations in the chamber pressure. The transient model is currently capable of simulating the dynamics of fluid flow at low Mach numbers and small density variations. In order to perform detailed ACPS analyses, a line model capable of taking into account larger variations in the fluid density, flow at higher Mach numbers and the effects of heat transfer into the lines should be incorporated. Also, the addition of the effects of a combustion time delay may be necessary in order to carry out detailed analyses of combustor start transients. This time delay results from the time that it takes for the gases to mix, or at the lower mixture ratios, the result of the time that it takes for them to chemically react. If the effect is significant, the initial ignition process should be modeled in more detail.

2.0 INTRODUCTION

The design and development of attitude control propulsion systems (ACPS) for future vehicles such as shuttle will require extensive analyses to establish optimum system concepts. These analyses will consist of parametrically generating sufficient component and subsystem data to permit evaluation of ACPS concepts which meet a variety of mission objectives for a wide range of operating conditions. Since emphasis will be placed upon reusability, high performance, safety, reliability and low cost for all components of future spacecraft, it is imperative that the analytical tools available for performing these analyses provide the capability and flexibility to parametrically integrate system components into a variety of ACPS configurations. These analysis programs must also be capable of evaluating point designs of candidate systems, determining the effects of component operation on overall system performance, determining system performance under both design and off-design conditions and characterizing final ACPS design configurations. Since the ACPS must be integrated with other vehicle subsystems to achieve optimum overall vehicle performance, the analysis programs must provide the additional capability of determining the effects on ACPS performance of subsystems integration and interaction.

MSC/TRW Task 705-1, "Characterization of Attitude Control Propulsion Systems," was initiated in order to develop programs with the capability to accomplish the requirements noted above. Specifically, the objectives of this task were to develop transient and steady-state analysis computer programs for a modular structure with generalized simulation capability suitable for

1. Evaluation of competing candidate ACPS;
2. Determining ACPS design criteria and operation constraints;
3. Determining the effect of component function on system performance, for a variety of system configurations;
4. Evaluating various point design concepts;

5. Failure mode evaluation;
6. Control system studies;
7. System operating sequence studies
8. Determining ACPS performance due to vehicle subsystem integration and interaction; and
9. Characterizing final design configuration operation.

Program capabilities required are shown in Table 1. Under this task all ACPS components have been modeled in sufficient detail to fully characterize the thermodynamic and fluid mechanics performance of each component and its effect on overall system performance. The resulting models provide the capability for determining fluid pressure and temperature profiles resulting from operating the ACPS during a particular mission duty cycle, and for determining methods of control and system operation compatible with a given mission duty cycle. In addition, the models can provide the ability to determine ACPS performance and behavior while simulating critical system component malfunctions.

The objectives of this Task have been achieved by performing the following three subtasks:

Subtask I : Identification and evaluation of various analytical techniques used to characterize the dynamic behavior and performance of propulsion systems and a definition of the recommended approach.

Subtask II : Application of the techniques selected in Subtask I to the development of general purpose computer programs to satisfy the requirements listed in Table I.

Subtask III: Demonstration and operation of the program by selecting a typical ACPS design and operating the program over a range of conditions on the MSC computer facilities.

This report presents the results of these subtasks, including a summary of the analytical techniques used to characterize the operation of the ACPS and a description of the resulting steady-state and transient computer programs.

TABLE I

COMPUTER PROGRAM CAPABILITY REQUIREMENTS

Transient Analysis Program

1. Component Sequencing
2. Subsystem energy requirements
3. Total impulse
4. System dynamics
5. System stability feedback:

   "line, valve and injector pressure surge, engine and feedline pressure overshoot"
6. Effects of geometry changes on start and shutdown
7. Effect of initial conditions
8. Component malfunction
9. Component performance
10. Varied component design and location
11. Varied engine configuration
12. Control system characteristics

Steady-State Program

1. System balance requirements
2. System and component performance
3. Varied component design and location
4. Effects of initial conditions
5. Effects of component malfunctions on system performance
6. Effects of component and control element tolerances on system performance

PRECEDING PAGE BLANK NOT FILMED

3.0 CHARACTERIZATION AND EVALUATION

Analytical techniques available for characterizing the dynamic behavior and performance of ACPS components (shown in Table 2) were evaluated on the basis of: state-of-the-art; efficiency; adaptability to solution by digital computer; previous usage; accuracy; availability of characterization parameters and adaptability to modular computer program construction. Basically, this subtask was divided into four phases:

Phase I	Literature/Computer Simulation Search
Phase II	Comparison Review
Phase III	Technique Evaluation
Phase IV	Recommended Techniques

The initial part of the subtask consisted of a survey of methods and programs currently used by industry and other NASA centers and governmental agencies including those at Lewis Research Center (LeRC), Marshall Space-Flight Center (MSFC), Jet Propulsion Laboratory (JPL), Arnold Engineering Development Center (AEDC), and Air Force Rocket Propulsion Laboratory (AFRPL). Contacts were established with companies performing ACPS simulation work on the Shuttle Vehicle, and the applicable computer programs formulated by these companies were reviewed.

3.1 LITERATURE/COMPUTER SIMULATION SEARCH (PHASE I)

Several literature search requests covering the entire scope of information deemed pertinent to the modeling of the Shuttle ACPS were submitted to the TRW Technical Information Center. The action taken on these literature search requests covered all available information sources as follows:

TABLE 3-1 TYPICAL ACPS COMPONENTS/SUBASSEMBLIES

- Combustors
  - Thrustors
  - Gas generators
  - Injectors
  - Manifolds
- Turbopumps
- Heat Exchangers
- Tanks
  - Accumulators
  - Liquid tanks
- Gas Lines
- Liquid Lines
- Orifices, Bends/Restrictions
- Regulators
- Control Valves

1 - Manually performed survey of all engineering and scientific publications including advanced degree theses.

2 - Manually performed review of indexes containing lists of computer programs shared by all NASA facilities and contractors. Among those indexes which contained the most pertinent information were COSMIC (Computer Software Management and Information Center) and the NASA ADP Resource Sharing System Computer Programs.

3 - Computerized search of all information available to NASA facilities and the Defense Documentation Center (DDC)

This effort resulted in a large bibliography of potentially applicable information and voluminous computer printouts of titles and abstracts. The information resulting from this effort is presented in Section 3.1 of Reference 33.

Upon receipt of the above information, a review of all titles and abstracts (if available) was carried out in order to select information for further examination under the Phase II comparison review. The ACPS Literature Search File was implemented to systematically control the receipt and filing of the ACPS information obtained under this portion of the Task.

3.2 COMPARISON REVIEW (PHASE II)

Upon review of the available bibliographies, those items indicating strong applicability for the ACPS were chosen for the comparison review. The selected literature and computer programs which are pertinent to this task are itemized in Section 3.2 of Reference 33. A preliminary review was made of this literature to determine which would be most suitable for comparison, and detailed documentation was ordered.

The second phase (Comparison Review) consisted of evaluating those items of information for which detailed documentation was received. Comparisons were made to determine similarities and differences between the analytical approaches as well as to ascertain their applicability to the ACPS task. Unique solution techniques were evaluated to the extent necessary to assess their validity and accuracy of approach.

3.3 TECHNIQUE EVALUATION (PHASE III)

The candidates defined in the comparison review were further reviewed to determine the final, pertinent information of the ACPS comparison evaluation. A synopsis of the technique evaluation phase information items is presented in Section 3.3 of Reference 33.

A cursory review was also performed of the Space Shuttle High and Low Pressure Auxiliary Control Propulsion Subsystem Definition studies (References 1, 2, 3, and 4). These studies were performed by McDonnell-Douglas Astronautics Co. - East and TRW Systems Group, Redondo Beach. A typical high pressure turbopump cycle was obtained from Reference 3 and is shown in Figure 2. A typical low pressure system cycle was obtained from Reference 4 and is shown in Figure 3. These figures represent configurations which were being considered for the Shuttle ACPS.

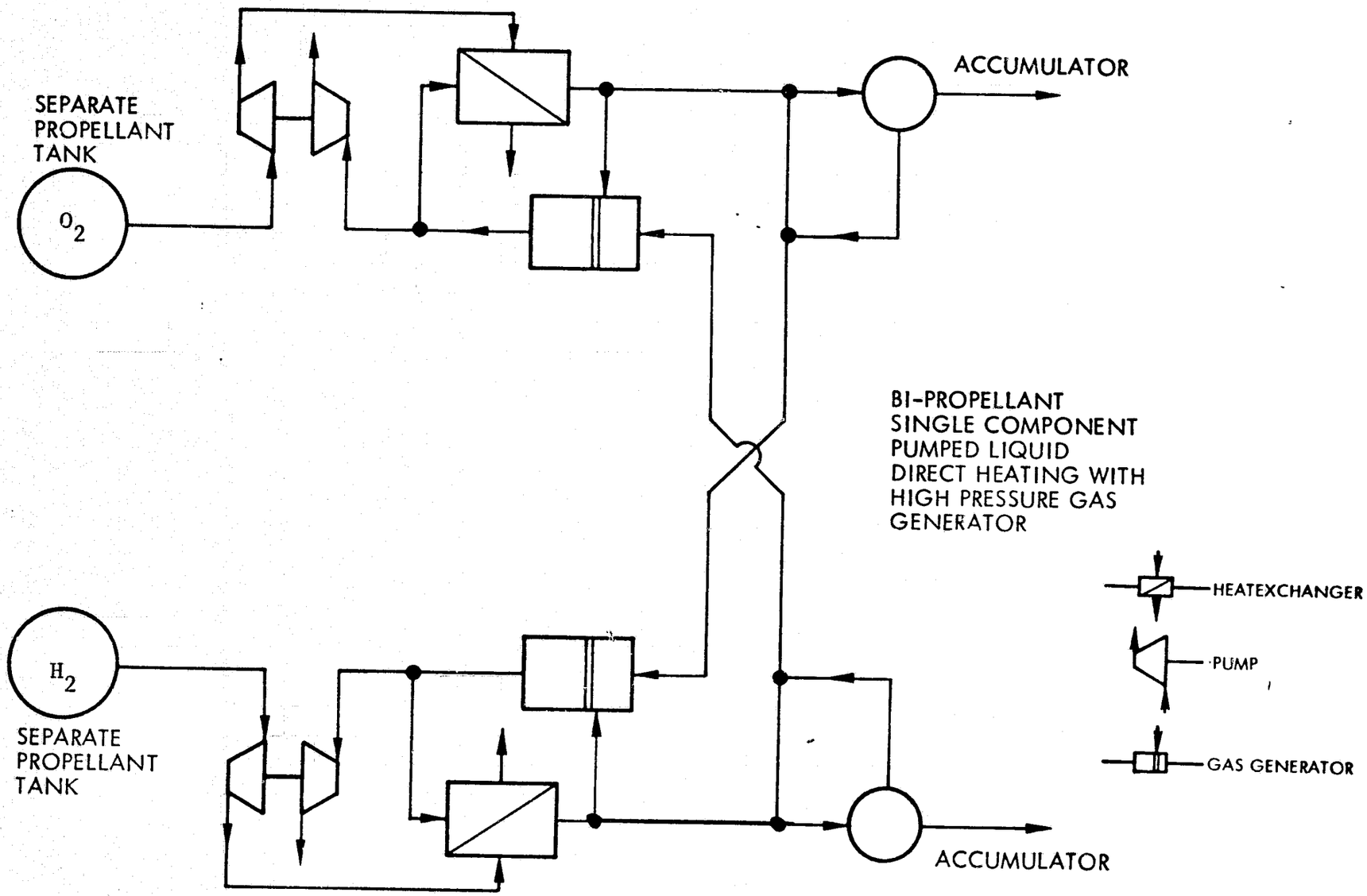

FIGURE 1
ACPS HIGH PRESSURE TURBOPUMP CYCLE

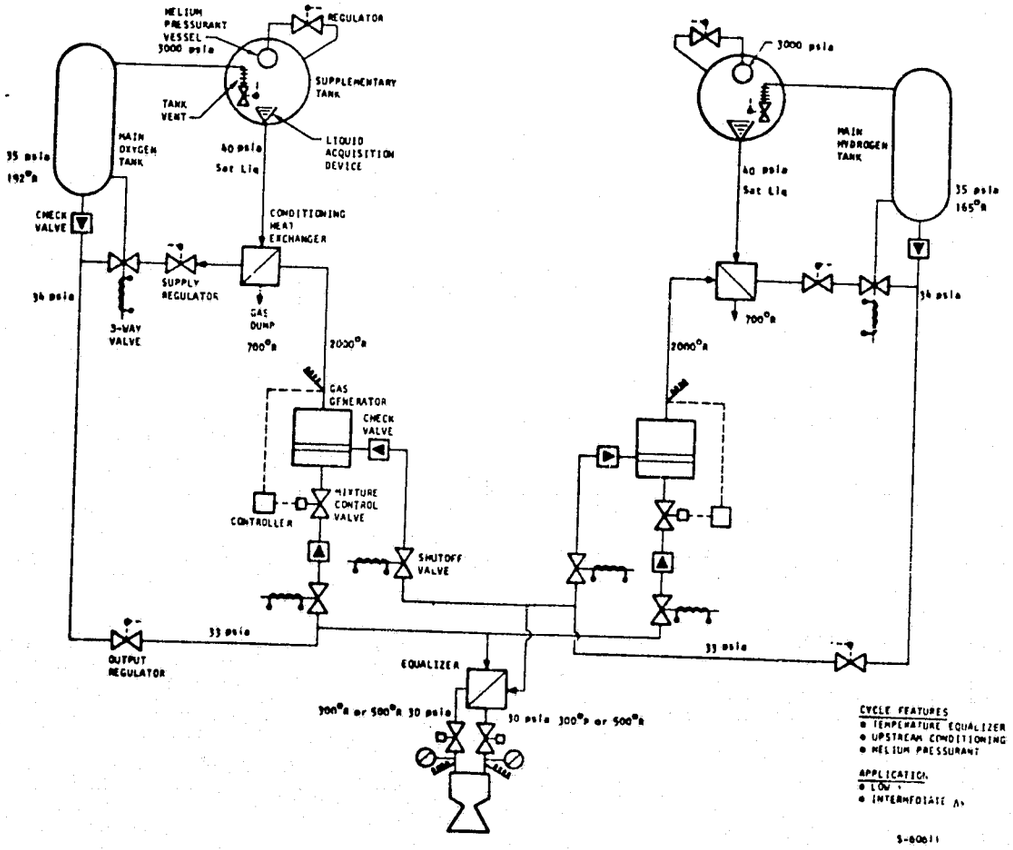

FIGURE 2
LOW PRESSURE ACPS

Extensive evaluation of techniques for characterizing supply line models, combustor models and general program organization was performed. Computer running time, integration techniques, model adequacy (accuracy) and digital computer adaptability (Univac 1108) were considered during this evaluation.

Program organization for generalized type of computer programs were evaluated by initially reviewing the Pipetran Computer Program (Reference 5), the Matrix Oriented Production Assembly System (MOPAS), Reference 6, the Propulsion Analysis Program (PAP), Reference 7, and the Hydraulic Transient Analysis Program (HTAP), Reference 34, supplied to TRW from MSC Auxiliary Propulsion and Pyrotechnics Branch. The ideas and formats associated with configuration selection, executive operation and the modularized form incorporated into these programs were useful in setting up the generalized ACPS programs. The Namelist data input was selected for program input due to ease of handling for the engineer. The executive program operation was fashioned after that of the Pipetran program with the configuration selection as input data and the executive driver handling the coupling of components and the solutions of simultaneous equations. The line model was established as the main program link due to its role of coupling segments with the other ACPS modularized components.

Since the line model was used as the main program link, considerable effort was expended in evaluating techniques for characterizing low Mach number gas and liquid lines. As a result of this effort, four programs were established as possible candidates and evaluated: (1) The ORI program, Reference 8; (2) the HTAP program; (3) Pipetran; and (4) a preliminary dynamics line model developed for the Space Shuttle Vehicle Definition study by TRW/Redondo Beach. The Pipetran Computer Program was eliminated immediately

because it was used mainly for long gas lines and the flow dynamics were not applicable. This program used the finite difference technique for evaluating the partial differential equations. The dynamics line model from TRW/Redondo Beach was eliminated because it is simplified and not generalized enough for this application. The remaining two programs (the ORI and HTAP programs) are closely related, although the HTAP program is a generalized model and the ORI program is not. However, both programs use the method of characteristics (Reference 9) to solve the transient fluid flow equations including friction terms. The method of characteristics technique transforms the partial differential transient fluid flow equations into ordinary differential equations which are then solved by the first order finite difference method. Although another method for solving the partial differential equations directly using the finite difference solution was considered (Reference 17), it was not used for this effort because of possible stability problems. Since both the HTAP and ORI programs use the method of characteristics for solving the partial differential equations and because these programs have been checked out; it was decided to incorporate this technique into the ACPS dynamic line model (Section 3.4.2). The ORI program has substantial documentation with several checkout cases, while the HTAP program has been used by the Auxiliary Propulsion and Pyrotechnics Branch at MSC to evaluate Apollo transient data and Skylab propulsion test transient data. The accuracy of the HTAP program has been demonstrated utilizing actual test data. Therefore, the ACPS line model developed for this task was verified by comparison with the HTAP model. Since the method of characteristics solution is well understood, and because neither the ORI nor the HTAP programs had the necessary flexibility to be readily adaptable to the ACPS problem, it

was most feasible to tailor an executive scheme to the ACPS problem. It was decided to use a modified method of characteristics for specified time intervals as described in Reference 11 (Chapters 2 and 3). This technique is tailored for the analysis of large networks such as those to be modeled by the ACPS Program. The numerical integration of the characteristics equations is accomplished by a simple first order finite-difference approximation.

In selecting a combustion chamber transient model, two TRW models were reviewed. The first was developed for solution on an analog computer and is the one adapted for use in this program. A Runge-Kutta integration scheme was incorporated to adapt it for use on a digital computer. This model is described in Section 3.4.12 and the results of the evaluation leading to its adoption are given in Section 4.0. The second model used an approach which consisted of linearizing the equations over each time step and obtaining a semi-analytical solution. Although this approach has some merit, because of the treatment of sonic flow into the chamber and of the valve forcing function, the chamber pressure differential equation was not in the form adaptable to the general transient case. The claimed advantage of this approach is, however, that the computational time step sizes can be twice the size as that required using the Runge-Kutta scheme. However, verification of this advantage would require that the two models be put on a more comparable basis, since they now differ in more than just their integration schemes. The effort required to make this comparison was not justified.

3.4 ACPS TRANSIENT AND STEADY-STATE CHARACTERIZATIONS

The ACPS transient and steady-state characterization computer models implement the best techniques identified in the Subtask 1 effort, and provide a flexible generalized characterization of ACPS components. The ACPS

characterization techniques provide a high degree of accuracy and are amenable to computer solutions. The results of this task provide NASA the framework of a program which can be utilized to simulate the vast majority of ACPS concepts in dynamic and steady-state modes of operation.

This section presents the transient and steady-state modeling techniques for the following components:

Combustors and gas generators

Manifolds and Injectors

Turbopumps

Junctions

Heat Exchangers

Accumulators and Pressure Vessels

Supply Lines

Pressure Regulators, Orifices, Pipebends and Valves.

The steady-state program consists of a main-driver program and subroutines representing the components in the form of non-linear implicit simultaneous algebraic equations. The choice of which variables are known and which ones are to be solved for are determined by input information specified by the user. For instance, in the thrust chamber model, the chamber pressure and flowrates may be stipulated and the throat area and injector orifice areas computed, or vice-versa. The user, of course, is constrained to pick a set of unknowns that result in an independent set of equations. In this respect, the steady-state program will be more flexible than the transient program. The nature of the equations in the transient model require that the hardware dimensions and characteristics (such as resistances) be input. From this input, the program computes the flow conditions (velocity, pressure, etc.) as functions of time.

characterization techniques provide a high degree of accuracy and are amenable to computer solutions. The results of this task provide NASA the framework of a program which can be utilized to simulate the vast majority of ACPS concepts in dynamic and steady-state modes of operation.

This section presents the transient and steady-state modeling techniques for the following components:

Combustors and gas generators

Manifolds and Injectors

Turbopumps

Junctions

Heat Exchangers

Accumulators and Pressure Vessels

Supply Lines

Pressure Regulators, Orifices, Pipebends and Valves.

The steady-state program consists of a main-driver program and subroutines representing the components in the form of non-linear implicit simultaneous algebraic equations. The choice of which variables are known and which ones are to be solved for are determined by input information specified by the user. For instance, in the thrust chamber model, the chamber pressure and flowrates may be stipulated and the throat area and injector orifice areas computed, or vice-versa. The user, of course, is constrained to pick a set of unknowns that result in an independent set of equations. In this respect, the steady-state program will be more flexible than the transient program. The nature of the equations in the transient model require that the hardware dimensions and characteristics (such as resistances) be input. From this input, the program computes the flow conditions (velocity, pressure, etc.) as functions of time.

3.4.1 Supply Lines Steady-State

Four steady-state supply line models were developed in order to provide simulation flexibility to the user. Three gas line models include the cases for (1) heat transfer with friction, (2) an isothermal line and (3) an adiabatic line. The liquid line model uses the momentum equation to determine the pressure drop in the line and the energy equation to calculate discharge fluid temperature. The following sections present the formulation of these models. The nomenclature for this formulation is given at the end of each section.

3.4.1.1 Gas Lines with Friction and Heat Transfer

The supply lines for the steady-state model are simulated assuming a constant temperature for the environment surrounding the lines (Figure 3). Therefore, the heat transfer coefficient (h) must be computed based on the Reynolds, Prandtl & Grashof numbers. Heat transfer into the fluid flowing in long gas lines is treated by numerical integration with respect to distance. The supply line model will handle the case of combined friction and heat transfer.

The general approach utilizes the energy equation expressed as a function of the heat transfer coefficient (page 243 of Reference 20) and is described below.

$$\dot{W}\, dQ = \frac{\pi}{4} D^2 \rho V (C_p dT_o) = h(dA)(T_E - T_{aw}) \qquad (1)$$

where T_{aw} = Adiabatic wall temperature (Figure 4).

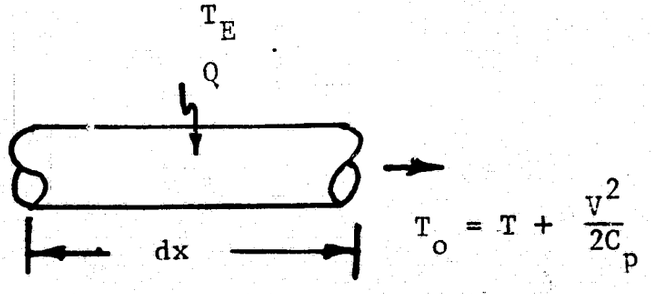

FIGURE 3 - CONSTANT HEAT FLUX INTO LINE ELEMENT

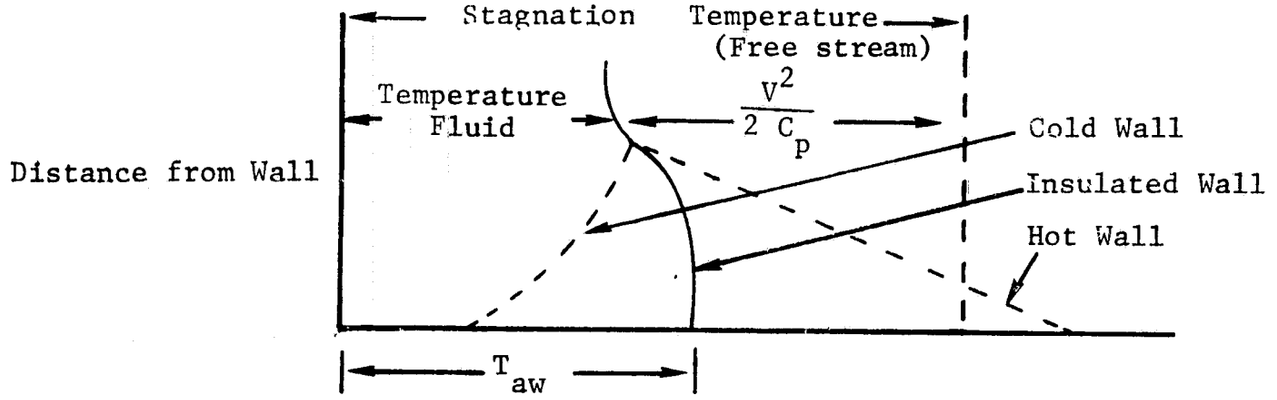

FIGURE 4 - DEFINITION OF ADIABATIC WALL TEMPERATURE

The dimensionless parameters are computed as follows for use in the energy balance.

Grashof Number

$$N_{Gr} = \frac{\beta_E G_{EE} (T_E - T_{o_1}) \rho_E^2 D^3}{\mu_E^2} \tag{2}$$

Prandtl Number

$$N_{Pr} = \frac{C_p \mu}{k} \tag{3}$$

Reynolds Number

$$N_{Re} = \frac{\dot{W} D \rho}{A \mu} \tag{4}$$

Outside film coefficient

$$H_o = \frac{.53k}{D_o} [N_{Re}^{.8} N_{Pr}^{.4}] \tag{5}$$

Inside film coefficient

$$H_i = \frac{.023k}{D_i} [N_{Gr} N_{Pr}]^{.25} \tag{6}$$

Overall Heat Transfer Coefficient

$$U = \frac{(H_o + H_{rad}) A_o H_i A_i W_c}{H_i A_i W_c + (H_o + H_{rad}) A_o W_c + H_i A_i (H_o + H_{rad}) A_K A_o} \tag{6a}$$

where

$$A_K = \frac{L}{A} = \ln \left(\frac{D_o}{D_i}\right) / 2\pi d_x$$

Radiation heat transfer coefficient

Calculation of radiation effects is performed by an iterative procedure of equations 7 thru 9.

The pipe wall temperature is estimated as follows:

$$T_w = \frac{(H_o + Rad)\ T_{Env} + H_i\ T_o}{(H_o + Rad + H_i)} \tag{7}$$

The radiation heat transfer coefficient is calculated as follows:

$$Rad = 0.1714 \times 10^{-8} (T_E - T_w)\ (T_E^2 + T_w^2) \tag{8}$$

$$Hrad = Rad \tag{9}$$

The friction factor is based on the Reynolds number:

$$f = 0.0014 + 0.125/(N_{Re})^{0.32} \tag{9a}$$

For subsonic flow the adiatatic wall temperature, T_{aw}, does not differ significantly from the stagnation temperature T_o (for $M < 0.3$ the error less than 0.3 percent). Therefore, $T_{aw} = T_o$ and Equation 1 becomes.

$$\frac{dT_o}{T_E - T_o} = \frac{4\,dU}{\rho\ V\ C_p D^2} \tag{10}$$

integrating with respect to distance;

$$\ln \left(\frac{T_E - T_{o_1}}{T_E - T_{o_2}}\right) = \frac{4\ U}{\rho C_p \pi D^2 V} \tag{11}$$

solving Equation 11 for T_{o_2}:

$$T_{o_2} = T_E - (T_E - T_{o_1})\ e^{-\left(\frac{4\ U}{\rho \pi D^2 C_p V}\right)} \tag{12}$$

Therefore, T_o can be calculated for any value of line length (dx).

Mach numbers are obtained by a finite difference iterative integration as follows;

$$dM^2 = F_{T_o} \frac{dT_o}{T_o} + F_f \, 4f \frac{dx}{D} \tag{13}$$

where the influence coefficients are as follows:

$$F_{T_o} = \frac{M^2(1+\gamma M^2)(1+\frac{\gamma-1}{2} M^2)}{1 - M^2} \tag{14}$$

$$F_f = \frac{\gamma M^4(1 + \frac{\gamma-1}{2} M^2)}{1 - M^2} \tag{15}$$

the finite difference equation is then written:

$$M_2^2 - M_1^2 = \left[\frac{2 \overline{F_{T_o}}}{\left(\frac{T_{o_2}}{T_{o_1}} + 1\right)} + \frac{\overline{F_f} \, 4 \, f \, dx}{D\left(\frac{T_{o_2}}{T_{o_1}} - 1\right)} \right] \left(\frac{T_{o_2}}{T_{o_1}} - 1 \right) \tag{16}$$

where $\overline{F_{T_o}}$, $\overline{F_f}$ are influence coefficients evaluated at $\frac{M_1 + M_2}{2}$ & $\overline{T_o} = \frac{T_{o_1} + T_{o_2}}{2}$.

3.4.1.2 Liquid Line

The liquid line model was derived for an incompressible fluid (constant density) and calculates the discharge pressure utilizing the momentum equation and a discharge fluid temperature which is based on the energy equation. The following equations represent the component model formulation.

The momentum equation is used to obtain the discharge pressure and is written as follows:

$$P_2 = P_1 + \rho_L \frac{G_{EE}}{g_c} \sin(\alpha) - \frac{\dot{W}^2}{\rho_L A^2 g_c} \left(f\frac{L}{D} + K_{LT}\right) \tag{17}$$

The hydraulic resistance may be input or calculated as follows:

$$H_R = \left(f\frac{L}{D} + K_{LT}\right) \frac{1}{2g_c A^2} \tag{18}$$

The discharge pressure in lbm/lb^2 is represented by:

$$P_2 = P_1 + \rho_L \frac{G_{EE}}{g_c} Z \sin(\alpha) - H_R \left(\frac{\dot{W}^2}{\rho_L}\right) \tag{19}$$

The energy equation is used to calculate the fluid discharge temperature and is given by:

$$W\ Cv\ dT = dQ + d\ F \tag{20}$$

$$\dot{W}\ Cv\ dT = U(T_E - \overline{T_f})\ dx + dF \tag{21}$$

$$T_{f_2} = \frac{U(T_E - \overline{T}_f)\ \Delta x}{\dot{W}\ Cv} + f\ \frac{\Delta x}{D}\ \frac{V^2}{2gCv} + T_{f_1} \tag{22}$$

The overall heat transfer coefficient (U) is calculated in the same manner as the gas line per Equations (2-11).

3.4.1.3 Isothermal Lines

Isothermal flow with friction is of interest in transporting gas over long distances. Although the Mach numbers for such flows are usually quite low, there are substantial changes in pressure due to the great lengths over which friction acts. Therefore, the flow may not be treated as incompressible.

The isothermal line model obtains the Reynolds number from Equation (4) and the gas properties from the property routines. The friction is obtained

from Equation (9a).

The following equation (Reference 20, pg. 182) is evaluated for the pressure drop as a function of Mach number using a Newton Raphson solution process.

$$P_1^2 - P_2^2 = 155.6943 \frac{\dot{W}^2 T}{(MW)D^4} \left(24\frac{fL}{D} - \ln \frac{P_2}{P_1}\right)$$

3.4.1.4 Adiabatic Lines

The analytical solution of adiabatic constant area flow in a pipe had been forumulated assuming the fluid is a perfect gas. Incorporation of the compressibility factor could be performed as a future model improvement.

The assumptions for adiabatic flow are: a) the flow is one-dimensional, b) the flow is steady, c) there is no external heat transfer or shaft work, d) the differences in elevation produce negligible changes compared with friction effects, and e) the duct is of constant area.

The adiabatic model obtains the Reynolds number from Equation (4), and the properties from the property data. The friction factor is calculated from Equation (9a).

The following equation (Reference 20, pg. 167) is utilized to obtain the discharge Mach number using a Newton Raphson solution process.

$$4\bar{f}\frac{L}{D} = \left[\frac{1-M^2}{\gamma M} + \frac{\gamma+1}{2\gamma}\ln\left\{\frac{(\gamma+1)M^2}{2(1+\frac{\gamma-1}{2}M^2)}\right\}\right]_1 - \left[\frac{1-M^2}{\gamma M} + \frac{\gamma+1}{2\gamma}\ln\left\{\frac{(\gamma+1)M^2}{2(1+\frac{\gamma-1}{2}M^2)}\right\}\right]_2$$

NOMENCLATURE (Section 3.4.1)

SYMBOL	DESCRIPTION	UNITS
A	Inside cross-sectional area of pipe	in^2
A_K	Length divided by area	1/ft
α	Angle pipe makes with horizontal	deg
β	Volume coefficient of thermal expansion	$1/^oR$
C_p	Specific heat at constant pressure	$BTU/^oR$-lbm
Cv	Specific heat at constant volume	$BTU/lbm-^oR$
dF	Frictional loss	BTU/lbm
dQ	Differential heat	BTU/lbm
dT	Differential temperature	^oR
dx, Δx	Pipe length segment	ft
D	Diameter of line	in.
E	Emissivity	-
f	Friction factor	-
F	Influence coefficient	-
g_c	32.174	$lbm-ft/sec^2lbf$
G_{EE}	Local gravitation	ft/sec^2
N_{Gr}	Grashof number	-
γ	Specific heat ratio, C_p/C_v	-
H_o	Outside film coefficient	$BTU/hr-ft^2-^oR$
H_i	Inside film coefficient	$BTU/hr-ft^2-^oR$
H_R	Hydraulic resistance	$sec^2/ft-in^2$
H_{Rad}	Radiation heat transfer coefficient	$BTU/hr-ft^2-^oR$
h	Heat transfer coefficient	$\frac{BTU}{hr\ ft^2\ ^oF}$
K_{LT}	Total loss coefficients; bends, contractions, etc.	-

NOMENCLATURE (Section 3.4.1) (Continued)

SYMBOL	DESCRIPTION	UNITS
k	Fluid thermal conductivity	BTU/hr-ft-^{o}R
L	Length of pipe	ft
MW	Molecular weight	-
μ	Viscosity	lbm/ft-sec
M	Mach number down pipe	-
N_{Re}	Reynolds number	-
N_{Pr}	Prandtl number	-
P	Pressure	psia
Q	Constant heat flux into pipe	BTU/sec
ρ	Density fluid	lbm/ft^3
σ	Stefan-Boltzmann constant, 0.1714×10^{8}	BTU/hr-ft^2-^{o}R
T_E	Temperature of environment	^{o}R
T_w	Temperature of wall	^{o}R
T_n	Temperature of fluid down pipe	^{o}R
T, To	Temperature of fluid or stagnation temperature fluid	^{o}R
U	Overall heat transfer coefficient	$\frac{BTU}{hr\ ^{o}R}$
V	Velocity fluid initial	ft/sec
$\dot{W}$	Flowrate	lbm/sec
W_c	Wall thermal conductivity	BTU/ft-hr-°R

SUBSCRIPTS

2	Discharge
1	Inlet
f	Fluid
L	Liquid
E	Environment
o	Outside
i	Inside

3.4.2 Supply Line Transients

The partial differential equations representing one-dimensional transient flow of a liquid in a pipe are given in Reference 11 as:

$$g \frac{\partial H}{\partial t} + a^2 \frac{\partial v}{\partial x} + gv \frac{\partial H}{\partial x} + gv \sin \alpha = 0 \qquad (1)$$

$$g \frac{\partial H}{\partial x} + v \frac{\partial v}{\partial x} + \frac{\partial v}{\partial t} + \frac{fv|v|}{2D} = 0 \qquad (2)$$

Equation (1) is the continuity equation while Equation (2) is the equation of motion. However, for use in circumstances where the local acceleration may be zero, or nearly zero, the above two equations are not satisfactory because H contains g in the denominator; and therefore, the product of gravity (g) times the total head (H) as g approaches zero becomes the indeterminate form of 0/0. The equations can be readily put into a form suitable for use at both zero and nonzero g; however, by making the substitution:

$$H = 144 \frac{g_c}{g} \frac{P}{\rho} + z \qquad (3)$$

Equations (1) and (2) are hyperbolic in form and can be solved either by substituting directly a finite-difference approximation for each term or by converting them into four equivalent ordinary differential equations by the method of characteristics and then substituting finite-difference approximations for each term (see References 17, 18, and 19). Although the former approach has certain advantages (see References 18 and 19), there appear to be no cases reported in the literature of equations having exactly the form of Equations (1) and (2) being solved in this manner. There are, however, examples for somewhat similar sets (References 17 and 19). In Reference 11, the method of characteristics was used to solve these equations. Several comparisons of the computational results with experimental data are presented. The agreement is excellent. Thus, for the sake of expediting the task, the method of characteristics was chosen to solve Equations (1) and (2).

Equations (1) and (2) are sufficient to describe the flow of a gas at low Mach numbers providing that the appropriate expression for the speed of sound is used. Assuming that elevation effects are negligible, Equations (1) and (2) become, respectively,

$$\frac{144\ g_c}{\rho}\ \frac{\partial P}{\partial t} + a^2\ \frac{\partial v}{\partial x} + 144\ g_c\ \frac{v}{\rho}\ \frac{\partial P}{\partial x} = 0 \qquad (4)$$

$$\frac{144\ g_c}{\rho}\ \frac{\partial P}{\partial x} + v\ \frac{\partial v}{\partial x} + \frac{\partial v}{\partial t} + \frac{f v|v|}{2D} = 0 \qquad (5)$$

The continuity equation and equation of motion suitable for the one-dimensional flow of a gas are (from Reference 20, page 972):

$$\frac{\partial \rho}{\partial t} + \rho\ \frac{\partial v}{\partial x} + v\ \frac{\partial \rho}{\partial x} = 0 \qquad (6)$$

$$\frac{144\ g_c}{\rho}\ \frac{\partial P}{\partial x} + v\ \frac{\partial v}{\partial x} + \frac{\partial v}{\partial t} + \frac{f v|v|}{2D} = 0 \qquad (7)$$

It should be noted that Equation (7) is identical to Equation (5)

Multiplying both sides of Equation (6) by $144\ \frac{\partial P}{\partial \rho}$ gives:

$$144\ \frac{\partial P}{\partial \rho}\ \frac{\partial \rho}{\partial t} + 144\ \rho\ \frac{\partial P}{\partial \rho}\ \frac{\partial v}{\partial x} + 144\ v\ \frac{\partial P}{\partial \rho}\ \frac{\partial \rho}{\partial x} = 0 \qquad (8)$$

For an isentropic process:

$$\frac{144\ \partial P}{\partial \rho} = \frac{a^2}{g_c} \qquad (9)$$

and after substitution, Equation (8) becomes identical to Equation (4).

The equations that follow are based on the speed of sound remaining constant in the pipe and the density being independent of the velocity. In a gas, these assumptions hold fairly well for Mach numbers less than about 0.2. For higher Mach numbers, the energy equation and the equation of state must be solved along with Equations (6) and (7).

Deriving the characteristic equations from Equations (1) and (2) converting them into finite difference form results in two relationships between flow rate and pressure at time equal to (n+1) Δt. (See Reference 11.)

$$\dot{w}_{i,j}^{n+1} + C_1 + C_2\ P_{i,j}^{n+1} = 0 \qquad (10)$$

$$\dot{w}_{i,j}^{n+1} + C_3 + C_4\ P_{i,j}^{n+1} = 0 \qquad (11)$$

C_1, C_2, C_3, and C_4 are functions of conditions at time $n\Delta t$.

$$C_1 = -\dot{w}_S^n - \frac{A_i}{a_i}(g\rho_i z_{i,j} - 144\, g_c P_S - g\rho_i z_S) - \frac{g\,\dot{w}_S^n (\sin\alpha_i)\Delta t}{a_i} + \frac{f_i \dot{w}_S^n |\dot{w}_S^n| \Delta t}{2(D_i/12)\rho_i A_i} \quad (12)$$

$$C_2 = -\frac{A_i}{a_i} g_c\, 144 \quad (13)$$

$$C_3 = -\dot{w}_R^n + \frac{A_i}{a_i}(g\rho_i z_{i,j} - 144\, g_c P_R^n - g\rho_i z_R) + \frac{g}{a_i}\,\dot{w}_R^n (\sin\alpha_i)\Delta t + \frac{f_i \dot{w}_R^n |\dot{w}_R^n| \Delta t}{2(D_i/12)\rho_i A_i} \quad (14)$$

$$C_4 = \frac{A_i}{a_i} g_c\, 144 \quad (15)$$

Values of $\dot{w}_R$, $\dot{w}_S$, z_R, z_S, P_R, and P_S are found from the following interpolation expressions.

$$\dot{w}_R^n = \frac{\dot{w}^n{}_{i,j} - \Theta_i a_i (\dot{w}^n{}_{i,j} - \dot{w}^n{}_{i,j-1})}{1 + \Theta_i (\dot{w}^n{}_{i,j} - \dot{w}^n{}_{i,j-1})/(\rho_i A_i)} \quad (16)$$

$$\dot{w}_S^n = \frac{\dot{w}^n{}_{i,j} - \Theta_i a_i (\dot{w}^n{}_{i,j} - \dot{w}^n{}_{i,j+1})}{1 - \Theta_i (\dot{w}^n{}_{i,j} - \dot{w}^n{}_{i,j+1})/(\rho_i A_i)} \quad (17)$$

$$z_R^n = z_{i,j} - \Theta_i \left(\frac{\dot{w}_R^n}{\rho_i A_i} + a_i \right) \left(z_{i,j} - z_{i,j-1} \right) \quad (18)$$

$$z_S^n = z_{i,j} + \Theta_i \left(\frac{\dot{w}_S^n}{\rho_i A_i} - a_i \right) \left(z_{i,j} - z_{i,j+1} \right)$$

$$P_R^n = P^n{}_{i,j} + \frac{g\,\rho_i\, z_{i,j}}{g_c\, 144} - \Theta_i \left(\frac{\dot{w}_R^n}{A_i \rho_i} + a_i \right) \left(P^n{}_{i,j} + \frac{g\,\rho_i z_{i,j}}{g_c\, 144} - \right. \quad (19)$$

$$\left. P^n{}_{i,j-1} - \frac{g\rho_i z_{i,j-1}}{g_c\, 144} \right) - \frac{g\rho_i z_R^n}{g_c\, 144} \quad (20)$$

$$P_S^n = P^n{}_{i,j} + \frac{g\,\rho_i z_{i,j}}{g_c\, 144} + \Theta_i \left(\frac{\dot{w}_S^n}{A_i \rho_i} - a_i \right) \left(P^n{}_{i,j} + \frac{g\rho_i z_{i,j}}{g_c\, 144} - \right.$$

$$p^n_{i,j+1} - \frac{g\rho_i z_{i,j+1}}{g_c 144}\Bigg) - \frac{g\rho_i z_S^n}{g_c 144} \tag{21}$$

$$\Theta_i = \Delta t/\Delta x_i \tag{22}$$

The speed of sound in a liquid pipeline is given by:

$$a_i = \sqrt{\frac{144\ B_i\ g_c}{\rho_i\left(1 + \frac{B_i D_i}{E\ e_i} c\right)}} \tag{23}$$

and by

$$a_i = \sqrt{\gamma_i g_c R_i T_i} \tag{24}$$

for a gas line.

The computational procedure is illustrated in Figure 5.

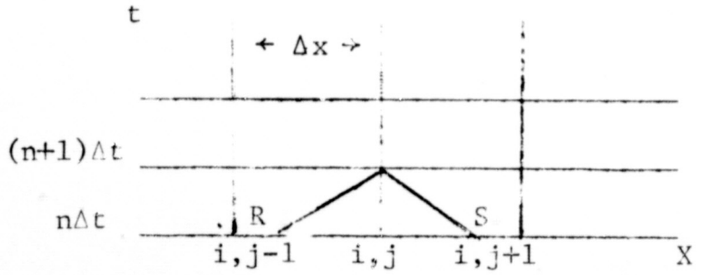

FIGURE 5 - COMPUTATIONAL GRID FOR INTERIOR POINTS

The problem requires that conditions at some initial time - zero or $n\Delta t$ - be known at each node j. Then to determine the conditions at $(n+1)\ \Delta t$ the values of $\dot{w}_R^n$, w_S^n, x_R^n, z_S^n, P_R^n, and P_S^n are found using the interpolation relations, Equations (16) through (21). Once these are known, C_1, C_2, C_3, and C_4 may be calculated and Equations (10) and (11) may be solved to yield:

$$P^{n+1}_{i,j} = (C_3 - C_1) / (C_2 - C_4) \tag{25}$$

$$\dot{w}^{n+1}_{i,j} = - C_2\ P^{n+1}_{i,j} - C_1 \tag{26}$$

The treatment of end points of the lines will be discussed in the following sections.

In selecting Δx and Δt the following numerical stability requirement must be met:

$$\Delta x_i \geq (1. + s)\ (\Delta t)\ a_i \tag{27}$$

where s is the maximum Mach number in the line during the transient. This requirement is stated in Reference 11 and discussions of it may be found in Section 4.0 and in References 19 and 21.

NOMENCLATURE (Section 3.4.2)

Symbol	Description	Units
A	Cross-sectional area of pipe	ft^2
a	Speed of sound	ft/sec
B	Bulk modulus of elasticity of liquid	psi
c	Correction for the effect of Poisson's ratio	
C_1, C_2, C_3, C_4	Defined by Equations (12) through (15)	
D	Pipe diameter	in
E	Young's modulus of pipe	psi
e	Pipe thickness	in
f	Friction factor	
g	Acceleration	ft/sec^2
g_c	32.174	lbm-ft/(sec^2-lbf)
H	Head	ft
P	Pressure	psia
R	Gas constant	ft-lbf/lbm-°R
s	Value that must equal or exceed maximum Mach number in line	
T	Temperature	°R
t	Time	sec
Δt	Time increment	sec
V	Volume	in^3
v	Velocity	ft/sec
$\dot{w}$	Flow rate	lbm/sec
x	Distance along pipe	ft
Δx	Length increment	ft

z	Elevation	ft
α	Angle pipe makes with horizontal	deg
γ	Ratio of specific heats	
ρ	Density	lbm/ft^3

SUBSCRIPTS

i	Indicates ith pipe
j	Indicates jth node in pipe

SUPERSCRIPTS

n	Indicates nth time interval

3.4.3 Accumulators and Pressure Vessels Steady-State

3.4.3.1 Accumulator/Storage Tank

The TANK module was developed to model a general tank which may be a gas-pressurized liquid propellant tank, a gas accumulator, or a surge damper. The basic function of this module is to provide the time-dependent pressure boundaries associated with a component containing a trapped gas volume. The gas pressure is computed from the ideal gas equation of state using the integrals of mass, volume, and heating rates. Mean gas properties are computed when two gaseous species co-exist in the volume. Figure 6 is a schematic of the tank component showing the various possible inlet and outlet ports and the heat input. Nomenclature is presented at the end of this section.

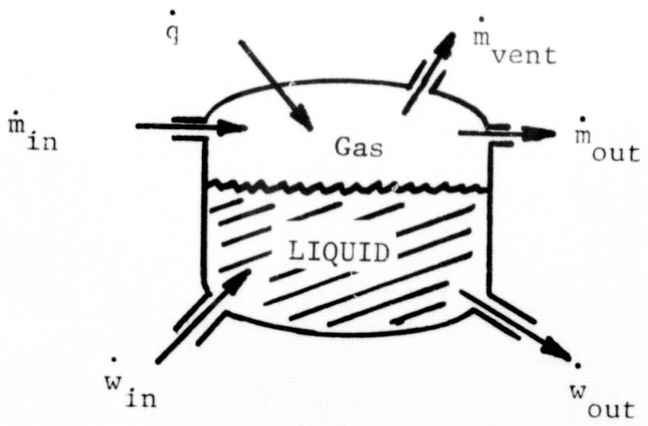

FIGURE 6

TANK COMPONENT SCHEMATIC

The flow and heating rates identified in Figure 6 are input to the program. For a given component, only those rates which apply to that particular component need to be input. All others are set to zero by the program. Similarly, the number of required initial conditions depends upon the generality of the component simulated.

Two gaseous species are considered to exist in the gas volume. The tank is pressurized initially with a quantity of species 1 computed from the specified initial pressure, temperature and volume conditions. The pertinent gas properties must be provided as input. Species 2 may be added to the gas volume at the flow rate, $\dot{m}_{in}$.

At any given time, the quantities of both species (m_1 and m_2) present in the tank are known. The total quantity is:

$$m_t = m_1 + m_2.$$

The two species are assumed to be thoroughly mixed such that the composition of the gas mixture is uniform throughout the volume. The proportion of species 2 in the mixture is:

$$\alpha = \frac{m_2}{m_1 + m_2}.$$

The gas mixture may be withdrawn from the volume by specifying $\dot{m}_{out} > 0$. A vent valve is simulated which opens at the specified pressure, P_{vent}. The gas mixture vents at the rate:

$$\dot{m}_v = \frac{32.2\ A_v P\ f(\gamma)}{\sqrt{\frac{32.2}{778.}\ \gamma RT}},$$

where $f(\gamma)$ is a tabular function of γ which is evaluated by linear interpolation.

The net rates of change of the two gas species are given by:

$$\dot{m}_1 = (\alpha - 1) \quad (\dot{m}_o + \dot{m}_v) \quad \text{and;}$$

$$\dot{m}_2 = \dot{m}_1 - \alpha(\dot{m}_o + \dot{m}_v).$$

Updated gas quantities are obtained by numerical integration of the rates. Specifically, the trapezoidal rule is employed so that:

$$\dot{m}_1^{n+1} = \dot{m}_1^{n} + 1/2 \; (\dot{m}_1^{n} + \dot{m}_1^{n+1}) \; \Delta t$$

$$m_2^{n+1} = m_2^{n} + 1/2 \; (\dot{m}_2^{n} + \dot{m}_2^{n+1}) \; \Delta t$$

The net rate of change of liquid in the tank is given as:

$$\dot{W}_n = \dot{W}_i - \dot{W}_o .$$

The integrated liquid weight is:

$$W_n^{n+1} = W_n^{n} + 1/2 \; (\dot{W}_n^{n} + \dot{W}_n^{n+1}) \; \Delta t.$$

If V_t is the total tank volume, and ρ is the liquid density, the gas volume is:

$$V_g = V_t - \frac{W}{\rho} .$$

For a mixture of two calorically perfect gases, the effective gas properties are given by:

$$\bar{R} = (R_1 \; m_1 + R_2 \; m_2) \; / m_t ,$$

$$\bar{C}_p = (Cp_1 \; m_1 + Cp_2 \; m_2) \; / m_t ,$$

$$\bar{C}_v = \bar{C}p - \bar{R} ,$$

$$\bar{\gamma} = \bar{C}p \; / \bar{C}v .$$

The enthalpy of the incoming gas is:

$$\dot{h}_k = m_k \, Cp_1 \, T_k \, .$$

The enthalpy of the gas mixture leaving the volume is:

$$\dot{h}_o = \dot{m}_o \, \bar{C}p \, \bar{T} \, ,$$

$$\dot{h}_v = \dot{m}_v \, \bar{C}p \, \bar{T} \, .$$

Work is performed on the gas volume at the rate:

$$\dot{P}w = P \, \dot{W}n/\rho \quad (\frac{144}{778}) \, .$$

By the first law, the rate of change of internal energy in the open system shown in Figure 1 is:

$$\dot{u} = \dot{q} + \dot{h}_k - \dot{h}_o - \dot{h}_v + \dot{W}k \, .$$

The integrated internal energy is computed as:

$$u^{n+1} = u^{n} + 1/2 \, (u^{n} + u^{n+1}) \Delta t \, .$$

The average temperature of the gas mixture is given by:

$$T = \frac{u}{m_t \, \bar{C}_v} \, .$$

Assuming the gas mixture to be thermally perfect, the pressure is obtained from the equation of state:

$$P = m_t \, \bar{R} \, \bar{T} \, / \, V_g \, (\frac{778}{144}) \, .$$

3.4.3.2 Pressure Boundary

The pressure boundary (P_b) is used to specify the pressure at either a large accumulator or some other boundary condition and input to the program. The line connected to this boundary condition is specified as line i. If the pressure boundary is at the upstream end of the line, the node j = 1. If the boundary is at the downstream end of the line the node j = number of nodes in the respective line. The flow constraint equation is as follows:

$$\frac{\dot{m}}{A_I} = \sqrt{\frac{ge\gamma}{R\,T_{ij}}}\; P_b M_{ij} \sqrt{1 + \left(\frac{\gamma-1}{2}\right) M^2_{ij}} \quad .$$

Pressure boundary constraint:

$$PB = P - P_b = 0 \quad .$$

NOMENCLATURE (Section 3.4.3)

Symbol	Description	Units
A	Flow area	in^2
A_I	Inside line area	in^2
C_p	Specific heat at constant pressure	B/lbm-°R
C_v	Specific heat at constant volume	B/lbm-°R
M	Mach number	-
m	Mass of gas	lbm
$\dot{m}$	Flowrate of gas	lbm/sec
P	Pressure	psi
PB	Pressure boundary constraint equation	-
q	Heat input to tank	$\frac{BTU}{lbm}$
R	Gas constant	ft-lbf/lbm-°R
T	Gas temperature	°R
t	Time	sec
V	Volume	ft^3
W	Mass of liquid	lbm
$\dot{W}$	Flowrate of liquid	lbm/sec
Pw	Power	$\frac{BTU}{sec}$
α	Mass ratio, $m_2/(m_1 + m_2)$	-
γ	Specific heat ratio, C_p/C_v	-
ρ	Density	lbm/ft^3

SUBSCRIPTS

Symbol	Description
b	Boundary
g	Gas
i	Line number

NOMENCLATURE (Section 3.4.3 Continued)

Symbol	Description
j	Node of line
k	in
n	net
o	out
v	vent
t	total
ℓ	liquid
1	Gas species 1 (initial)
2	Gas species 2 (inlet)
5	Total, tank

SUPERSCRIPTS

Symbol	Description	Units
g	gas	
ℓ	liquid	
($\dot{}$) (dot)	rate (time derivative)	sec^{-1}
($\bar{}$) (bar)	mean gas property	

3.4.4 Accumulator, Pressures and Flowrate Boundaries for Transient Program

3.4.4.1 Pressure and Flowrate Boundaries

The computational grid at the end of a line is shown in Figure 7 below. At the upstream and downstream ends either 1) the flowrate or pressure must be specified, or 2) there must be a set of equations specifying a relationship between flowrate and pressure.

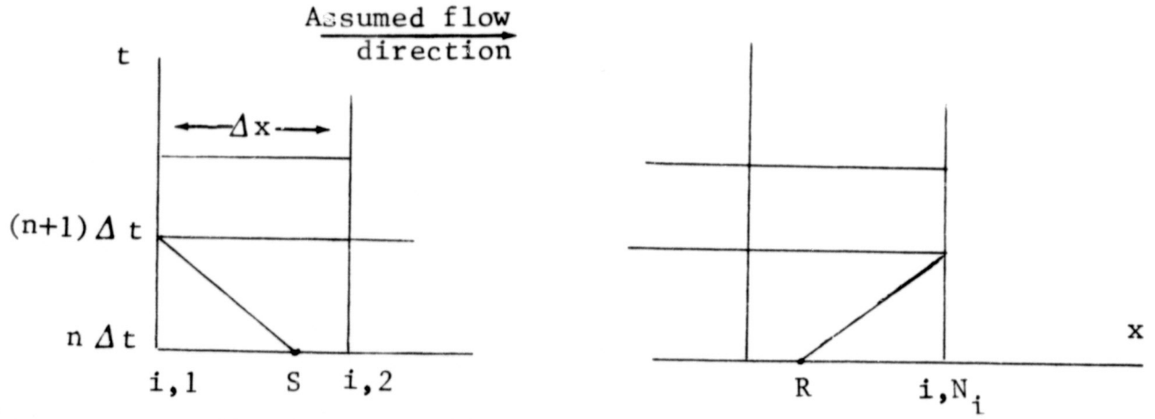

FIGURE 7 - COMPUTATIONAL GRID FOR END POINTS

When pressure or flow rate as a function of time is specified at the end of a line, either Equation (25) or (26) of Section 3.4.2 must be solved, depending upon whether the pressure is specified at the upstream or downstream end.

At the upstream end, the flowrate is

$$\dot{w}_{i,j}^{n+1} = -C_1 - C_2 P_b^{n+1} \quad , j = 1 \tag{1}$$

if the pressure is specified at the boundary and given by:

$$P_{i,j}^{n+1} = \frac{-\dot{w}_b^{n+1}}{C_2} - \frac{C_1}{C_2} \quad , j = 1 \; ; \tag{2}$$

C_1 and C_2 are computed in the same manner as for the interior line points. Similarly, for either flowrate or pressure specified at the downstream end,

the equations become, respectively,

$$\dot{w}_{i,j}^{n+1} = -C_3 - C_4 P_b^{n+1}, \quad j = N_i$$

$$P_{i,j}^{n+1} = -\frac{\dot{w}_b^{n+1}}{C_4} - \frac{C_3}{C_4}, \quad j = N_i$$

3.4.4.2 Pressure Boundary with Variable Resistance

A line with a lumped resistance (such as a valve) at the end of a line followed immediately by a pressure boundary is shown schematically in Figure 8 below:

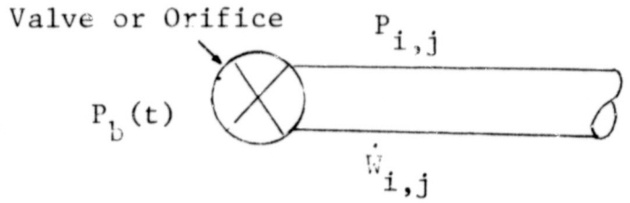

FIGURE 8 - PRESSURE BOUNDARY WITH VARIABLE RESISTANCE

The resistance is treated as being of a length small enough to be disregarded when compared to the other lengths in the system. The relationship between the pressure drop across the resistance and the flowrate is given by:

$$\dot{w}_{i,j}^{n+1} = \pm K\sqrt{2\, g_c\, \rho\, (144)\, |P_b^{n+1} - P_{i,j}^{n+1}|}, \quad j = 1 \text{ or } N_i \qquad (1)$$

The effective area, K, of the resistance may also be a function of time. If the boundary is at the assigned upstream end of the pipe, the characteristic relation between flowrate and pressure is:

$$\dot{w}_{i,j}^{n+1} + C_1 + C_2 P_{i,j}^{n+1} = 0, \quad j = 1 \qquad (2)$$

Equations 1 and 2 may be solved to yield:

$$\dot{w}_{i,j}^{n+1} = \frac{\pm C_5 \pm \sqrt{C_5^2 + 4C_6}}{2} \qquad (3)$$

where

$$C_5 = K^2\, 2\, g_c \rho\, \frac{144}{C_2} \quad \text{and} \quad C_6 = 144\, K^2\, 2 g_c\, \rho\, \left(P_b^{n+1} + \frac{C_1}{C_2}\right) \qquad (4)$$

The positive signs should be used in Equation 3 if $C_6 > 0$. The pressure at the first node in the pipeline is:

$$P_{i,j}^{n+1} = -\frac{C_1}{C_2} - \frac{\dot{w}_{i,j}^{n+1}}{C_2} \quad , \quad j = 1 \tag{5}$$

At an assigned downstream end, Equation (2) is replaced by:

$$\dot{w}_{i,j}^{n+1} + C_3 + C_4 P_{i,j}^{n+1} = 0 \quad , \quad j = N_i \tag{6}$$

Equations (6) and (1) may be solved for the flowrate to give:

$$\dot{w}_{i,j}^{n+1} = \frac{\pm C_7 \pm \sqrt{C_7^2 - 4C_8}}{2} \tag{7}$$

where:

$$C_7 = \frac{K^2 \, 2g_c \, \rho 144}{C_4} \text{ and } C_8 = \left(\frac{C_3}{C_4} + P_b^{n+1}\right) 144 \, K^2 \, 2g_c \, \rho \tag{8}$$

The upper signs in Equation (7) should be used if $C_8 < 0$, otherwise use the lower signs. The pressure at the last node in the pipe is then

$$P_{i,j}^{n+1} = \frac{-C_3}{C_4} - \frac{\dot{w}_{i,j}^{n+1}}{C_4} \quad , \quad j = N_k \tag{9}$$

3.4.4.3 Accumulator and Pressure Vessel Transients

The accumulator model is similar to that of the pressure boundary but includes friction (schematic shown in Figure 9)

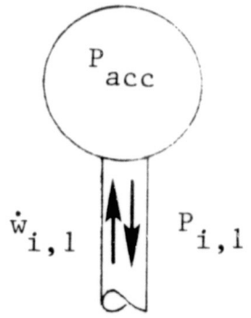

FIGURE 9 - ACCUMULATOR

except that instead of specifying the pressure as a function of time, the pressure is obtained by integrating the following differential equation.

$$\frac{dP_{acc}}{dt} = \frac{12\ a_i^2\ \dot{w}_{i,j}}{V_{acc}\ g_c}$$

A second order Runge-Kutta scheme is used in the computer program. The accumulator pressure (P_{acc}) is then used in the equations in Section 3.4.4.2 in place of P_b.

If an accumulator is large enough and the time interval selected for the system is such that it requires at least two nodes to describe the accumulator it can be treated in the program as a line. The entry and exit losses if it is treated as a line can be accounted for using the valve-orifice model described in Section 3.4.6. Large pressure vessels can be treated as constant pressure boundaries.

NOMENCLATURE (Section 3.4.4)

a	Speed of sound	ft/sec
C_1, C_2, C_3, C_4	Defined by Equations (12) through (15), Section 3.4.2	
C_5, C_6, C_7, C_8	Defined by Equations (4) and (8)	
g_c	32.174	lbm-ft/(sec^2-lbf)
K	Effective area of a valve or other lumped resistance	ft^2
N	Number of nodes in pipe	
P	Pressure	psia
t	Time	sec
V	Volume	in^3
$\dot{w}$	Flow rate	lbm/sec
ρ	Density	lbm/ft^3

SUBSCRIPTS

acc	Accumulator
b	Value specified at end of pipe
i	Indicates ith pipe
j	Indicates jth node in pipe

SUPERSCRIPTS

n	Indicates nth time interval

3.4.5 Manifolds, Injectors, Orifices, Valves and Pipends

The manifolds and injectors are treated as lines and orifices (Figure 10). Calculations for flow parameters through these components are dependent on the state of the fluid. If the fluid is a gas, the downstream pressure is calculated using Equation (1), while for a liquid, the downstream pressure is calculated from Equation (2).

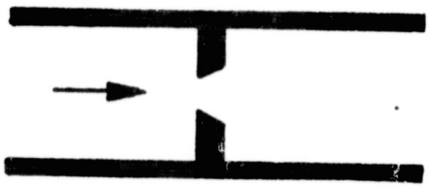

FIGURE 10 - SIMPLIFIED MANIFOLD ORIFICE

The downstream pressure through the gas valve is calculated as follows:

$$\dot{W} - P_1 \, XK \sqrt{\frac{gc}{RT}\left(\frac{2\gamma}{\gamma-1}\right)\left[\left(\frac{P_2}{P_1}\right)^{2/\gamma} - \left(\frac{P_2}{P_1}\right)^{\frac{\gamma+1}{\gamma}}\right]} \qquad (1)$$

This equation is solved for the discharge pressure (P_2) using the Newton-Raphson method of solution.

The liquid valve is simulated by calculating the discharge pressure as follows:

$$P_2 = P_1 - \left(\frac{\dot{W}}{XK}\right)^2 \Big/ 288.gc \, \rho_2 \, . \qquad (2)$$

NOMENCLATURE (Section 3.4.5)

Symbol	Description	Units
gc	32.174	lbm-ft/lbf-sec^2
P	Pressure	psia
R	Gas Constant	ft-lbf/lbm-°R
T	Temperature line	°R
$\dot{W}$	Flowrate	lbm/sec
XK	Cross sectional area times valve discharge coefficient	in^2
γ	Ratio of specific heats	-
ρ	Density	lbm/ft^3

SUBSCRIPTS

1	Upstream
2	Downstream

3.4.6 Orifices, Valves, and Linebends Transients

The computational scheme for treating orifices, valves, and linebend transients is similar to the one described in Section 3.4.4.2 for pressure boundaries with variable resistance.

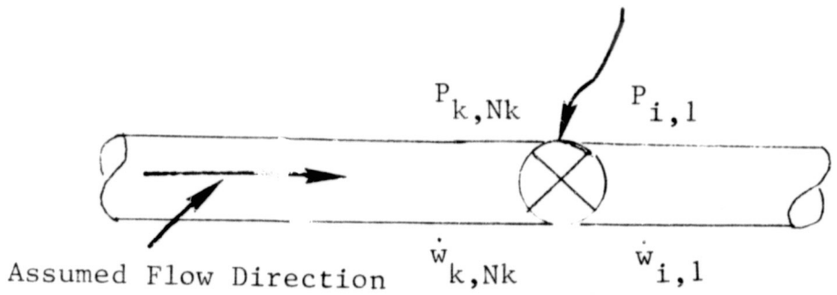

FIGURE 11 ORIFICE OR VALVE IN A LINE

The characteristic equation for the line downstream of the resistance is given by:

$$\dot{w}_{i,1}^{n+1} + C_1 + C_2 P_{i,1}^{n+1} = 0 \tag{1}$$

and for the line upstream:

$$\dot{w}_{k,N_k}^{n+1} + C_3 + C_4 P_{k,N_k}^{n+1} = 0 \tag{2}$$

The flowrate across the resistance is given by:

$$\dot{w}_{i,1}^{n+1} = \pm K \sqrt{2g_c \rho 144 \mid P_{k,N_k}^{n+1} - P_{i,1}^{n+1} \mid} \tag{3}$$

in which K may be a function of time.

In addition,

$$\dot{w}_{i,1}^{n+1} = \dot{w}_{k,N_k}^{n+1} \tag{4}$$

Solving the above equations for the flowrate yields:

$$\dot{w}_{i,1}^{n+1} = \dot{w}_{k,N_K}^{n+1} = \frac{\pm C_9 \pm \sqrt{C_9^2 - 4C_{10}}}{2} \tag{5}$$

in which:

$$C_9 = K^2\ 2g_c\ \rho 144\left(\frac{1}{C_4} - \frac{1}{C_2}\right) \tag{6}$$

$$C_{10} = K^2\ 2g_c\ \rho 144\left(\frac{C_3}{C_4} - \frac{C_1}{C_2}\right) \tag{7}$$

The upper signs are used in Equation (5) if $C_9>0$. By a suitable choice of K, the above formulation can be used to account for the changes in velocity head brought about by changes in cross-sectional area of the line. For instance, assuming that there is a sudden change in cross-section with no loss in total pressure, then:

$$K = \sqrt{\frac{A_i^{\,2}\ A_k^{\,2}}{A_k^{\,2} - A_i^{\,2}}} \tag{8}$$

The above relationship is easily derived from Bernoulli's equation for steady flow.

NOMENCLATURE (Section 3.4.6)

C_1, C_2, C_3, C_4	Defined by Equations (12) through (15), Section 3.4.2	
C_9, C_{10}	Defined by Equations (9) and (10)	
g_c	32.174	lbm-ft/ (sec^2-lbf)
K	Valve effective area	ft^2
N	Number of nodes in pipe	
P	Pressure	psia
$\dot{w}$	Flow rate	lbm/sec
ρ	Density	lbm/ft^3

SUBSCRIPTS

i	Indicates ith pipe
j	Indicates jth node in pipe
k	Indicates kth pipe

SUPERSCRIPTS

n	Indicates nth time interval

3.4.7 Line Junction Subroutine (JUNCL)

The JUNCL module permits as many as six lines to be joined together at a line junction. Any combination of inlet and outlet lines may be specified and a total of ten line junctions are permitted. The fluid in the lines connected by a junction may be either a liquid or a gas.

The junction temperature is obtained as a weighted average of the fluid temperatures in the inlet lines and is represented by:

$$T_{junc} = \sum_{k=1}^{N_{in}} (\dot{W}\ C_p\ T)_k \Big/ \sum_{k=1}^{N_{in}} (\dot{W}C_p)_k$$

The inlet conditions to each of the outlet lines become:

$$P_{out,\ k} = P_{junc}$$

$$T_{out,\ k} = T_{junc}$$

The flowrates in the inlet and outlet lines are supplied to this subroutine from other subroutines based upon the pressures existing in the system. However, to preserve mass continuity for steady-state operating conditions, the total flowrate into the junction must equal the total flowrate out of the junction. This equality is achieved by specifying the non-dimensional constraint equation:

$$F_W = 1 - \frac{\dot{W}_{out,t}}{\dot{W}_{in,t}}$$

The junction pressure was estimated as the average of the inlet line end pressures. The physical requirement that the line pressures approach a common value at the junction is imposed by the constraint equations:

$$F_{P,k} = 1 - \frac{P_{in,k}}{P_{junc}}$$

The flowrate and pressure constraints, $F_W \to 0$, $F_{P,k} \to 0$, are achieved iteratively by proper determination of adjacent line flowrates and upstream pressures.

NOMENCLATURE (Section 3.4.7)

Symbol	Description	Units
C_p	Specific heat at constant pressure	B/lbm-°R
F_P	Pressure constraint	
F_W	Flowrate constraint	
N	Number of inlet or outlet lines	-
P	Pressure	psi
T	Temperature	°R
$\dot{W}$	Mass flowrate	lbm/sec

SUBSCRIPTS

Symbol	Description
in	Inlet
junc	Junction
k	Index designating line number
out	Outlet
t	Total

3.4.8 Junction Transients

A schematic of a pipe junction is shown in Figure 12.

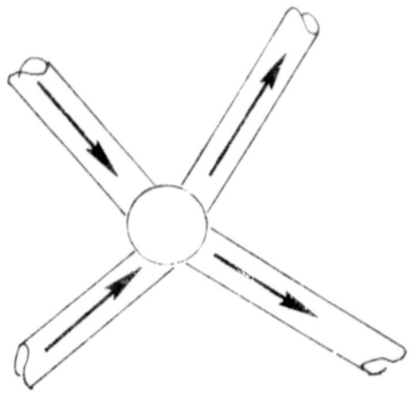

FIGURE 12 JUNCTION

The conditions at a junction are computed assuming the sum of the flows entering and leaving the junction is zero and that the pressures at the end of each line connected to the junction are equal. That is:

$$\sum_{i} \dot{w}^{n+1}_{i,N_i} - \sum_{K} \dot{w}^{n+1}_{k,1} = 0 \tag{1}$$

$$P^{n+1}_{i,N_i} = P, \quad P^{n+1}_{k,1} = P \tag{2}$$

where i takes on the values for the upstream lines and k takes on the values of the downstream lines. The characteristic relations for each line are given by:

$$\dot{w}^{n+1}_{i,N_i} + C_{3,i} + C_{4,i}\, P^{n+1}_{i,N_i} = 0 \tag{3}$$

$$\dot{w}^{n+1}_{k,1} + C_{1,i} + C_{2,i}\, P^{n+1}_{k,N_i} = 0 \tag{4}$$

Equations (1) through (4) are solved explicitly for the junction pressure (P) using the following relation:

$$P = \frac{\sum C_{1,K} - \sum C_{3,i}}{-\sum C_{2,k} + \sum C_{4,i}} \tag{5}$$

The flow rates are then computed using Equations (3) and (4)

NOMENCLATURE (Section 3.4.8)

Symbol	Description	Units
C_1, C_2, C_3, C_4	Defined by Equations (12)-(15), Section 3.4.2	
N	Number of nodes in pipe	
P	Pressure	psia
$\dot{w}$	Flow rate	lbm/sec

SUBSCRIPTS

i	Indicates ith pipe
j	Indicates jth node in pipe
k	Indicates kth pipe

SUPERSCRIPTS

n	Indicates nth time interval

3.4.9 Pressure Regulator Steady-State

The pressure regulator is modeled as a pressure boundary and both the stagnation temperature and flowrate are held constant across the regulator. The pressure can be specified either by input or computed using the non-linear equation solver, From the pressure and temperature the density is calculated by:

$$P_{reg} = \text{constant}$$

$$T_2 = T_1$$

$$\rho = P_{reg}(144)/RT$$

Assuming sonic flow through an orifice, the area of the regulator required to obtain the desired flowrate is calculated using:

$$A_{reg} = \frac{\dot{W}_{reg}}{P_1 \sqrt{\frac{g_c}{RT}\gamma\left(\frac{2}{\gamma+1}\right)^{\frac{\gamma+1}{\gamma-1}}}}$$

This area is calculated as a check to determine if the desired flow rate can be passed through the regulator at maximum flow conditions.

28

NOMENCLATURE (Section 3.4.9)

Symbol	Description	Units
P_{reg}	Regulator downstream pressure	psia
R	Gas constant	$\frac{\text{ft-lbf}}{\text{lbm-°R}}$
T	Temperature	°R
ρ	Density	lbm/ft^3

SUBSCRIPTS

1	Upstream
2	Downstream

3.4.10 Pressure Regulator Transients

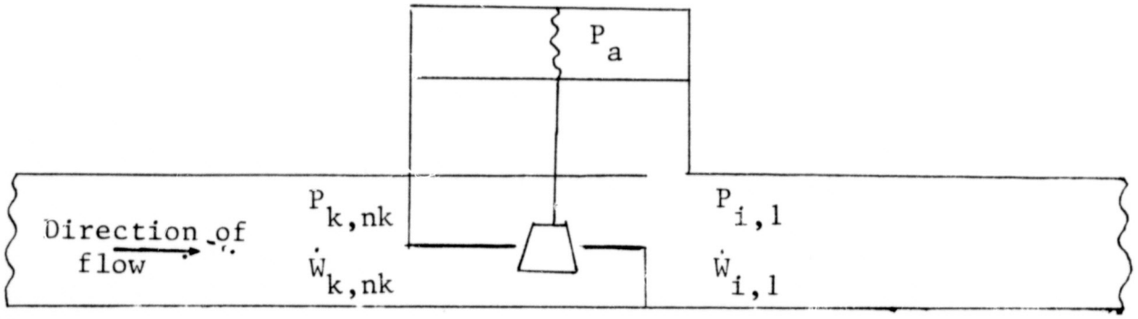

FIGURE 13 PRESSURE REGULATOR

The pressure regulator response is governed by an assumed time delay, t_{reg}. The downstream and upstream characteristic equations are, respectively, given by:

$$\dot{w}_{i,1}^{n+1} + C_1 + C_2 P_{i,1}^{n+1} = 0 \tag{1}$$

$$\dot{w}_{k,N_k}^{n+1} + C_3 + C_4 P_{k,N_k}^{n+1} = 0 \tag{2}$$

The flow rate across the regulator is governed by the relationship:

$$\dot{w}_{reg} = A_{reg}(t)\, P_{k,N_k}^{n+1} \sqrt{\frac{g_c\,\gamma}{RT}\left(\frac{2}{\gamma+1}\right)^{\frac{\gamma+1}{\gamma-1}}} \tag{3}$$

providing:

$$\frac{P_{i,1}^{n+1}}{P_{k,N_k}^{n+1}} \leq \left(\frac{2}{\gamma+1}\right)^{\frac{\gamma}{\gamma-1}} \tag{4}$$

Otherwise,

$$\dot{w}_{reg} = A_{reg}(t)\, P_{k,N_k}^{n+1} \sqrt{\frac{g_c\,\gamma}{RT}\left(\frac{2\gamma}{\gamma-1}\right)\left[\left(\frac{P_{i,1}^{n+1}}{P_{k,N_k}^{n+1}}\right)^{\frac{2}{\gamma}} - \left(\frac{P_{i,1}^{n+1}}{P_{k,N_k}^{n+1}}\right)^{\frac{\gamma+1}{\gamma}}\right]} \tag{5}$$

Also,

$$\dot{w}_{reg} = \dot{w}_{i,1}^{n+1} = \dot{w}_{k,N_k}^{n+1} \tag{6}$$

and:

$$t = (n+1)\ \Delta t \tag{7}$$

The force on the spring is given by:

$$F_{sp} = F_{spo} + Ky \tag{8}$$

and force on the diaphragm:

$$F_{dia} = \left(P_{i,1}^{n+1} - P_a\right) A_{rege} \tag{9}$$

The regulator flow area is assumed to be a linear function of the spring position such that:

$$A_{reg} = A_{reg,\,mx} - \sigma y \tag{10}$$

If the effects of inertia and damping are accounted for by the inclusion of a time delay, then the flow area of the regulator at the time $t+t_{reg}$ is determined by combining Equations (8), (9), and (10) resulting in:

$$A_{reg}(t+t_{reg}) = A_{reg,\,mx} - \frac{\sigma}{K}\left\{\left(P_{i,1}^{n+1} - P_a\right) A_{rege} - F_{spo}\right\} \tag{11}$$

For choked flow through the regulator Equations (1), (2), and (3) result in:

$$P_{k,N}^{n+1} = \frac{-C_3}{A_{reg}(t)\sqrt{\frac{g_c\,\gamma}{RT}\left(\frac{2}{\gamma+1}\right)^{\frac{\gamma+1}{\gamma-1}}} + C_4} \tag{12}$$

$P_{i,1}^{n+1}$ and $\dot{w}_{reg}$ are then computed from Equations (1) and (2).

When the flow is not choked, Equations (1), (2), and (5) are combined to obtain an implicit expression for the regulator flow rate resulting in:

$$\dot{w}_{reg}^2 - A_{reg}^2(t) \frac{g_c \gamma}{RT} \left(\frac{2\gamma}{\gamma+1}\right) \left[\left(- \frac{\dot{w}_{reg}}{C_2} - \frac{C_1}{C_2} \right)^{\frac{2}{\gamma}} \left(- \frac{\dot{w}_{reg}}{C_4} - \frac{C_3}{C_4} \right)^{\frac{2(\gamma-1)}{\gamma}} - \right.$$

$$\left. \left(- \frac{\dot{w}_{reg}}{C_2} - \frac{C_1}{C_2} \right)^{\frac{\gamma+1}{\gamma}} \left(- \frac{\dot{w}}{C_4} - \frac{C_3}{C_4} \right)^{\frac{\gamma-1}{\gamma}} \right] = 0 \qquad (13)$$

This expression is solved using a Newton-Raphson scheme.

NOMENCLATURE (Section 3.4.10)

Symbol	Description	Units
A	Effective flow area	in^2
C_1, C_2, C_3, C_4	Defined by Equations (12) through (15), Section 3.4.2	
K	Spring constant	lbf/in
F	Force	lbf
g_c	32.174	lbm-ft/(sec^2-lbf)
P	Pressure	psia
R	Gas constant	ft-lbf/lbm-°R
T	Temperature	°R
$\dot{w}$	Flow rate	lbm/sec
y	Distance moved by regulator spring	in
γ	Ratio of specific heats	
σ	Change in regulator flow area with change in spring position	in^2/in

SUBSCRIPTS

dia	Regulator diaphragm
i	Indicates ith pipe
k	Indicates kth pipe
mx	Maximum value
reg	Regulator
rege	Indicates effective area for a pressure balance in regulator

sp	Regulator spring
spo	Regulator spring in the closed position
a	Reference

SUPERSCRIPTS

n	Indicates nth time interval

3.4.11 Combustors Steady-State

The combustor component models have been developed with options for either bi-propellant or monopropellant fluids. The bi-propellant model uses curve fits to obtain the combustion properties and the specific impulse. The monopropellant model assumes a constant ratio of specific heats throughout the combustion chamber and nozzle. The development of both models gives the program a wide range of flexibility in modeling ACPS combustors.

3.4.11.1 Bi-Propellant Combustor Steady-State

The steady-state model of an ACPS combustor uses curve fits of chamber performance data (calculated using the ICRPG programs) to describe the steady-state operation of combustion chamber parameters. These curves are presently incorporated into the program, but must be expanded to account for effects of chamber pressure inlet propellant temperatures and expansion ratio variations. Curve fit evaluations were performed by comparing them with data from TRW Redondo Beach's high and low pressure ACPS studies. The chamber pressure utilized in the curve fits was 300psia and the expansion ratio was 40:1.

The model calculations are performed as follows:

Flowrate through the oxidizer/fuel injections is implemented as a constraint equation.

$$\dot{W}_{o,f} = P_c C_d A_{inj} \sqrt{\frac{g_c}{RT}\left(\frac{2\gamma}{\gamma-1}\right)\left(\left(\frac{Pc}{P_{o,f}}\right)^{2/\gamma} - \left(\frac{Pc}{P_{o,f}}\right)\right)^{\frac{\gamma+1}{\gamma}}} \qquad (1)$$

The mixture ratio is given by

$$MR = \frac{\dot{W}_o}{\dot{W}_f} \qquad (2)$$

The specific impulse is given by:

$$ISP_v = f(MR) \qquad (3)$$

The characteristic exhaust velocity is given by:

$$C^* = f(MR) \tag{4}$$

The thrust coefficient is given by:

$$C_{fv} = \frac{gISP_v}{C^*} \tag{5}$$

The nozzle flowrate is given by:

$$\dot{W}_n = \dot{W}_o + \dot{W}_f \tag{6}$$

The combustion gas temperature is given by:

$$T_c = f(MR) \tag{7}$$

Constraint equation

$$\text{Constraint} = P_c - \frac{F\ C^*}{ISP_v A_t gc} \tag{8}$$

3.4.11.2 Monopropellant Combustor

The monopropellant combustor is based on calculations which assume a constant ratio of specific heats. The nozzle area ratio is utilized to define the exit Mach number. The boundary conditions can be specified as either specific impulse, chamber pressure, or engine thrust. The following equations define the component model.

The nozzle exit Mach number (Me) is calculated from the following equation using the Newton-Raphson technique.

$$\varepsilon = \frac{1}{Me} \left[\frac{1 + \left(\frac{\gamma-1}{2}\right) M_e^2}{1 + \frac{\gamma-1}{2}} \right] \frac{\gamma + 1}{2\ (\gamma - 1)} \tag{9}$$

The injector flow equation is given by:

$$\dot{W}_n = P_c A_{inj}\ C_d \sqrt{\frac{g_c\ \gamma}{RT} \left(\frac{2}{\gamma-1}\right) \left[\left(\frac{P_c}{P_T}\right)^{2/\gamma} - \left(\frac{P_c}{P_T}\right)^{\frac{\gamma+1}{\gamma}} \right]} \tag{10}$$

The nozzle sonic flowrate is a constraint equation:

$$\text{Constraint} = C_d A_t P_o \sqrt{\frac{g_c \gamma}{RT_o} \left(\frac{2}{\gamma+1}\right)^{\frac{\gamma+1}{\gamma-1}}} - \frac{F}{ISP} \tag{11}$$

Nozzle exit pressure is given by:

$$P_e = P_0 \Big/ \left(1 + \frac{\gamma-1}{2} M_e^2\right)^{\frac{\gamma}{\gamma-1}} \tag{12}$$

The thrust is given by:

$$F = A_e P_e \left(1 + \lambda\gamma M_e^2\right) - \text{Patm } A_e \tag{13}$$

Specific Impulse

$$ISP = \frac{F}{\dot{W}_{noz}} \tag{14}$$

The boundaries are implemented as constraint equation and are specified for one of the following conditions:

Thrust Boundary

$$BC = FI - F \tag{15}$$

Specific Impulse Boundary

$$BC = ISPI - ISP \tag{16}$$

Chamber Pressure Boundary

$$BC = PC - PCI \tag{17}$$

NOMENCLATURE (Section 3.4.11)

Symbol	Description	Units
A_{inj}	Injector area	in^2
A_t	Area combustor throat	in^2
C*	Characteristic exhaust velocity	ft/sec
C_d	Discharge coefficient through injector	-
C_{fv}	Vacuum thrust coefficient	-
F	Thrust	lbf
gc	Conversion constant (32.174)	$\frac{lbm\text{-}ft}{sec^2\text{-}lbf}$
ISP_v	Vacuum specific impulse	sec
MR	Mixture ratio	-
P_c	Chamber pressure	psia
R	Gas constant	$\frac{ft\text{-}lbm}{lbf\text{-}°R}$
T_c	Chamber temperature	°R
T_{H_2}	Inlet temperature	°R
T_{O_2}	Inlet temperature	°R
$\dot{W}_{H_2}$	Fuel flowrate	lbm/sec
$\dot{W}_n$	Nozzle flowrate	lbm/sec
$\dot{W}_{O_2}$	Oxidizer flowrate	lbm/sec
ε	Expansion area ratio	-
γ	Ratio specific heats	-
B_c	Constraint equation	-
A_e	Nozzle exit area ratio	in^2
FI	Thrust boundary	lbf

Symbol	Description	Units
ISPI	Specific impulse boundary	sec.
M_E	Nozzle exit Mach number	-
PCI	Chamber pressure boundary	psia
λ	Nozzle divergence coefficient	-

Subscripts

f	Fuel	-
o	Oxidizer	-
e	Exit	

3.4.12 Combustor Transients

A schematic of the thrust chamber and its associated parts is shown in Figure 14

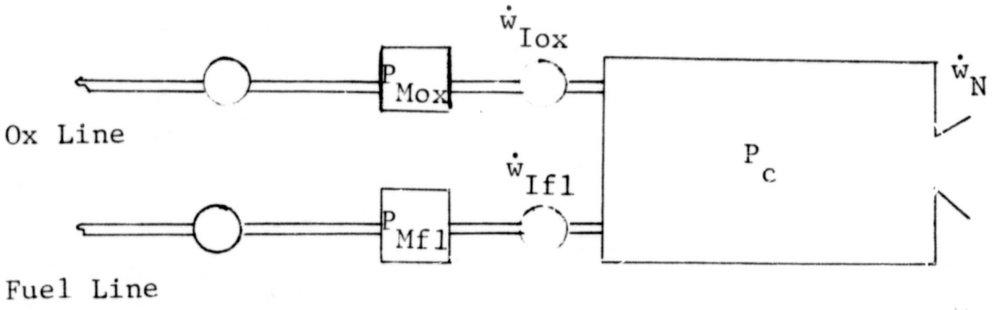

FIGURE 14 COMBUSTOR

The characteristic relation at the end of the oxidizer line is given by:

$$\dot{w}_{iox,N_i} = -C_3 - C_4 P_{iox,\ Ni} \tag{1}$$

If

$$\frac{P_{Mox}}{P_{iox,N_{iox}}} \leq \left(\frac{2}{\gamma_{ox}+1}\right)^{\frac{\gamma_{ox}}{\gamma_{ox}-1}} \tag{2}$$

the flow rate through the oxidizer thrust chamber valve is given by:

$$\dot{w}_{iox,N_{iox}} = A_{vox}\ C_{vox}\ P_{iox,N_{iox}} \sqrt{\frac{g_c\ \gamma_{ox}}{R_{ox}\ T_{ox}} \left(\frac{2}{\gamma_{ox}+1}\right)^{\left(\frac{\gamma_{ox}+1}{\gamma_{ox}-1}\right)}} \tag{3}$$

If Equation (2) is not satisfied, then the flow rate through the valve is dependent upon the manifold pressure and is obtained from:

$$\dot{w}_{iox,N_i} = A_{vox}\, C_{vox}\, P_{iox,N_i} \left\{ \frac{g_c}{R_{ox}\, T_{ox}} \left(\frac{2\gamma_{ox}}{\gamma_{ox}-1}\right) \left[\left(\frac{P_{Mox}}{P_{iox,N_i}}\right)^{\frac{2}{\gamma_{ox}}} - \left(\frac{P_{Mox}}{P_{iox,N_i}}\right)^{\frac{\gamma_{ox}+1}{\gamma_{ox}}} \right] \right\}^{\frac{1}{2}} \tag{4}$$

The oxidizer injector flowrates are given by:

$$\dot{w}_{Iox} = A_{Iox}\, P_{Mox} \sqrt{\frac{g_c\, \gamma_{ox}}{R_{ox}\, T_{ox}} \left(\frac{2}{\gamma_{ox}+1}\right)^{\frac{\gamma_{ox}+1}{\gamma_{ox}-1}}} \tag{5}$$

if,

$$\frac{P_c}{P_{Mox}} \leq \left(\frac{2}{\gamma_{ox}+1}\right)^{\frac{\gamma_{ox}}{\gamma_{ox}-1}} \tag{6}$$

otherwise,

$$\dot{w}_{Iox} = A_{Iox}\, P_{Mox} \sqrt{\frac{g_c}{R_{ox}\, T_{ox}} \left(\frac{2\gamma_{ox}}{\gamma_{ox}-1}\right) \left[\left(\frac{P_c}{P_{Mox}}\right)^{\frac{2}{\gamma_{ox}}} - \left(\frac{P_c}{P_{Mox}}\right)^{\frac{\gamma_{ox}+1}{\gamma_{ox}}} \right]} \tag{7}$$

The change in pressure with time in the oxidizer manifold is computed using:

$$\frac{dP_{Mox}}{dt} = \frac{12\, a_{iox}^2}{V_{Mox}\, g_c} \left(\dot{w}_{iox,N_{iox}} - \dot{w}_{iox}\right) \tag{8}$$

Relationships identical to Equation (1) through (8) are valid for the fuel side as well as for the oxidizer side. The change in quantities of fuel and oxidizer residing in the chamber are given by:

$$\frac{dW_{ox}}{dt} = \dot{w}_{iox} - \frac{MR}{MR + 1} \dot{w}_{n\phi z} \tag{9}$$

$$\frac{dW_{fl}}{dt} = \dot{w}_{Ifl} - \frac{1}{MR + 1} \dot{w}_{n\phi z} \tag{10}$$

The mixture ratio used in the above two equations is computed using the quantities of fuel and oxidizer present in the chamber and is given by:

$$MR = \frac{W_{ox}}{W_{fl}} \tag{11}$$

The chamber pressure is derived from the ideal gas law such that:

$$P_c = \frac{\left(W_{ox} + W_{fl}\right) \; 1545 \; T_C}{12 \qquad MW \qquad V_C} \tag{12}$$

and the flow out of the nozzle is determined using the characteristic velocity as follows:

$$\dot{w}_{n\phi z} = \frac{P_c \; A_{n\phi z} \; g_c}{C^*} \tag{13}$$

The molecular weight, chamber temperature, characteristic velocity, and specific impulse are determined from polynomial least squares curve fits of these variables as a function of mixture ratio. Functionally, these parameters can be represented as follows:

$$
\begin{aligned}
MW &= f(MR) \\
T_c &= f(MR) \\
C^* &= f(MR) \\
I_{sp} &= f(MR)
\end{aligned}
\qquad (14)
$$

Given the conditions at time, n Δt, the conditions at time, (n+1)Δt, are determined by first integrating the differential equations for manifold pressures and quantities of propellants in the chamber using a Runge-Kutta fourth order integration scheme. Once W_{ox}, W_{fl}, P_{Mox}, and P_{Mfl} are known, the remaining variables for the pressures and flow rates upstream of the propellant valves are solved using the above equations. If the flow through the propellant valve is choked, Equations (1) and (3) are combined to give an explicit expression for the pressure as follows:

$$
P_{iox},\ N_{iox} = \frac{-C_3}{C_4 + A_{Vox}\ C_{Vox} \sqrt{\frac{g_c\ \gamma_{ox}}{R_{ox}\ T_{ox}} \left(\frac{2}{\gamma_{ox}+1}\right)^{\frac{\gamma_{ox}+1}{\gamma_{ox}-1}}}} \qquad (15)
$$

When the flow is unchoked, Equations (1) and (4) are combined to yield an expression implicit in P_{iox,N_i}, which is represented by:

$$
\begin{aligned}
&-C_3^2 - 2\ C_3\ C_4\ P_{iox,N_{iox}} - C_4^2\ P^2_{iox},\ N_{iox} + \\
&A^2_{Vox}\ C^2_{Vox}\ \frac{g_c}{R_{ox}\ T_{ox}} \left(\frac{2\gamma_{ox}}{\gamma_{ox}-1}\right) \Bigg\{ \left(P_{Mox}\right)^{\frac{2}{\gamma_{ox}}} \left(P_{iox,N_{iox}}\right)^{\frac{2\ \gamma_{ox}-2}{\gamma_{ox}}} \\
&\qquad - \left(P_{Mox}\right)^{\frac{\gamma_{ox}+1}{\gamma_{ox}}} \left(P_{iox,\ N_{iox}}\right)^{\frac{\gamma_{ox}-1}{\gamma_{ox}}} \Bigg\} = 0 \qquad (16)
\end{aligned}
$$

The above equation is solved for P_{i,N_i} using a Newton-Raphson scheme. Once P_{i,N_i} is known, $\dot{w}_{i,N_i}$ is calculated using Equation (1).

NOMENCLATURE (Section 3.4.12)

a	Speed of sound	ft/sec
C	Valve discharge coefficient	
C*	Characteristic velocity	ft/sec
C_3, C_4	Defined by Equations 12 and 13, Section 3.4.2	
g_c	32.174	lbm-ft/(sec^2-lbf)
I_{sp}	Specific Impulse	lbm-sec/lbm
MW	Molecular weight	lbm/lbm-mole
P	Pressure	psia
R	Gas constant	ft-lbf/lbm-°R
T	Temperature	°R
V	Volume	in^3
W	Quantity	lbm
$\dot{w}$	Flow rate	lbm/sec
γ	Ratio of specific heats	

SUBSCRIPTS

c	Combustion chamber
Iox	Oxidizer injector
iox	Oxidizer line
Mox	Oxidizer manifold
N	Number of nodes in pipe
noz	Nozzle
ox	Oxidizer
Vox	Oxidizer valve
Vfl	Fuel valve

3.4.13 Turbopumps Steady-State

Relationships of the type shown in Figures 26 and 27 are sufficient to represent the turbopump and turbine in a steady-state program when the turbine and pump power equality constraints are satisfied simultaneously with the propellant continuity constraints. The turbomachinery relationship is in the form of curve fit equations where the equation constants may be varied to simulate the characteristics of different hardware. The turbopump equations have been formulated based on pump and turbine characteristic curves combined with turbopump similarity parameters.

The pressure rise at design speed is curve fit using pump characteristic curves based on flowrates.

$$\Delta P_R = P_{W0} + P_{W1} \dot{W}_R + P_{W2} \dot{W}_R^2 \qquad (1)$$

The pump relationships are based on geometrically similar pumps, which have similar flow conditions.

$$\dot{W}_R = \frac{\dot{W}_p}{\frac{N_p}{N_D}\left(\frac{D_p}{D_D}\right)^3} \qquad (2)$$

$$\Delta P_R = \frac{\Delta P_p}{\left(\frac{N_p}{N_D}\right)^2 \left(\frac{D_p}{D_D}\right)^2} \qquad (3)$$

Substituting Equations (2) and (3) into Equation (1) gives:

$$P_p = P_{W0}\left(\frac{D_p}{D_D}\right)^2\left(\frac{N_D}{W_D}\right)^2 + \dot{W}_p P_{W1}\left(\frac{D_D}{D_p}\right)\left(\frac{N_p}{N_D}\right) + P_{W2}\left(\frac{D_D}{D_p}\right)^4 \dot{W}_p^2 \qquad (4)$$

Solving the quadratic equation for the speed ratio, $\frac{N_p}{N_D}$, gives the following equation:

$$\frac{N_p}{N_D} = \frac{-\frac{P_{W1}\dot{W}_p}{(D_p/D_D)} \pm \sqrt{\left(\frac{P_{W1}\dot{W}_p}{(D_p/D_D)}\right)^2 - 4P_{Wo}\left(\frac{D_p}{D_D}\right)^2\left(\frac{P_{W2}\dot{W}_p^{\,2}}{(D_p/D_D)^4} - \Delta P_p\right)}}{2\left(\frac{D_p}{D_D}\right)^2 P_{Wo}} \tag{5}$$

Solving for the pump speed:

$$N_p = N_D\left(\frac{N_p}{N_D}\right) \tag{6}$$

The pump power based on the characteristic curves at design speeds is presented as a third order curve fit based upon flowrate.

$$P_{OWD} = P_{OW} + P_{OW1}\,\dot{W}_R + P_{OW2}\,W_R^{\,2} + P_{OW3}\,\dot{W}_R^{\,3} \tag{7}$$

substituting Equation (2) into Equation (7):

$$P_{OWD} = P_{OW} + P_{OW1}\,\frac{\dot{W}_p}{SX} + P_{OW2}\left(\frac{\dot{W}_p}{SX}\right)^2 + P_{OW3}\left(\frac{\dot{W}_p}{SX}\right)^3 \tag{8}$$

where: $S = \left(\frac{N_p}{N_D}\right)$ and

$$SX = S\left(\frac{D_p}{D_D}\right)^3$$

Ratio of actual pump diameter to pump design diameter:

$$RD = \left(\frac{D_p}{D_D}\right) \tag{8a}$$

The pump similarity relationship is as follows:

$$\frac{P_{OWP}}{N_p^3 D_p^5} = \frac{P_{OWD}}{N_D^3 D_D^5} \tag{9}$$

The pump power is calculated combining the similarity relationship in Equation (9) between pump power and speed and Equation (8).

$$P_{OWP} = \left[S^3 RD^5 (P_{GW}) + S^2 RD^2 (P_{OW1}) \dot{W}_p + \frac{S (P_{OW2})}{RD} \dot{W}_p^2 + \frac{P_{OW3} W_p^3}{RD^4} \right] \tag{10}$$

The pump efficiency is obtained as follows:

$$\eta_p = \frac{\Delta P_p \dot{W}_p 144}{P_{OWP} \rho_L} \tag{11}$$

The temperature of the pump discharge, °R, assumes all the power dissipated is transferred into fluid heating and is given by:

$$T_{PO} = \frac{(1-\eta_p) P_{OWP}}{\dot{W}_p 778.26 C_v} + T_{PI} \tag{12}$$

The turbine speed, RPM, is calculated based upon the gear ratio GR such that:

$$\eta_T = \eta_p \cdot GR \tag{13}$$

The temperature inlet to the turbine is obtained from the temperature in the gas generator as follows:

$$T_{TI} = T_{GG} \tag{14}$$

The turbine isentropic discharge temperature (°R) is from equations based on choked flowrate through the turbine and through the turbine duct.

$$T_S = T_{TI} \left(\frac{A_{TI}}{A_{TD}}\right)^{2\left(\frac{\gamma-1}{\gamma+1}\right)} \tag{15}$$

The turbine inlet pressure, psia is calculated by:

$$P_{TI} = P_{GG} - \frac{K \dot{W}_T^2}{P_{GG}} \quad T_{GG} \; R \tag{16}$$

The isentropic spouting velocity is given as follows:

$$C_{vel} = \sqrt{2C_P(T_{TI}-T_S)(778.26)gc} \tag{17}$$

The turbine tip speed is calculated from the following equations:

$$u = \frac{\pi \; D_t \; N_t}{12(60)} \tag{18}$$

The turbine efficiency becomes:

$$\eta_t = a\left(\frac{u}{C_{vel}}\right)^2 + b\left(\frac{u}{C_{vel}}\right) \tag{19}$$

The turbine power, ft-lbf/sec, is given by:

$$P_{OWT} = \eta_T \; 778.26 \; C_P \; \dot{W}_T \; (T_{TI} - T_{TO}) \tag{20}$$

The turbine actual discharge temperature (°R) is given by:

$$T_{TO} = T_{GG} \; (1-\eta_T)(1-T_S/T_{GG}) \tag{21}$$

The turbine choked flowrate lbm/sec is calculated as follows:

$$W_T = P_{TI} A_{TI} K_{TI} \sqrt{\frac{MW \; gc \; \gamma}{1545 \; T_{TI}} \left(\frac{2}{\gamma+1}\right)^{\frac{\gamma+1}{\gamma-1}}} \tag{22}$$

The turbine discharge pressure, psia, is given by:

$$P_{TO} = \frac{WT}{A_{TD} K_{TD} \frac{MW\ gc\ \gamma}{1545\ T_{TO}} \left(\frac{2}{\gamma+1}\right)^{\frac{\gamma+1}{\gamma-1}}} \tag{23}$$

The turbine flowrate constraint equation becomes:

$$\text{Constraint} = \dot{W}_T - \dot{W}_{GG} \tag{24}$$

The pump/turbine power balance finalizes the computations:

$$\text{Constraint} = P_{OWP} - P_{OWT} \tag{25}$$

NOMENCLATURE (Section 3.4.13)

Symbol	Description	Units
a	Coefficient of turbine efficiency curve	-
A_{TI}	Turbine inlet area	in^2
A_{TD}	Turbine duct discharge area	in^2
b	Coefficient of turbine efficiency curve	-
C_p	Specific heat constant pressure	BTU/°R
C_{vel}	Isentropic spouting velocity	ft/sec
D_D	Pump design diameter	in
D_P	Pump diameter	in
D_t	Diameter of turbine rotor	in
K	Duct pressure loss coefficient	$\frac{psia\text{-}sec^2}{lbm\text{-}ft^3}$
K_{TD}	Turbine Discharge coefficient	-
K_{TI}	Turbine inlet coefficient	-
MW	Molecular weight	-
N_D	Pump design speed	RPM
N_p	Pump speed	RPM
N_T	Speed of turbine	RPM
P_{GG}	Pressure of gas generator	psia
$P_{OW,0,1,2,3}$	Coefficients of pump power design curve	-
P_{OWD}	Pump power at design speed	ft-lbf/sec
P_{OWP}	Pump power	ft-lbf/sec
P_{OWT}	Turbine power	ft-lbf/sec
P_{TD}	Turbine discharge pressure	psia
$P_{WO,1,2}$	Coefficients of pump pressure design curve	-
ΔP_{PD}	Design pump pressure rise	psia
ΔP_P	Pump pressure rise	psia

NOMENCLATURE (Section 3.4.13 Continued)

Symbol	Description	Units
ΔP_R	Pump pressure at design speed	psia
R	Gas constant	ft-lbf/lbm-°R
RD	Ratio pump of diameter to design pump diameter	-
T_{GG}	Temperature of gas generator	°R
T_{PO}	Temperature of pump discharge	°R
T_{PI}	Temperature of pump inlet	°R
T_S	Turbine isentropic discharge temperature	°R
T_{TI}	Temperature of turbine inlet	°R
$T_{T\emptyset}$	Temperature of turbine discharge	°R
$\dot{W}_P$	Flowrate of pump	lbm/sec
$\dot{W}_R$	Pump flowrate along design speed curve	lbm/sec
$\dot{W}_T$	Flowrate of turbine	lbf/sec
η_t	Efficiency of turbine	-
η_p	Efficiency of pump	-
γ	Ratio of specific heats	-
μ	Turbine tip speed	ft/sec

3.4.14 Turbopump and Gas Generator Transients

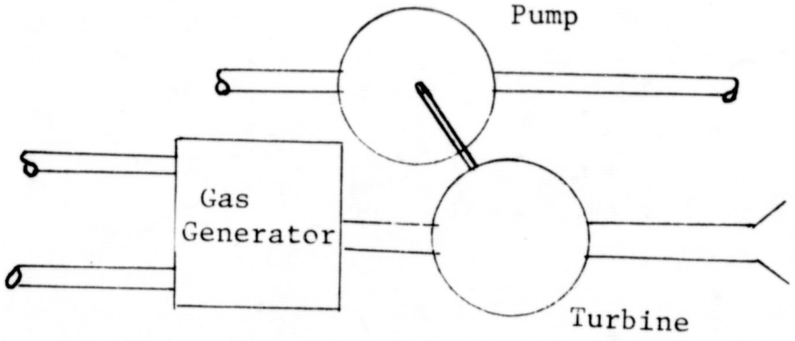

FIGURE 15 - TURBOPUMP AND GAS GENERATOR

The system shown in Figure 15 represents a schematic of the components utilized in the turbopump and gas generator model.

The equations used in modeling the gas generator are identical to those used for the thrust chamber except that Equation 1, below, for flow rate across the turbine replaces Equation 13, described in Section 3.4.12. The flows through the pump and turbine are treated as being quasi-steady, i.e., the steady flow relationships are assumed to be valid at any instant in the transient. The flow rate through the turbine is given by:

$$\dot{w}_T = A_T P_c \sqrt{\frac{g_c \gamma_c}{R_c T_c} \left(\frac{2}{\gamma_c+1}\right)^{\frac{\gamma_c+1}{\gamma_c-1}}} \qquad (1)$$

The turbine efficiency is given by

$$\eta_T = a \left(\frac{U}{v_{TOI}}\right) + b \left(\frac{U}{v_{TOI}}\right)^2 \qquad (2)$$

The isentropic spouting velocity is

$$v_{TOI} = \sqrt{2\, c_p (778.26)(T_c - T_{TOI})\, g_c} \qquad (3)$$

where T_{TOI} is:

$$T_{TOI} = T_c \left(\frac{P_{TO}}{P_c}\right)^{\frac{\gamma_c - 1}{\gamma_c}} \quad (4)$$

The turbine tip speed is:

$$U = \frac{\pi}{(12)} \frac{D_{TR}\omega_T}{(60)} \quad (5)$$

The turbine power and torque is obtained from:

$$\phi_T = \eta_T (778.26) c_p \dot{w}_T (T_c - T_{TOI}) \quad (6)$$

$$\tau_T = \frac{\phi_T 60}{2\pi \omega_T} \quad (7)$$

The turbine outlet temperature is:

$$T_{TO} = T_c \left[1 - \eta_T \left(1 - \frac{T_{TOI}}{T_c}\right)\right] \quad (8)$$

The change in turbopump speed with time is:

$$\frac{d\omega_T}{dt} = \frac{g_c (144) (60))}{2\pi} I_{TP} (\tau_T - \tau_P) \quad (9)$$

The final two equations required to describe the turbine are those giving the change in turbine exit duct pressure with time and the flow rate through the turbine duct exit nozzle. These parameters are given by:

$$\frac{dP_{TD}}{dt} = \frac{\gamma_c \ 1545 \ T_{TO} \ (\dot{w}_T - \dot{w}_{TD})}{MW \ L_{TD} \ A_{TD}} \tag{10}$$

$$\dot{w}_{TD} = A_{TDN} \ P_{TD} \sqrt{\frac{g_c \gamma_c}{R_c T_{TO}} \left(\frac{2}{\gamma_c + 1}\right)^{\frac{\gamma_c + 1}{\gamma_c - 1}}} \tag{11}$$

The characteristic equations relating flow rate and pressure at the ends of the liquid lines attached to the pump are given by:

$$\dot{w}_P + C_1 + C_2 \ P_{PO} = 0 \tag{12}$$

$$\dot{w}_P + C_3 + C_4 \ P_{PI} = 0 \tag{13}$$

The pressure rise across the pump is expressed in terms of the variables in the above two equations and is given by:

$$\Delta P_P = P_{PO} - P_{PI} = C_9 \ \dot{w}_P + C_{10} \tag{14}$$

where:

$$C_9 = \left(\frac{1}{C_4} - \frac{1}{C_2}\right) \quad , \quad C_{10} = \left(\frac{C_3}{C_4} - \frac{C_1}{C_2}\right) \tag{15}$$

The pressure rise across the pump and the pump power at the pump design speed are expressed as functions of the flow rate as shown below:

$$\Delta P_r = a_o + a_1 \dot{w}_r + a_2 \dot{w}_r^2 \tag{16}$$

$$\phi_r = b_o + b_1 \dot{w}_r + b_2 \dot{w}_r^2 + b_3 \dot{w}_r^3 \tag{17}$$

The coefficients in the above equations are derived from least squares fits. The pump similarity relations are:

$$\frac{\Delta P_P}{\Delta P_r} = \left(\frac{\omega_P}{\omega_D}\right)^2 \quad , \quad \frac{\dot{w}_P}{\dot{w}_R} = \frac{\omega_P}{\omega_D} \tag{18}$$

$$\frac{\phi_P}{\phi_R} = \left(\frac{\omega_P}{\omega_D}\right)^3$$

Using the three similarity relations, expressions for the pressure rise and pump power as a function of both speed and flow rate are derived such that:

$$\Delta P_P = a_o \psi^2 + a_1 \psi \dot{w}_P + a_2 \dot{w}_P^2 \tag{19}$$

$$\phi_P = \psi^3 b_o + \psi^2 b_1 \dot{w}_P + b_2 \psi \dot{w}_P^2 + b_3 \dot{w}_P^3 \tag{20}$$

In the above two equations:

$$\psi = \frac{N_P}{N_D} \tag{21}$$

Equations (14) and (19) are combined to give the flow rate and are expressed as follows:

$$\dot{w}_P = - \frac{C_{11} - \sqrt{C_{12}^2 - 4\, a_2\, C_{12}}}{2\, a_2} \tag{22}$$

where:

$$C_{11} = a_1\, \psi - C_9$$

$$C_{12} = a_0\, \psi^2 - C_{10}$$

Once the pump flow rate is determined, the pump power is computed using Equation (20) and the pump torque is computed from:

$$\tau_P = \frac{\phi_P\, 60}{2\Pi\ \omega_p} \tag{23}$$

The differential relations for turbine speed and turbine output pressure are integrated using a Runge-Kutta fourth order scheme.

NOMENCLATURE (Section 3.4.14)

A	Effective flow area	in^2
a	Speed of sound	ft/sec
g_c	32.174	$lbm\text{-}ft/(sec^2\text{-}lbf)$
L	Length	ft
P	Pressure	psi
R	Gas constant	ft-lbf/lbm-°R
T	Temperature	°R
t	Time	sec
U	Turbine tip speed	ft/sec
v	Velocity	ft/sec
$\dot{w}$	Flow rate	lbm/sec
γ	Ratio of specific heats	
η	Efficiency	
τ	Torque	ft-lbf
ϕ	Power	ft-lbf/sec
ψ	Ratio of speed to design speed	
ω	Rotational speed	rev/min.

SUBSCRIPTS

c	Combustion chamber
D	Steady-state design conditions
P	Pump
PI	Pump inlet
PO	Pump outlet
r	Value at design speed
T	Turbine
TOI	Turbine outlet based on an isentropic expansion

NOMENCLATURE (Continued)

TR	Turbine rotor
TO	Turbine outlet
TD	Turbine exit duct
TDN	Turbine exit duct throat

3.4.15 Steady-State Heat Exchanger Model

A heat exchanger computer program was formulated to analyze and simulate the performance of a heat exchanger operating under steady-state conditions. This program is equipped to analyze parallel, counterflow and cross flow types of heat exchangers; and has provisions for simulating vaporization of the cold side fluid. The heat exchanger geometry is assumed to consist of two concentric tubes for the parallel and counterflow simulations.

At the present time the thermodynamic properties of oxygen, hydrogen and their gas generator combustion products at a mixture ratio of 1.0 are included in the program. It is assumed that the gas generator combustion products will flow through the hot gas side of the exchanger and the cold side will contain flow of either cryogen. When this model is used as part of the ACPS model, the thermodynamic condition of the hot gas side of the heat exchanger will be determined from the inlet model interface. If the gas combustor is close coupled to the heat exchanger, the mixture ratio and combustor products data will be determined in the combustor model and interfaced into this model. If no feed back is necessary and a long length of line is connected at the hot-gas-side inlet to the exchanger, the model is formulated to use gas generator combustor products data at a mixture ratio of 1.0. If a detailed gas generator is connected to the heat exchanger the mixture ratio of the gas generator will be utilized. The chamber pressure, specific heat, nozzle flowrate and combustion temperature are fed into the heat exchanger from the gas generator. At present the heat exchanger cannot be connected to the turbopump assembly effluent. Program modification will have to be performed in order to model systems having turbine/heat exchanger series connections.

Although the correlations defining the heat transfer film coefficients were specifically identified for oxygen and hydrogen heat exchangers, the temperature correction (T_w/T_b) in the equations below can be set to unity. This reduces the correlations to the Dittus Boelter or Colburn form which can be used at moderate temperatures and pressures for all gases and liquids excepting liquid metals ($P_r < .1$).

The heat exchanger discharge conditions are computed from the condition of the inlet fluid streams. The outlet conditions for parallel flow types of heat exchangers are computed directly from the inlet conditions. For counter-flow heat exchangers the discharge conditions are computed utilizing the method of false positions. This method is explained in Section 3.4.18.

The following basic equations are used in the steady-state heat exchanger model and are listed in the order they appear in the model. The nomenclature is defined at the end of the section.

Reynolds number

$$N_{Re_{o,i}} = \frac{2\,\dot{W}_{o,i}}{\pi\, R_o\, \mu} \tag{1}$$

Hydraulic diameter, inches

$$H_{Dy} = \frac{4(\text{Flow Area})}{(\text{Wetted Perimeter})} \tag{2}$$

Various tests are performed to determine if the fluid has entered the two phase region. ($T \leq Tsat$). The calculation of the quality of the fluid is based on its enthalpy.

Quality:

$$X_{i,o} = \frac{h_{i,o} - h_L}{h_L - h_G} \tag{3}$$

If the fluid is in the two phase region, the thermal conductivity, viscosity and the Prandtl numbers are evaluated at the saturated gas condition. The Martinelli parameter, specific volumes, and specific heats are calculated as follows:

$$MART = \left(\frac{X}{1-X}\right)^{-0.9} \left(\frac{\mu G}{\mu L}\right)^{-0.1} \frac{SV_G}{SV_L}^{-0.5} \tag{4}$$

$$SV = (X) SV_G + (1-X)\ SV_L \tag{5}$$

$$CP = (X) C_{PG} + (1-X)\ C_{PL} \tag{6}$$

The pressure drop correction term for two phase flow is calculated as follows:

$$P_{co} = \left[1 + MART^{.25} \left(\frac{1-X}{X}\right)^{0.75} \left(\frac{\mu L}{\mu G}\right)^{0.83} \left(\frac{SV_L}{SV_G}\right)^{0.416}\right]^{2.4} \tag{7}$$

The Nusselt number is

$$N_{nu} = f\ (N_{Re},\ N_{pr}) \tag{8}$$

The primary point of engineering interest is the selection of the film coefficient correlations. The correlations used in the program are presented below. The boiling heat transfer correlation is derived from hydrogen tests only. No correlation for boiling heat transfer of oxygen was available. In the absence of a boiling oxygen correlation, the boiling hydrogen correlation was used for oxygen. For this reason the oxygen boiling results should be considered as best estimates.

The correlations used in the program are:

1. Hydrogen and H_2-O_2 combustion products at low mixture ratio (Reference 27)

$$N_{NU} = 0.025\left(N_{Re}\right)^{0.8}\left(N_{PR}\right)^{0.4}\left(\frac{T_W}{T_B}\right)^{-0.55}\left(\phi_1\ \phi_2\ \phi_3\ \phi_4\right) \tag{9}$$

$$\phi_1 = f\ (T_B)$$

$$\phi_2 = 1.0 \qquad N_{Re} < 5 \times 10^5$$

$$= 0.92 \qquad N_{Re} > 5 \times 10^5$$

2. Oxygen (Reference 27)

$$N_{NU} = 0.023\left(N_{Re}\right)^{0.8}\left(N_{Re}\right)^{0.4}\left(\frac{T_W}{T_B}\right)^{-0.34}\left(\phi_1\ \phi_2\ \phi_3\right) \tag{10}$$

$$\phi_1 = 1.0$$

$$\phi_2 = 1.0$$

$$\phi_3 = f\ (T_B, T_W)$$

3. Boiling Heat Transfers (Reference 28)

$$N_{NU} = \frac{0.023\left(N_{Re}\right)^{0.8}\left(N_{Re}\right)^{0.4}}{0.611 + 1.93\ MART} \tag{11}$$

MART = Marinelli Parameter (Refer to Equation (4).

Heat Balance

The heat transfer coefficients are computed as follows:

$$H_{o,i} = N_{NU_{o,i}}\ \frac{K}{D_{hy_{o,i}}} \tag{12}$$

Wall conductivity

$$Hw = \frac{Kw}{th} \tag{13}$$

Equivalent heat transfer coefficient (constant area assumption Ai,= Aw = Ao).

$$H_e = \frac{1}{\frac{1}{Hi} + \frac{1}{Hw} + \frac{1}{Ho}} \tag{14}$$

The energy balance of the heat exchanger assumes that the heat transfer flux is a function of the inside and outside temperature differences only:

$$dQ_T = dQ_j - dQ_o = 0 \tag{15}$$

$$dQ_o = dQ_i \tag{16}$$

Temperature change:

$$T_{o,i_n} = T_{o,i_{(n-1)}} - \frac{(T_o - T_i)\ He\ A}{\dot{W}\ C_{P_{avg}}} \tag{17}$$

If the fluid is two phase, the temperature is equated to the saturated temperature at the respective pressure.

The pressure drop through the heat exchanger is based upon the loss in energy due to momentum change and friction.

The friction factor is given by:

$$f = 0.316/\ (N_{RE})^{0.25} \tag{18}$$

The pressure drop is given by:

$$\Delta P = (\frac{\dot{W}}{A})^2\ \frac{1}{gc}\ [dSV + f\ \overline{SV}\ \frac{dx}{4R_i}] \tag{19}$$

If the fluid is two phase the pressure drop correction term P_{co} is applied to the momentum pressure drop term resulting in:

$$P = (\frac{W}{A})^2\ \frac{1}{gc}\ [P_{co}\ dSV + f\ \overline{SV}\ \frac{dx}{4R_i}] \tag{20}$$

NOMENCLATURE (Section 3.4.15)

SYMBOL	DESCRIPTION	UNITS
A	Cross-sectional flow area	in^2
Cp	Specific heat at constant pressure	BTU/lbm-^oR
$d\dot{Q}$	Heat flux	BTU/sec-in^2
dSV	Change in specific volume	in^3/lbm
dx	Length	in
ε	Estimate of error used as the convergence criteria	-
f	Friction factor	-
g_c	Gravitational constant = 32.174	$\frac{\text{ft-lbm}}{\text{sec}^2\text{-lbf}}$
H	Heat transfer coefficient	BTU/in^2-sec-^oR
He	Equivalent heat transfer coefficient	BTU/in^2-^oR
H_{DY}	Hydraulic diameter	in
h	Enthalpy	BTU/lbm
K	Fluid thermal conductivity	BTU/in-sec-^oR
MART	Martinelli parameter	-
μ	Viscosity	lbm/in-sec
N_{Nu}	Fluid Nusselt Number, $\frac{HD}{K}$	-
N_{pr}	Fluid Prandtl Number, $\frac{Cp\mu}{K}$	-
N_{Re}	Fluid Reynolds Number, $\frac{VD\rho}{\mu}$	-
Pco	Pressure drop correction for two-phase flow	-
P	Fluid pressure	psia
ϕ_1	Correction for two-phase flow boiling	-
ϕ_2	Correction entrance effects	-
ϕ_3	Correction asymetric heating	-
ϕ_4	Correction surface roughness	-

NOMENCLATURE (Section 3.4.15) (Continued)

SYMBOL	DESCRIPTION	UNITS
R	Radius	in
SV	Specific volume	in^3/lbm
$\overline{SV}$	Average specific volume	in^3/lbm
th	Wall thickness	in
T	Temperature	^oR
Π	Pi, constant = 3.1416	-
$\dot{W}$	Flowrate	lbm/sec
X	Fluid quality dependent upon enthalpy ratio of gas to liquid	-
Y	Variable chosen to show regula Falsi Method	-

SUBSCRIPTS

avg	Average
B	Bulk
Δ	Delta or change of
d	Differential operator
G	Gas
i	Inner
L	Liquid
o	Outer
T	Total
w	Wall

3.4.16 Transient Heat Exchanger Model

This program module was formulated to analyze and simulate the transient performance of an ACPS heat exchanger. The model is an extension of the steady-state heat exchanger program discussed in paragraph 3.4.15.

Ideally, the effect of changes in the heat exchanger inlet conditions (pressure, temperature, and flow) upon the outlet conditions can be determined. However, the relative response times for each of these parameters are considerably different, as shown in Table 1, which present problems in modeling these effects. The nomenclature for the symbols shown in Table 3 is presented at the end of this section.

Table 3. Heat Exchanger Response Time Comparison

Step Change in	Relative response time
Pressure	$\theta << \theta_d$ (Reference 29)
Flowrate	$\theta_{\dot{w}} \leq \theta_d$ (Reference 30, 31)
Temperature	$\theta_t >> \theta_d$ (Reference 22)

Most of the investigations to date are limited to solutions for correct temperature response modeling. Typical temperature response values for heat exchangers have been reported to lie between 10 to 1000 dwell times (length of time fluid resides (θ_d) within the heat exchanger (Reference 22)). Treatment of heat exchanger pressure response has not been found in the literature.

The effect of each independent parameter must be determined for a number of boundary and initial conditions to establish the transient performance of heat exchangers. A general solution for the transient operation of a two-fluid heat exchanger is practically impossible, because of the complexity of the differential equations, boundary conditions and the number of independent parameters. Most solutions have been limited to very simple cases and have been solved by one of the following three methods: (1) analytical, (2) numerical, or (3) analog. The analytical methods described in the literature were found to be complex and contained severe limitations. Numerical methods such as a formulation by Northern Research and Engineering Corporation (NREC) (Reference 29) have widespread

application, but require a large amount of computer time and core space and are generally too specific. Analog methods such as the Kays and London Effectiveness (ε) - NTU approach (Reference 32), are desirable because a "physical feel" for the problem is maintained.

Two separate computer models utilizing the numerical and analog methods were initiated to simulate the transient operation of an ACPS model heat exchanger. The two models used are the NREC and London methods mentioned above. The existing NREC program (N70-10069) is operational at NASA/MSC and simulates both one and two phase flow and is capable of simulating the effects of fluid condensation on one side of the heat exchanger. However, the ACPS model must be capable of simulating evaporation rather than condensation. Therefore, an effort was initiated to correct this program for simulating evaporation. The NREC program excludes the pressure response, but includes the flow and temperature response parameters. The program uses an iterative finite difference scheme to solve the differential equations. Unfortunately completion of the modifications required to convert this program to simulate evaporation was deemed too extensive for the time allowed.

Although the most common technique for solving an exchanger heat balance is the log-mean-delta-T (ΔT_{lm}) method, it requires numerous iterations to obtain a solution (Reference 32). The analog type of solution (ε-NTU) based upon the work of A. L. London and others (References 30-32) allows solution of the heat balance without iteration. Consequently, the London model was employed in the development of the transient heat exchanger program. The London model parameters are shown schematically in Figure 16 Nomenclature is presented at the end of this section.

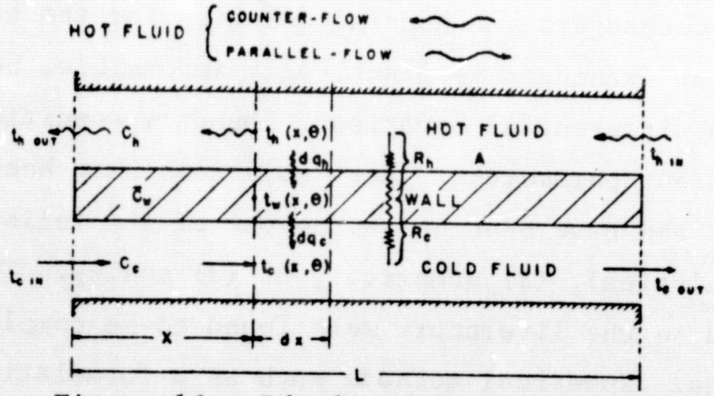

Figure 16 Idealized Heat Exchanger

The heat transfer rate with the London method is identified by its effectiveness level (ε) as follows:

$$\varepsilon = \frac{\dot{q}\ \text{actual}}{\dot{q}\ \text{max}} \tag{1}$$

$$\text{where:}\quad \dot{q}\ \text{actual} = (\dot{w}\ Cp)_f\ (t_{in}-t_{out})_f \tag{2}$$

$$\dot{q}\ \text{max} = (\dot{w}\ Cp)_{min}\ (t_{in_{hot}} - t_{in_{cold}}) \tag{3}$$

The smallest capacitance ($C = \dot{w}\ Cp$) value for each of the two fluid streams is defined as $(\dot{w}\ Cp)_{min}$ or C_{min}. With this method, the emphasis is placed upon the determination of the effectiveness (ε) to determine the heat exchanger duty (identified above as $\dot{q}$ actual). The ε-NTU relationship for heat exchangers operating under steady-state conditions is depicted in Figure 17.

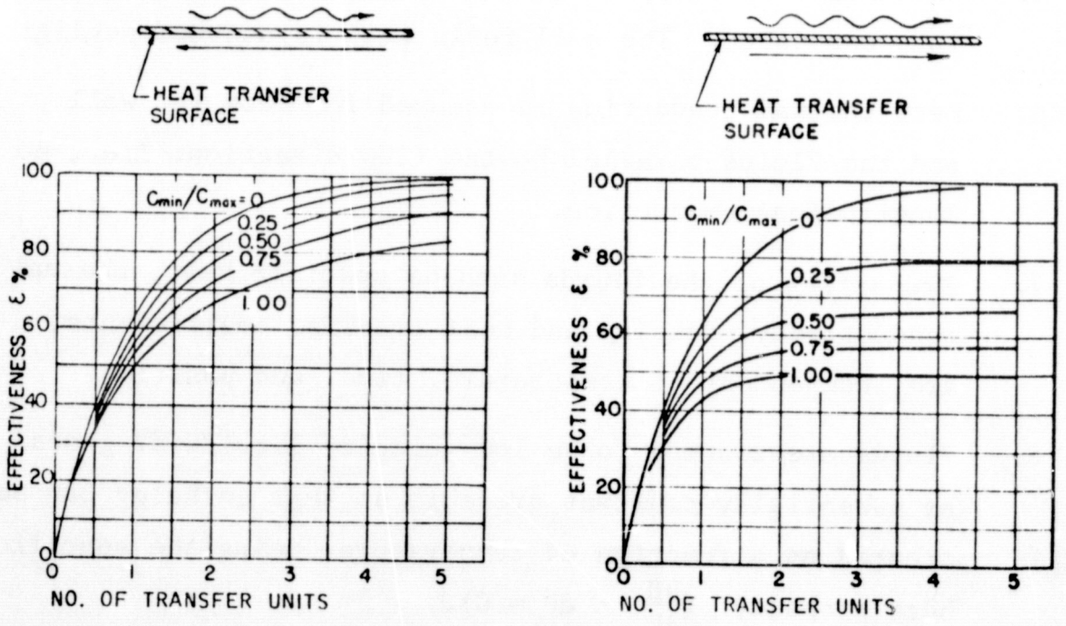

Figure 17. ε-NTU Effect for Counterflow and Parallel Flow Heat Exchange

The number of Transfer Units (NTU) is defined as:

$$NTU = \frac{(UA)}{C_{min}} \tag{4}$$

and represents a characteristic conductance to capacitance ratio for heat exchanger design.

Because the analysis of the transient response of heat exchangers is not amenable to simple mathematical treatment, the following simplifying assumptions are necessary to achieve the solutions described in this model development.

1. The temperature (t) of each of the fluids and the wall are functions of time (θ) and distance (x) only; $t - t(x,\theta)$.
2. The mass-flow rates ($\dot{w}_c$ and $\dot{w}_h$) are constant within the exchanger.
3. The system is overall adiabatic.
4. No internal source for thermal-energy generation exists, such as nuclear fission, chemical reaction, or electrical heating.
5. The heat-transfer resistance for each fluid is lumped into one value. The wall resistance is assumed negligible.
6. Zero thermal conduction is assumed for both the wall and the fluids parallel to the flow direction; i.e., no longitudinal conduction.
7. Properties of the fluids such as specific heat, thermal conductivity, density and heat-transfer coefficients, are independent of temperature, time, and position.
8. Fluids are assumed to be low-velocity liquids or gases at essentially constant pressure so that enthalpy can be treated as a function of temperature, using the specific heat property $(\frac{\partial H}{\partial P} \cdot dP = 0)$.
9. The thermal capacity of the shell of the exchanger is considered negligible relative to that of the heat-transfer surface.
10. Pressure changes and viscous dissipation terms in the energy equation are negligible.
11. No shaft work is done ($W = 0$).

Assumptions 1, 3, 4, 5, 9, and 11 appear to be justified. However, the remaining assumptions require additional comment about their effects upon

model accuracy. Assumption 2 requires that once a fluid has entered the exchanger inlet it does not change flowrate. Under transient operating conditions, this assumption might result in a severe restriction for heat exchangers in which two-phase flow occurs. If the ACPS exchangers are made of aluminum or copper materials, significant longitudinal heat transfer will be present and Assumption 6 will then represent a relatively large error in the predicted value of heat transfer flux. However, this can be adequately handled as an ε loss at the end of each computation step. Assumption 7 has been relaxed in the London method computer model. An average of the thermal properties (Cp, k, μ, h) from the 20 segmental steady-state program results is used in this program. Assumption 8 was verified by examining the fluid conditions for an ACPS exchanger. The results of examining the fluid thermal properties, showed that enthalpy can be approximately expressed as follows:

$$\text{for } H = H(P,T) \tag{5}$$

$$dH = \left(\frac{\partial H}{\partial T}\right)_P dT + \left(\frac{\partial H}{\partial P}\right)_T dP \tag{6}$$

$$dH_{H_2} \tilde{=} (5 \pm 2)\, dT - (.03 \pm .03) dP \tag{7}$$

$$dH_{O_2} \tilde{=} (.7 \pm .2)\, dT - (.02 \pm .02)\, dP \tag{8}$$

From Equations (7) and (8) it can be concluded that the pressure term is negligible; i.e., 160 psia change represents a 1°F change. Assumption 10, although hard to justify is necessary to solve the differential equations. It is not known at this time what the effect of deleting these terms will have upon the final solutions. With these limiting assumptions, however, the energy equation takes the form of:

$$\frac{\partial q}{\partial x} = \dot{w}\, Cp\, \frac{\partial t}{\partial x} + \rho A\, Cp\, \frac{\partial t}{\partial \theta} \tag{9}$$

Expressed in the ε-NTU nomenclature.

$$\text{Variable Capacitance, } C = \dot{w}\, Cp \tag{10}$$

$$\text{Fixed Capacitance, } \overline{C} = \rho AL\, Cp \tag{11}$$

$$\text{Heat transfer resistances, } R = \frac{1}{(hA)_f} \text{ fluid case} \tag{12}$$

$$R = \frac{Tw}{kA} \quad \text{wall case} \tag{13}$$

Expanding Equation (9) for the fluids and the wall heat exchange, results in the following.

$$\frac{t_h - t_w}{R_h L} = -\frac{\bar{C}_h}{L}\frac{\partial t_h}{\partial \theta} \pm C_h \frac{\partial t_h}{\partial x} \tag{14}$$

$$\frac{t_w - t_c}{R_c L} = \frac{\bar{C}_c}{L}\frac{\partial t_c}{\partial \theta} + C_c \frac{\partial t_c}{\partial x} \tag{15}$$

$$\frac{t_h - t_w}{R_h} - \frac{t_w - t_c}{R_c} = \bar{C}_w \frac{\partial t_w}{\partial \theta} \tag{16}$$

Note that Equation (14) uses a (-) for parallel hot gas flow and a (+) for counter flow of the hot gas streams.

A set of non-dimensionalized parameters introduced to simplify the program solution are shown in Table 4.

Table 4. Non-Dimensionalized Parameters, ε-NTU Approach

Dependent Parameters	Independent Operating And Design Parameters	
t_h^*	NTU	(Steady State)
t_w^*	Cmin/Cmax	(Steady State)
t_c^*	x *	(Steady State)
ε_c^*	θ *	(Transient)
ε_h^*	θ_d^*	(Transient)
	R *	(Transient)
	$\bar{C}_w^*$	(Transient)

See the Nomenclature at the end of this section for a description of these parameters. Rewriting the energy Equations (14), (15), and (16) in non-dimensionalized form, results in the following:

$$t_h^* - t_w^* = \frac{\left(\frac{-1}{\theta_d}\right)\frac{\partial t_h^*}{\partial \theta^*} + \frac{\partial t_h^*}{\partial \theta^*}}{(R^*+1)(NTU)\ (Cmin/Cmax)} \tag{17}$$

$$t_w^* - t_c^* = \frac{\left(\frac{R^*}{R^*+1}\right)\left(\frac{\partial t_c^*}{\partial \theta^*} + \frac{\partial t_c^*}{\partial x^*}\right)}{NTU} \tag{18}$$

$$R^*\ (t_h^* - t_w^*) - (t_w^* - t_c^*) = \left(\frac{R^*}{R^*+1}\right)\left(\frac{\bar{C}_w^*}{NTU}\right)\left(\frac{\partial t_w^*}{\partial \theta^*}\right) \tag{19}$$

To simplify the problem further only two conditions of flow have been considered for this model.

Case 1. A gas/gas heat exchanger where Cmin/Cmax $\geq$ .8 is modeled with a Cmin/Cmax = 1.0.

Case 2. For a cryogenic ACPS type of heat exchanger, Cmin/Cmax $\leq$ .2, so a Cmin/Cmax = 0. is used in the model.

These two cases result in solutions to the energy equations shown in Figures (18) and (19) (Reference 32).

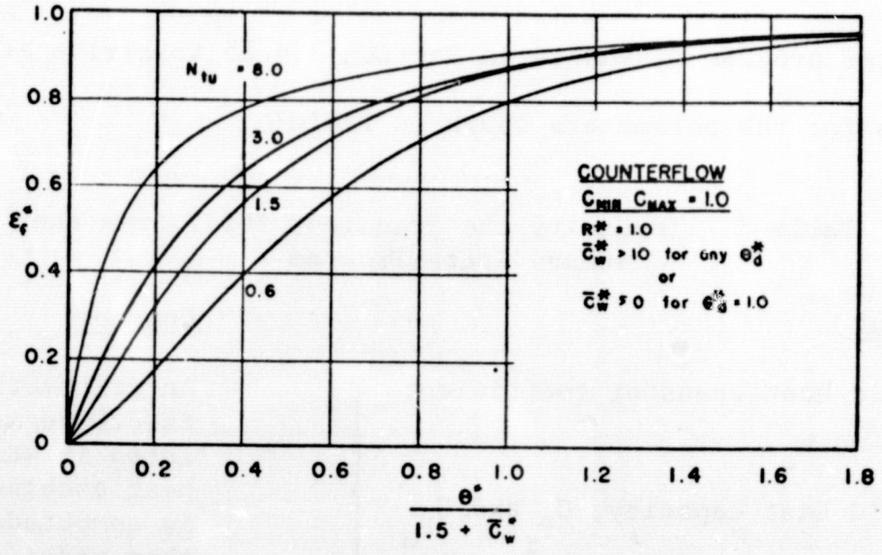

Figure 18. Gas/gas heat exchange
Cmin/Cmax $\geq$ .8

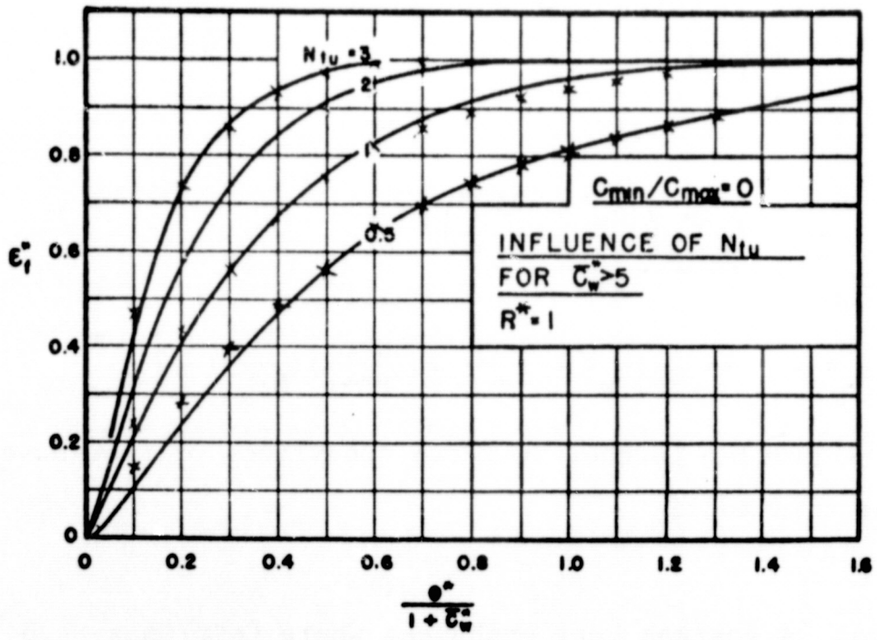

Figure 19. ACPS Type Cryogenic Exchanger
Cmin/Cmax $\leq$ .2

An additional constraint of $\bar{C}_w^* > 10$ or 5 is shown in Figures (18) and (19). This constraint is justified by existing designs with $\bar{C}_w^* \approx 1000$.

The transient program has been structured to use the steady state heat exchanger program discussed in Section 3.4.15 to arrive at the steady state values for the parameters shown in Table 5.

Table 5. Inputs to the Transient Model from the Steady State Program

Parameter	Comment
1. Fluid heat transfer coefficients h_i and h_o	An arithmetic average of the 20 segments calculated in steady state heat exchanger model is computed and used in this model.
2. Fluid heat capacity, C_{P_i} and C_{P_o}	
3. Fluid specific Volume, $\overline{V}_i$ and $\overline{V}_o$	
4. Heat Transfer Areas (Inside/Outside)	Direct data transfer
5. Heat Exchanger Volumes (Inside, Outside, Wall)	Direct data transfer

The calculations are performed within the program in the order they appear below.

1. Calculations of the fluid capacitances:

$$C_c = \dot{w}_c \; C_{p_c} \tag{20}$$

$$C_h = \dot{w}_h \; C_{p_h} \tag{21}$$

test to identify Cmin and Cmax.

calculate Cmin/Cmax.

2. Calculations of the overall heat transfer conductance (UA) wall conductance assumed negligible - Assumption 5:

$$(UA) = \frac{1}{\frac{1}{h_c A_c} + \frac{1}{h_h A_h}} \tag{22}$$

3. Calculations of the Number Transfer Units (NTU):

$$NTU = \frac{(UA)}{Cmin} \tag{4}$$

4. Calculations of the length of time for fluid residence within the heat exchanger [(dwell time) (θ_d)]

$$\theta_{dh} = \frac{V_h \rho_h}{C_h} \tag{23}$$

$$\theta_{dc} = \frac{V_c \rho_c}{C_c} \tag{24}$$

Ratio of the dwell times for the fluids in the same relationship as used to calculate Cmin/Cmax.

For ACPS heat exchanger $C_h = C_{min}$.

So.

$$\theta_d \text{ Ratio} = \frac{\theta_{dh}}{\theta_{dc}} \tag{25}$$

$$\theta_{dmin} = \theta_{dh} \tag{26}$$

$$\theta_{dmax} = \theta_{dc} \tag{27}$$

5. Calculation of the heat transfer resistance ratio (R*):

$$R^* = \frac{Rmin}{Rmax} \tag{28}$$

$$\text{For ACPS case } R^* = \frac{\left(\frac{(1)}{hA}\right)_h}{\left(\frac{1}{hA}\right)_c} \tag{29}$$

$$\text{or } R^* = \frac{(hA)c}{(hA)h} \tag{30}$$

6. Calculate the dimensionless time (θ^*)

$$\theta^* = \frac{\theta}{\theta_{dmin}} \tag{31}$$

7. Calculate the wall-to-fluid capacity ratio ($\overline{C}_w^*$)

$$\overline{C}_w^* = \frac{\overline{C}_w}{\overline{C}_{min}} \tag{32}$$

$$= \frac{\overline{C}_w}{(Cmin)(\theta_{dmin})} \tag{33}$$

8. Calculate the time argument parameter (ϕ).

$$\phi = \frac{\theta^*}{1+C_w^*} \tag{34}$$

9. Calculate the transient heat exchanger effectiveness (ε_f^*)

Curve fits to Figure 19 as follows:

$$\text{NTU} = .5, \quad \varepsilon_f^* = 1-e^{-1.70\phi} \tag{35}$$

$$\text{NTU} = 1.0, \quad \varepsilon_f^* = 1-e^{-2.80\phi} \tag{36}$$

$$\text{NTU} = 2.0, \quad \varepsilon_f^* = 1-e^{-4.50\phi} \tag{37}$$

$$\text{NTU} = 3.0, \quad \varepsilon_f^* = 1-e^{-6.60\phi} \tag{38}$$

If NTU $\leq$ .5, ε_f^* for NTU = .5 is used

If NTU $\geq$ 3.0, ε_f for NTU = 3.0 is used

10. Calculate the steady state heat exchanger effectiveness (ε_{ss})

For crossflow and counterflow:

$$\varepsilon_{ss} = \frac{1.0-e^{-NTU\ (1-\frac{Cmin}{Cmax})}}{1-\frac{Cmin}{Cmax}\ e^{-NTU\ (1-\frac{Cmin}{Cmax})}} \tag{39}$$

For parallel flow:

$$\varepsilon_{ss} = \frac{1 - e^{-NTU \quad (1+\frac{Cmin}{Cmax})}}{1 + Cmin/Cmax} \tag{40}$$

11. Calculate the heat transfer for this transient condition (q(t)):

$$\varepsilon(t) = \varepsilon_f^*(o) + \varepsilon_f^* \ (\varepsilon_{ss} - \varepsilon_f^*(t) \tag{41}$$

$$\dot{q}(t) = \varepsilon(t) \quad \varepsilon_{ss} \ C_{min} \ (T_{h_{in}} - T_{c_{in}}) \tag{42}$$

12. Calculate exit stream temperatures

$$t_{hout} = t_{h_{in}} - \frac{\dot{q}(t)}{C_h} \tag{43}$$

$$t_{cout} = t_{c_{in}} + \frac{\dot{q}(t)}{C_c} \tag{44}$$

This completes the main data calculation block. At this point all of the data for this transient time step is printed and the data for the next transient time is fed in.

NOMENCLATURE (Section 3.4.16)

SYMBOL	DESCRIPTION	UNITS
A	Heat-transfer area	in^2
C	Fluid capacity rate, mass flow rate times specific heat	BTU/sec-^oF
$\overline{C}$	Fixed capacity	BTU/^oF
C_p	Fluid heat capacity	BTU/lbm-^oF
$\overline{C}_w$*	Wall capacity relative to fluid capacity, Equation (32)	-
ξ, ε	Heat-transfer effectiveness, dimensionless	-
h	Heat transfer film coefficient	$\frac{BTU/sec}{in^2-^oF}$
k	Wall thermal conductivity	$\frac{BTU/sec}{in-^oF}$
L	Total flow length	ft
NTU	Number of transfer units, dimensionless = A/C_{min} or Equation (4)	-
ϕ	Denotes a functional relation	-
$\dot{q}$	Heat transfer rate	BTU/sec
ρ	Density	lbm/in^3
R	Total heat-transfer resistance	$\frac{sec-^oF}{BTU}$
R*	Defined Equation (28)	-
t	Temperature	^oF
T_w	Wall thickness	in
θ	Time	sec
θ_d	Dwell time = (C/C) = (L/V)	sec
θ_P	Pressure response time	sec
θ_t	Temperature response time	sec

NOMENCLATURE (Section 3.4.16) (Continued)

SYMBOL	DESCRIPTION	UNITS
θ_w	Fluid flowrate response time	sec
θ^*	Time relative to dwell time, Equation (31)	-
θ_d^*	Dwell-time ratio	-
t_h^*, t_c^*	Relative temperature differences	-
U	Overall unit heat-transfer conductance	$\frac{BTU/sec}{in^2-{}^oF}$
V	Flow velocity	ft/sec
x	Flow-length variable	ft

SUBSCRIPTS

c	Cold fluid or cold fluid side
d	Dwell time of fluid
f	Fluid, either hot or cold
h	Hot fluid or hot fluid side
in	Inlet section
max	Maximum capacity rate or associated with C_{max}
min	Minimum capacity rate or associated with C_{min}
out	Outlet section
ss	Steady state
w	Wall

3.4.17 Steady-State Modeling - Gas Generator (high & low pressure)

The gas generator (GG) is essentially a combustor model operating at a mixture ratio different from that of the main combustors. The model uses the same basic fluid flow equations as the combustor model with additional calculations to determine the thermodynamic conditions at the gas generator exits (duct entrance) (Reference Section 3.4.2, Steady-State Combustor for Modeling and Basic Input/Output). The combustion equations are based on curve fits of data calculated with the ICRPG program (References 12-16). The gas generator exhaust gas may be ducted to a turbine or to a heat exchanger.

The approach used for modeling the GG is described by the following equations. The nomenclature for these equations is found at the end of this section.

The flowrate through oxidizer/fuel injectors is implemented as a constraint equation and is given by:

$$\text{Constraint} = \dot{W}_{o,f} - P_c C_d A_{inj} \sqrt{\frac{g_c}{RT}\left(\frac{2\gamma}{\gamma-1}\right)\left(\left(\frac{P_c}{P_{o,f}}\right) - \left(\frac{P_c}{P_{o,f}}\right)^{\frac{\gamma+1}{\gamma}}\right)}$$

The characteristic exhaust velocity temperature, specific impulse, combustion temperature, gas generator, specific heat, and molecular weight are calculated from the following curve fits:

$$C^* = f(MR) \quad (1)$$

$$T_c = f(MR) \quad (2)$$

$$ISP = f(MR) \quad (3)$$

$$T_{GG} = f(MR) \quad (4)$$

$$C_p = f(MR) \quad (5)$$

$$MW = f(MR) \quad (6)$$

The duct pressure

$$P_x = P_{GG} - \frac{K \dot{W}^2}{P_{GG}} T_{GG} \cdot R \tag{7}$$

The duct temperature

$$T_x = T_{GG} \tag{8}$$

NOMENCLATURE (Section 3.4.17)

SYMBOL	DESCRIPTION	UNITS
A_{inj}	Area injector	in^2
CD	Discharge coefficient through injector	-
C_F	Thrust coefficient	-
C*	Characteristic exhaust velocity	ft/sec
C_p	Specific heat constant pressure	BTU/^oR-lbm
γ	Specific heat ratio	-
gc	Conversion constant	32.2 $\frac{lbm\text{-}ft}{sec^2\text{-}lbf}$
ISP	Specific impulse	lbf/sec/lbm
K	Duct pressure loss coefficient	$\frac{psia\text{-}sec^2}{lbm\text{-}ft^2}$
MR	Mixture ratio	-
MW	Molecular weight	-
P	Pressure	psia
R	Gas constant	$\frac{lbm}{lb\text{-}mole}$
T	Temperature	^oR
$\dot{W}$	Flowrate	lbm/sec

SUBSCRIPTS

x	Duct
GG	Gas generator
c	Combustion
o	Oxidizer
f	Fuel

3.4.18 Feedback Constraint Steady State

The feedback constraint subroutine was formulated in order to obtain feedback connections between downstream components and upstream components. The subroutine calculates constraint equations for flowrate, pressure and temperature. These constraint equations are minimized using a nonlinear equation solver to obtain the desired feedback parameters.

The flowrate constraints are calculated as follows:

$$\text{Constraint}_1 = 1 - \frac{\dot{W}}{WFB}$$

$$\text{Constraint}_2 = 1 - \frac{P}{PFB}$$

$$\text{Constraint}_3 = 1 - \frac{T}{TFB}$$

NOMENCLATURE (Section 3.4.18)

Variables	Description	Units
T	temperature	°R
P	pressure	psia
$\dot{W}$	flowrate	Lbm/sec
TFB	temperature state variable	°R
PFB	pressure state variable	psia
WFB	flowrate state variable	Lbm/sec

3.4.19 Solution of a System of Implicit Equations

In the steady-state analysis program, it is necessary to have a subroutine or set of subroutines that computes a solution to the system of equations $F(X) = 0$. These routines must be accurate, reliable, and easy to use. They must require a minimum of care and execution time as they are used extensively. During the listerature search, a set of subroutines were discovered which meet these specifications.

BEGS is a subroutine that, given N functions $F = (f_1, \ldots, f_N)$ in M variables $X = (x_1, \ldots, x_M)$, computes X such that $||F(X)||^2 = \sum_{i=1}^{n} f_1^2(X)$ is a minimum. If M = N, it seeks the solution of the system of equations $F(X) = 0$ using the Newton Method. BEGS requires two auxiliary subroutines. One routine must be provided to compute F(X) for a given value of X. The other is subroutine LEGS. LEGS is used to solve an overdetermined linear system of equations AX = B using the least squares method, i.e., to solve the normal equations $A^TAX = A^TB$. These routines have proven to be accurate and reliable and have been used successfully in several programs at both TRW/Houston and TRW/Redondo Beach.

In the heat exchange model only one implicit equation is solved, therefore, the regula falsi method (method of false positions) was used. The regula falsi method is a numerical linear method of finding the roots of an equation by determining the point at which the secant of the curve crosses the Y axis. The two points Y1, f(Y1) and Y2, f(Y2) are used to determine the intersection of the secant to the curve with the Y axis. From similar traingles $\frac{f(Y1)}{Y3-Y1} = \frac{f(Y2)}{Y3-Y2}$, and solving for Y3 we obtain the interpolation equation

$$Y3 = \frac{Y2\ (fY1) - Y1\ (fY2)}{f\ (Y1) - f\ (Y2)}$$

The method has linear convergence as shown in Figure 20.

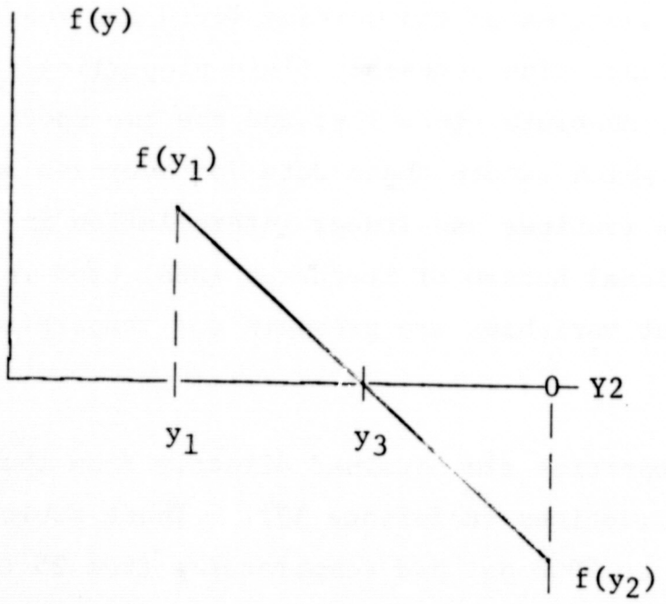

FIGURE 20. REGULA FALSI METHOD

3.4.20 Integration Subroutine

The transient analysis program requires an integration subroutine for the combustor model. Through the use of the TRW/TSS terminal system, a library integration subroutine was located. The subroutine is capable of solving a set of N simultaneous, first order, ordinary differential equations of the form:

$$y_i' = f_i(X, Y_1, Y_2, \ldots, Y_n),\ i = 1, \ldots, n$$

using a classical fourth-order Runge-Kutta method.

3.4.21 Thermodynamic Property Subroutines

Thermodynamic properties of the working fluid are required in many of the program calculations. The necessary fluid properties include density, thermal conductivity, absolute viscosity, and the two specific heats: C_v and C_p. Subroutines which return these data for hydrogen and oxygen have been included. These routines use linear interpolation in data tables generated by the National Bureau of Standards (NBS) from real fluid property data. The independent variables are pressure and temperature.

Hydrogen

All hydrogen properties are obtained directly from the accepted NBS hydrogen property subroutines (Reference 35). These subroutines apply for pressures from 1 to 5000 psi and temperatures from 25 to 5000°R as shown in Figure 21.

Oxygen

Oxygen properties are obtained from previously existing subroutines which employ property data from References 36 and 37. The data tables in the original subroutines were extended to increase the pressure range. The data presently covers the pressure range from 14.7 to 1249 psi and the temperature range from 144 to 540°R as shown in Figure 22. Since the pressure and temperature range is more restrictive for oxygen than for hydrogen, the oxygen subroutine was further modified to use the closest available data in the event the pressure or temperature fall outside the permissible range. However, the out-of-range density value is computed from the perfect gas equation if the pressure is out of range-low or if the temperature is out of range-high. Diagnostics are printed whenever the input pressure or temperature is out of range.

Two-Phase Fluid Properties

For the operation of the steady-state heat exchanger model with boiling fluid, properties are required at saturated liquid and saturated vapor conditions. Subroutines to compute the following two-phase boundary properties are supplied for both hydrogen and oxygen fluids.

Linear interpolation is used within special data tables to compute the saturation temperature and the enthalpies, densities, and, for oxygen,

the specific heat at the saturated liquid and saturated gas conditions. The thermal conductivity, viscosity, and specific heat of hydrogen are obtained by calls to the general cryogenic property routines. The fluid pressure and the corresponding saturation temperature plus or minus 0.5 degree are the independent variables used to produce values at saturated vapor and saturated liquid condition, respectively.

FIGURE 21. HYDROGEN PROPERTY DATA RANGE

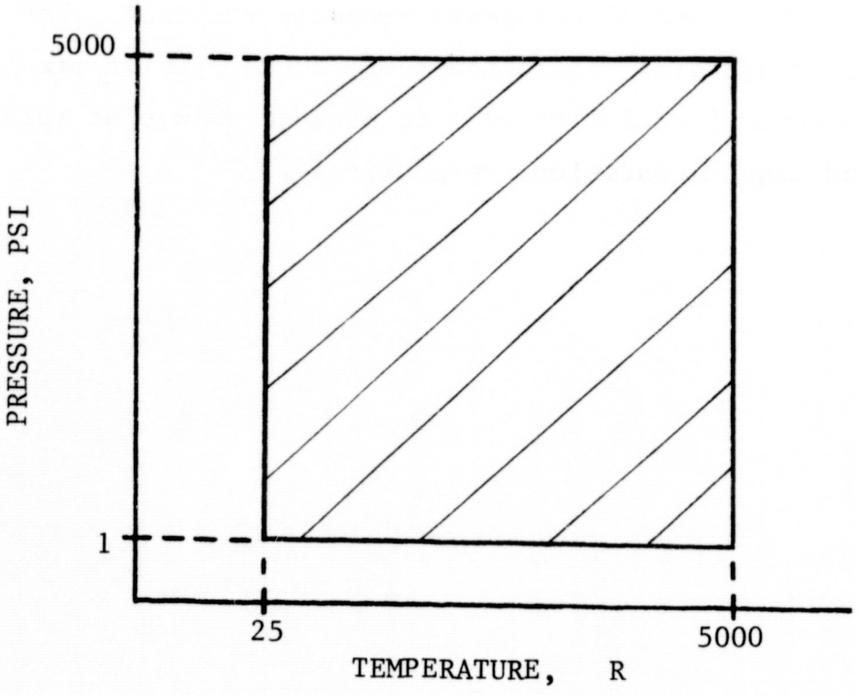

FIGURE 22. OXYGEN PROPERTY DATA RANGE

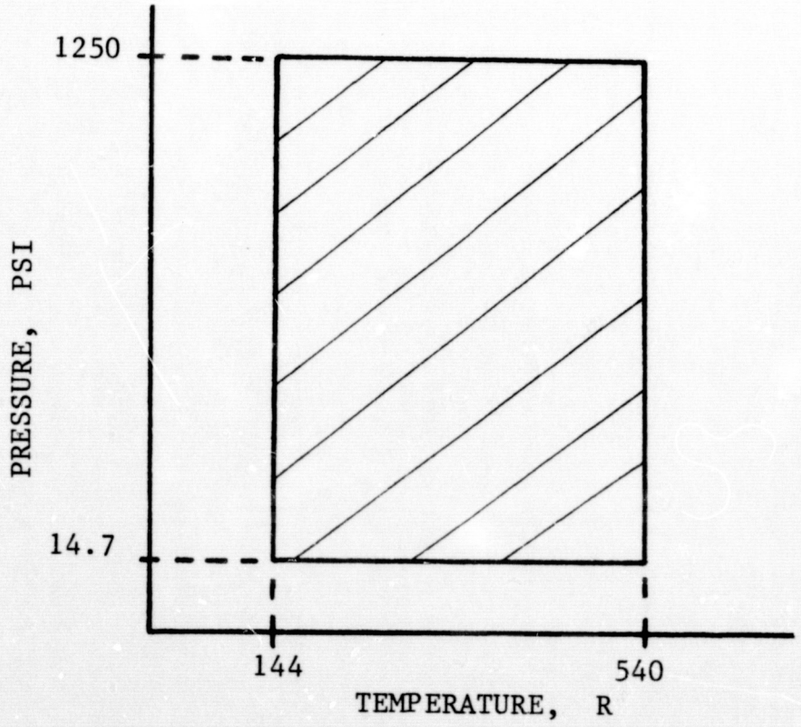

4.0 ACPS SYSTEM SIMULATION RESULTS CASES

The ACPS computer modeling was formulated as presented in Sections 3.4.1 through 3.4.19. Each module was checked out separately and then incorporated into the appropriate computer program. An overall system was set up to demonstrate both programs' capabilities. This section presents the demonstration case which exercises all of the respective component modules in both programs. Additional results of the transient program line and combustor models are presented.

The demonstration case system configuration is shown in Figure 23. The system was set up to exercise the hydrogen side of the system and to simulate the oxygen side as constant pressure boundaries. The system consists of hydrogen from a storage tank feeding a gas generator driven turbopump which increases the pressure to 1060 psia. The liquid is then fed through a heat exchanger (hot side heated by a gas generator) and vaporized which results in a final temperature of 500°R. The gas is then fed back through pressure regulators to both of the gas generators and also to the in-line H_2 accumulator. Downstream of the accumulators, the H_2 is fed to three bipropellant combustors. The steady-state flowrates, dimensions and temperatures are presented in Figure 23. The combustor thermochemical and performance data are presented in Figures 24 and 25. The pump head and power curves are shown in Figure 26. .The turbine efficiency curve for the hydrogen turbopump is shown in Figure 27.

To check the transient model, the flow rates and pressures at points in a 50-foot horizontal, frictionless steel pipe were calculated after the sudden closure of a valve (see Figure 28). Before the valve closure, the fluid which was water was flowing steadily. The calculations were repeated for differing time intervals and stability criteria. Equation (27) in Section 3.4.2 is the stability criterion. The plot of pressure

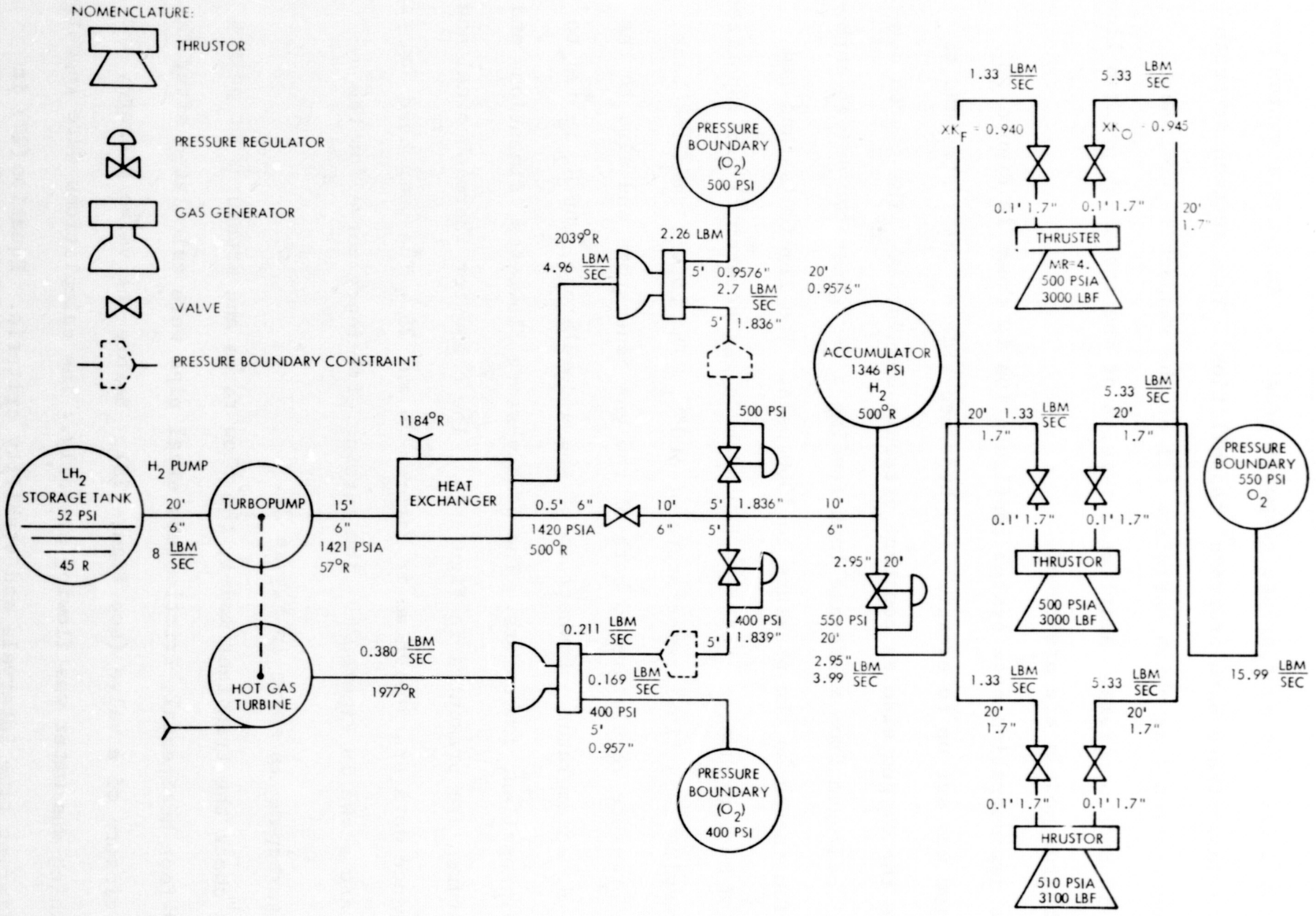

FIGURE 23. ACPS STEADY-STATE DEMONSTRATION SCHEMATIC

FIGURE 24

COMBUSTION CHAMBER GAS PROPERTIES AND PERFORMANCE FOR OXYGEN-HYDROGEN (ISP, TC, CP)

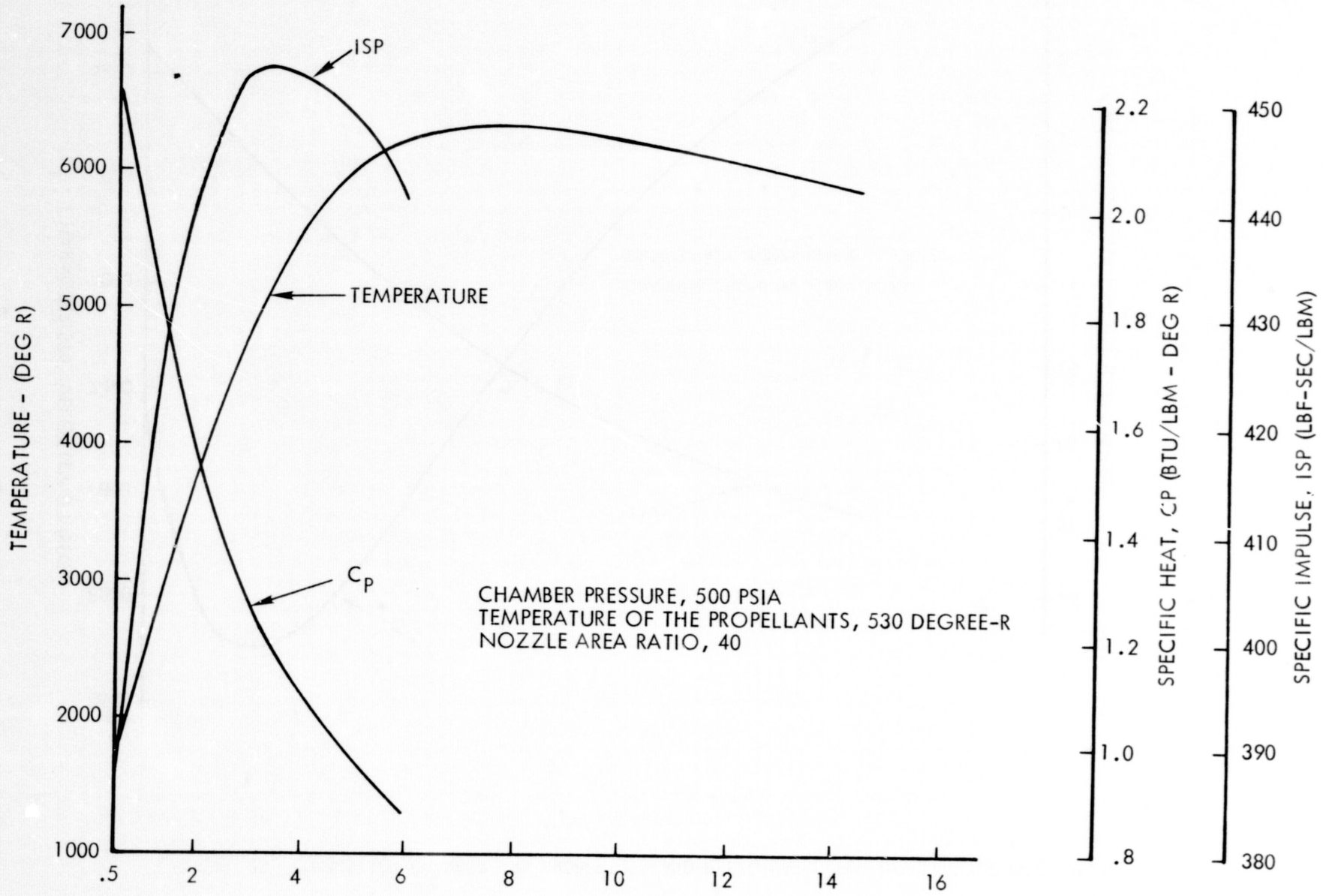

FIGURE 25 COMBUSTION CHAMBER GAS PROPERTIES AND PERFORMANCE FOR OXYGEN-HYDROGEN (C*,MW)

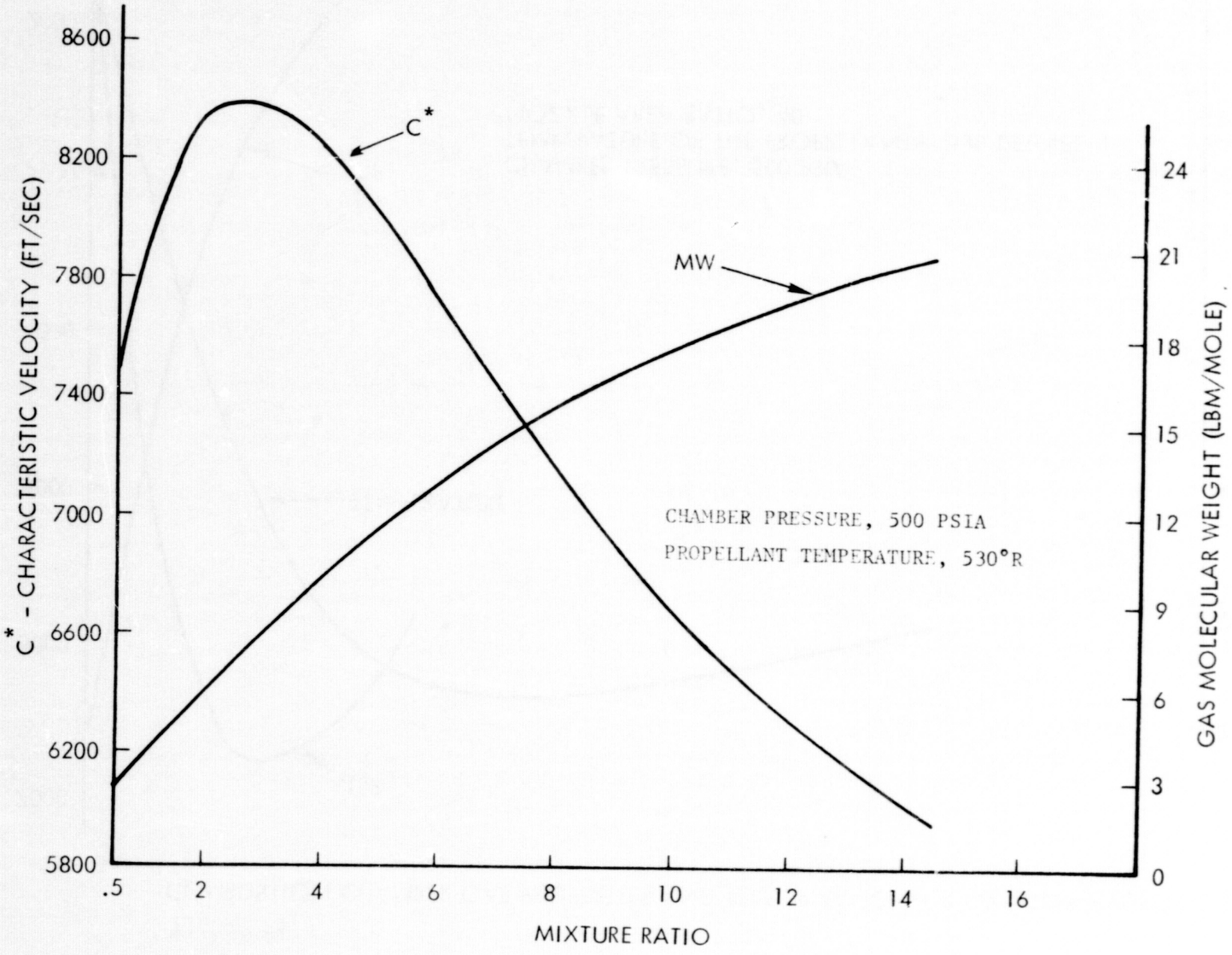

HYDROGEN PUMP CHARACTERISTICS, 50,000 RPM

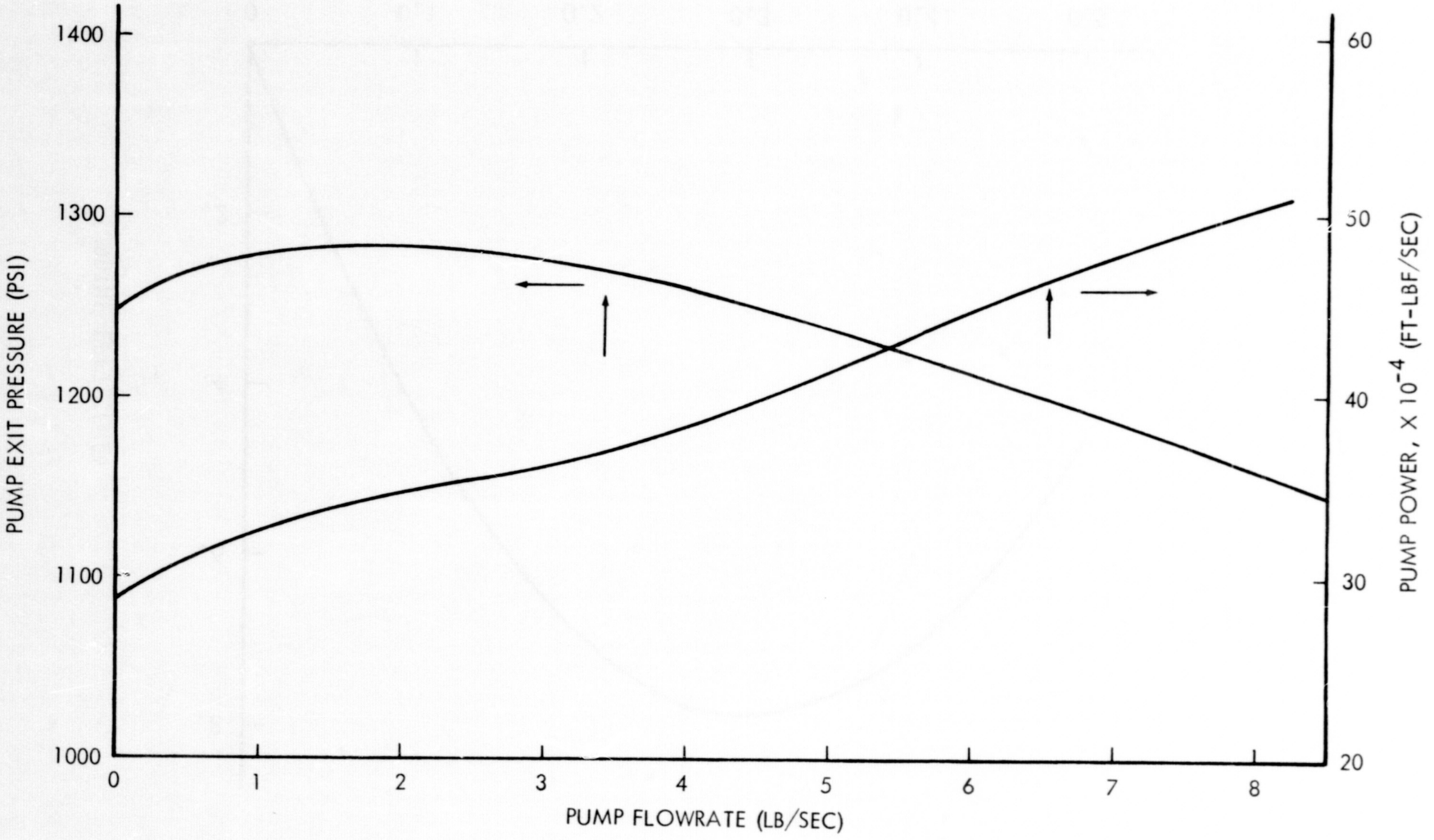

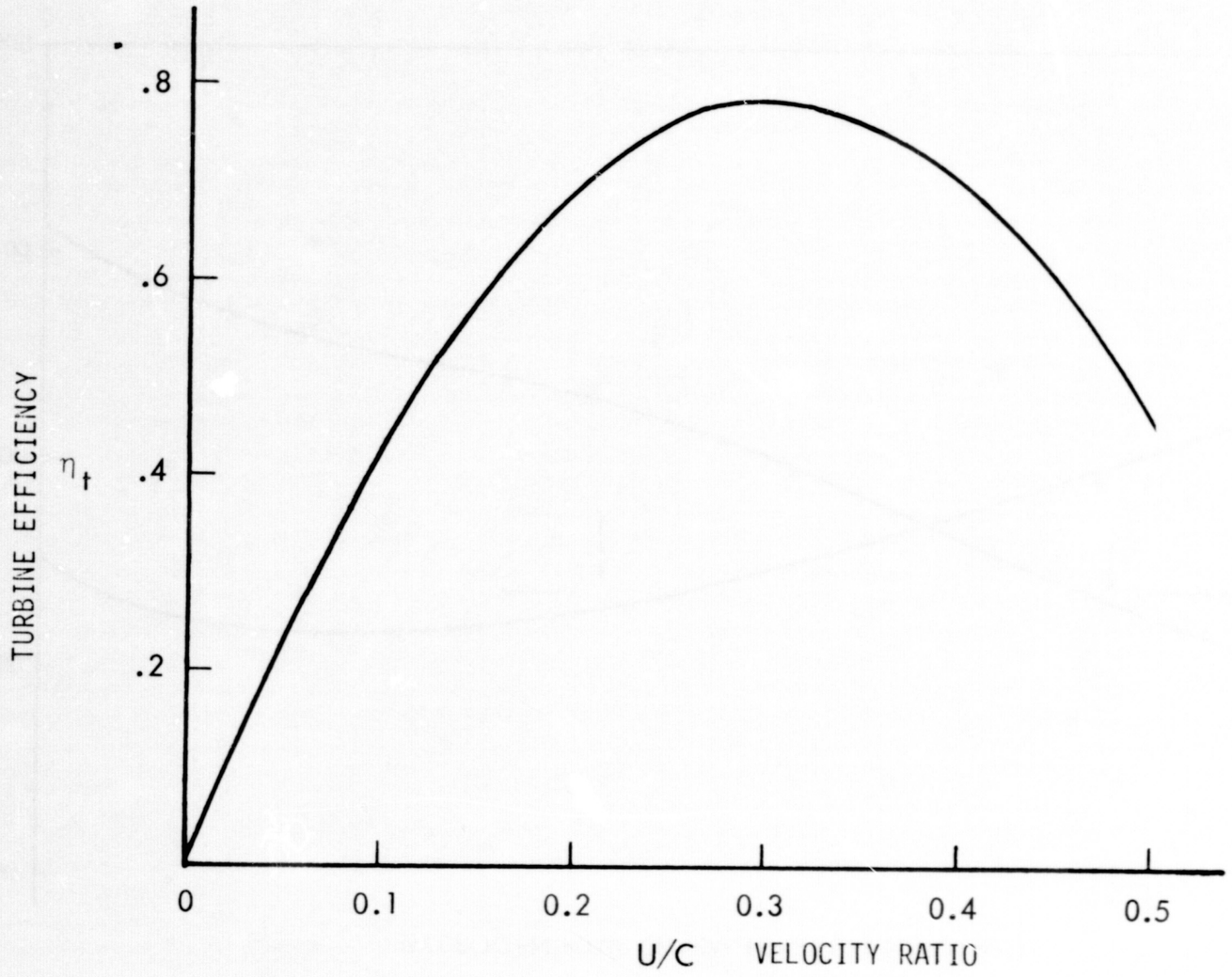

FIGURE 27 TURBINE EFFICIENCY CURVE FOR HYDROGEN TURBOPUMP

at the valve as a function of time should be nearly a perfect square wave. Since this analytical model takes into account the fact that the wave velocity with respect to the pipe travels at the speed of sound plus or minus the velocity of the fluid, the wave shape will differ from a square wave. However, at the fluid velocity used in this example, about 1.64 ft/sec, the difference should be imperceptible. At very high fluid velocities the wave shape will differ considerably from a square wave.

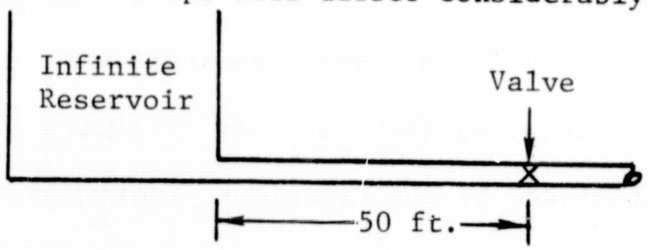

Fluid velocity, 1.64 ft/sec
Speed of sound in pipe, 4067 ft/sec
Friction factor, 0
Pressure in pipe before valve closure, 100 psia

FIGURE 28. TEST CASE FOR LINE MODEL

Four different computer "runs" were made. The first was for a computational time increment of 1.0 ms and a value of (s) of 0.001. The variable (s) is a value which determines the size of the length increment, ΔX, once the time increment, Δt has been selected (see Equation (27), Section 3.4.2). It is shown in References 19 and 22 that (s) must equal or exceed the ratio of the maximum velocity in the pipe to the speed of sound in the pipe. The pressure at the valve is shown in Figure 29 and the flowrate at the entrance to the pipe is shown in Figure 30. The results show good agreement with those anticipated. The pressure amplitude agrees exactly with that predicted by classical water hammer theory although there is some rounding of the wave with the passage of time. The rounding is caused by the numerical approximations that are used to solve Equations (1) and (2). In Figures 31 and 32, the computational time increment is the same, but (s) was set to

0.2. Increasing (s) has the effect of introducing an artificial dampening which again is the result of the numerical approximations. Reducing the time increment, however, will eliminate the effect. This is shown in Figures 33 and 34 where (s) is equal to 0.2, but the time increment is 0.15 ms. The effect of violating the stability criterion is depicted in Figures 35 and 36. In these, (s) is -0.2 and the time increment is 1.0 ms. In this case, the solution diverges wildly. The results given in Figures 7-10 indicate that for maximum accuracy for a given time increment, (s) should be as small as possible without violating the stability criterion.

The system simulated by the transient program is shown in Figure 38. It differs in a few details from the one used for demonstrating the steady-state program. The heat exchanger is represented by a step change in temperature. The design valves of pressure, temperature, and flowrate for each component are shown on the diagram. The combustor valve opening sequences and values of selected variables during the transient are shown on plots in Figure 39. The valve just downstream of the pump, the opening sequence of which is not shown in Figure 39, was opened at .25 seconds from the start of the transient in an interval of .02 seconds. The opening of this valve was delayed to allow the pressure on the downstream side of the pump to reach a value sufficiently high such that back flow through the pump would not occur. This opening accounts for the sudden fluctuations in many of the variables starting at about .25 seconds. Just before .25 seconds, the system seems to be close to a steady-state operating point. Since, in the arrangement shown in the schematic, the output of the pump exceeds the design point demand of the engines, the accumulator will in general be either filling or emptying, and the system as a whole will never be at a steady-state. Much of the fluctuation in the pressures and flowrates at the various components in caused by the opening and closing of the pressure regulators.

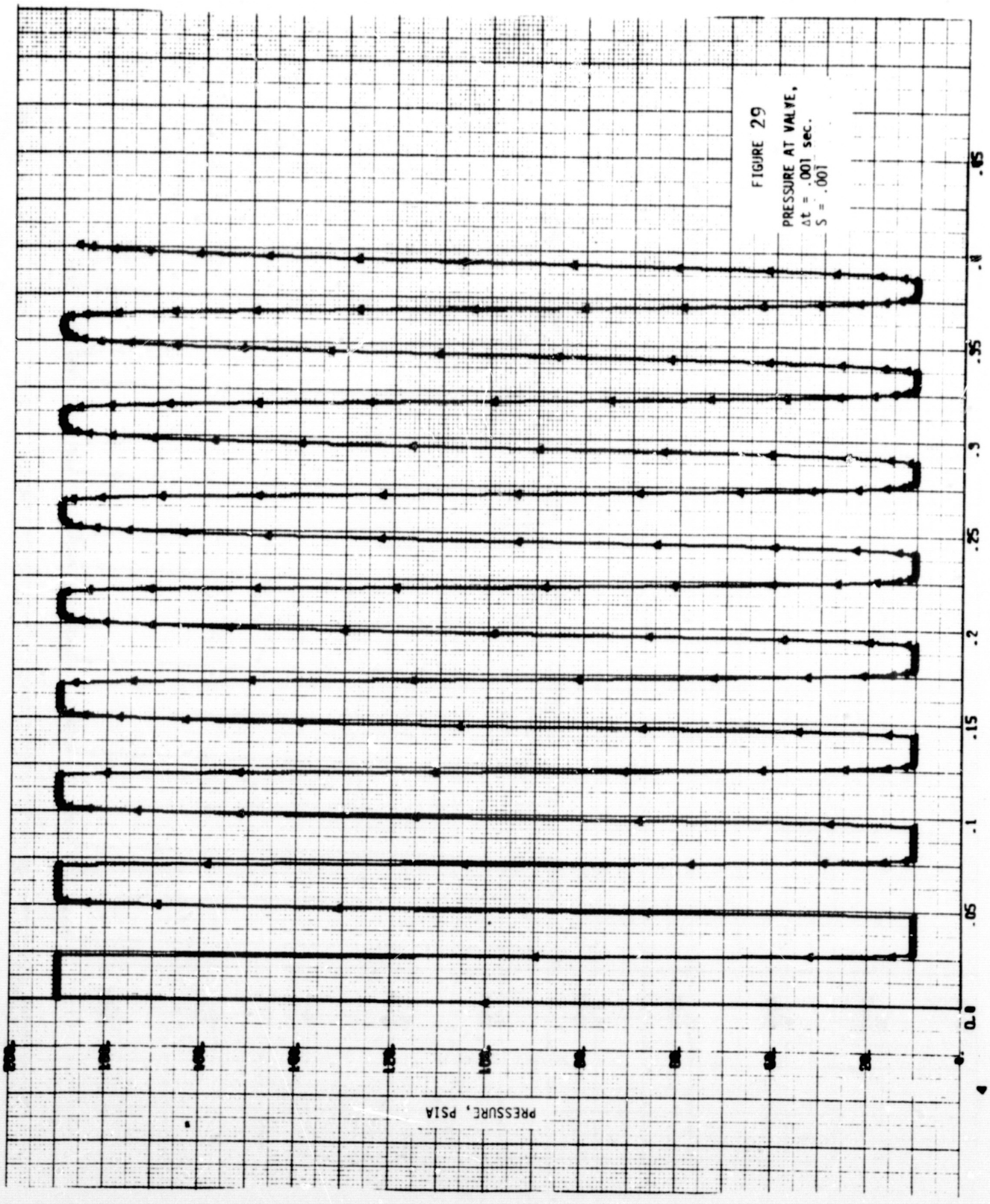
FIGURE 29
PRESSURE AT VALVE,
Δt = .001 sec.
S = .001
PRESSURE, PSIA
TIME, SEC
0.0
.05
.1
.15
.2
.25
.3
.35
.4
.45

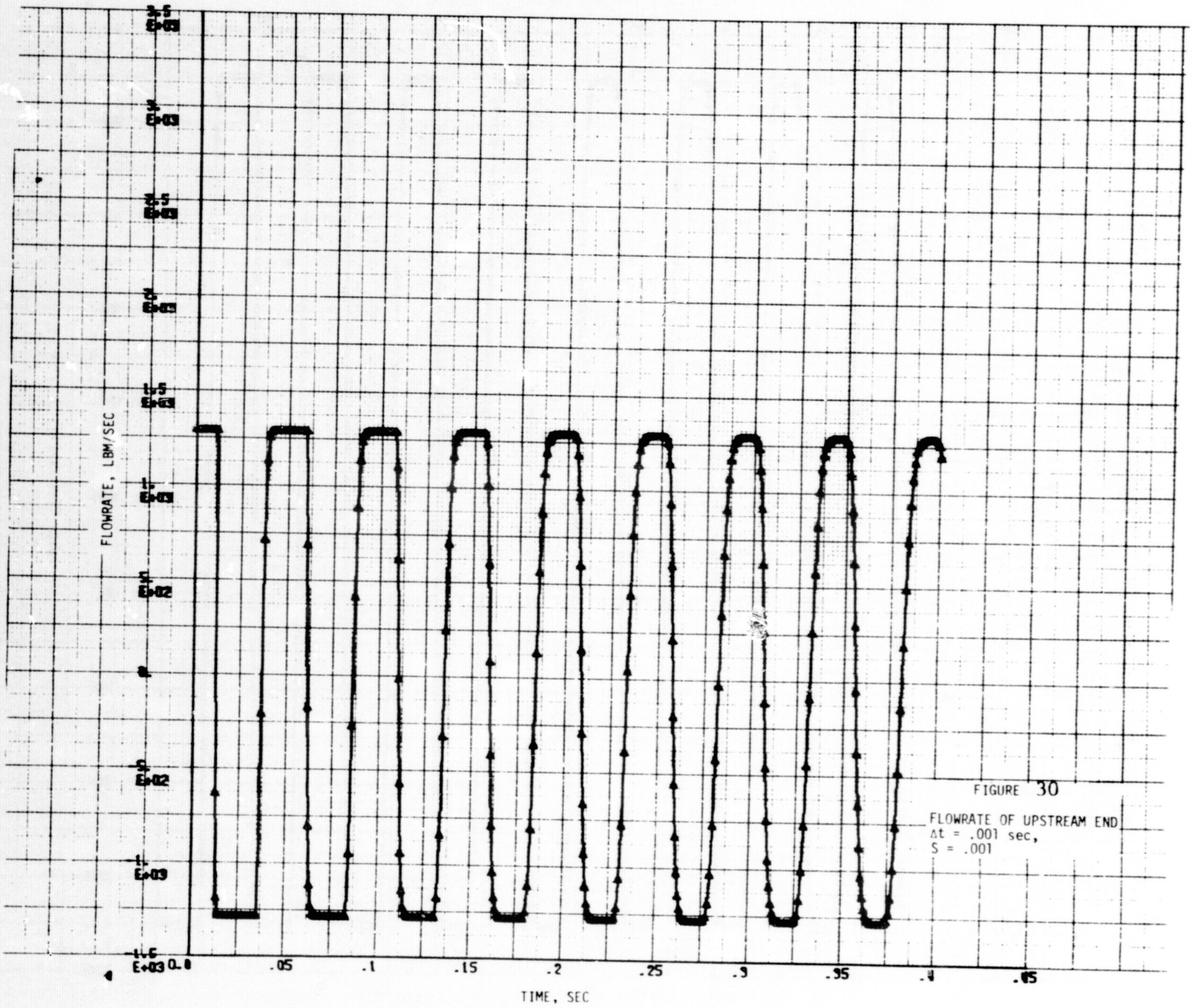

FIGURE 30

FLOWRATE OF UPSTREAM END
Δt = .001 sec,
S = .001

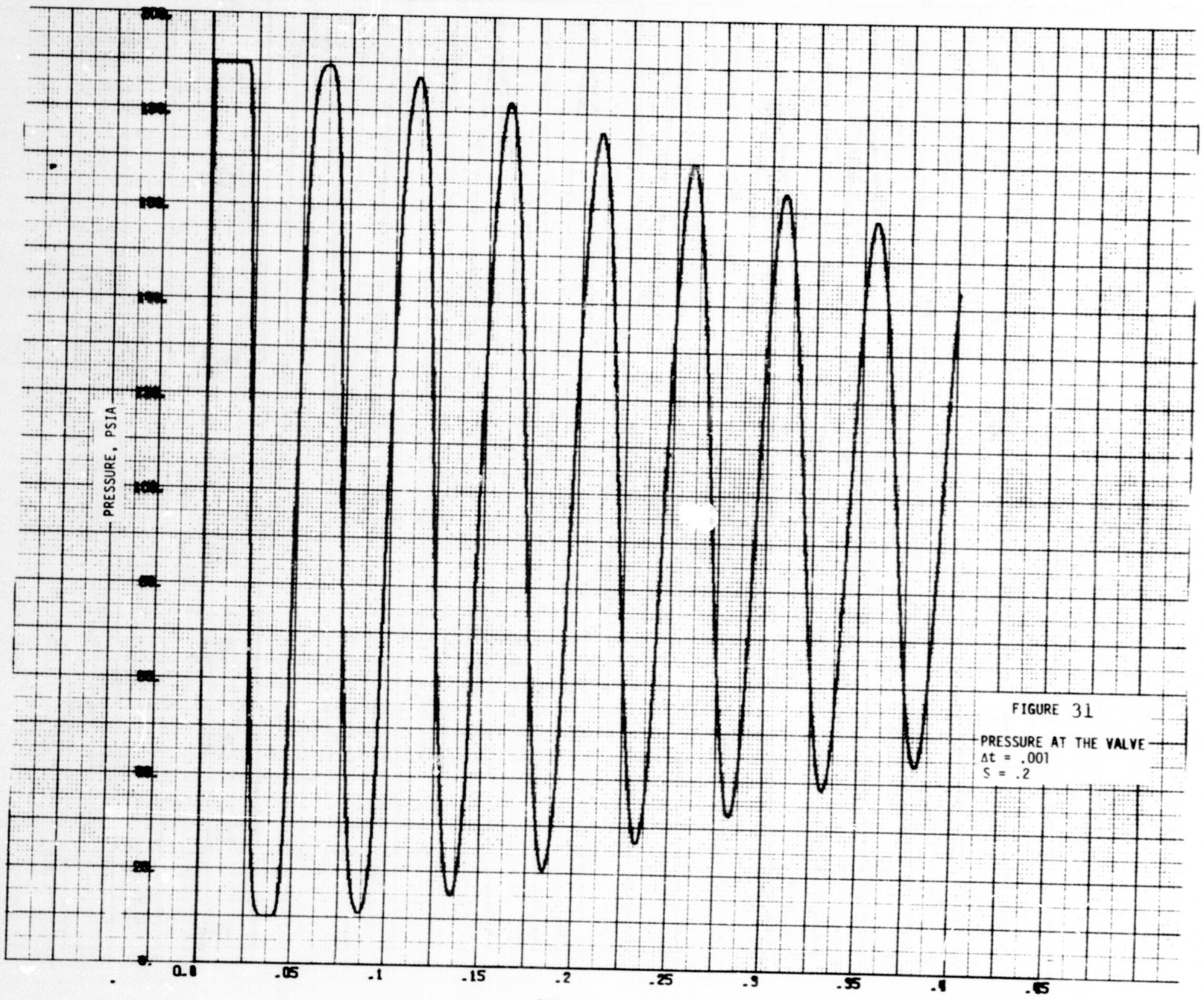

FIGURE 31

PRESSURE AT THE VALVE
Δt = .001
S = .2

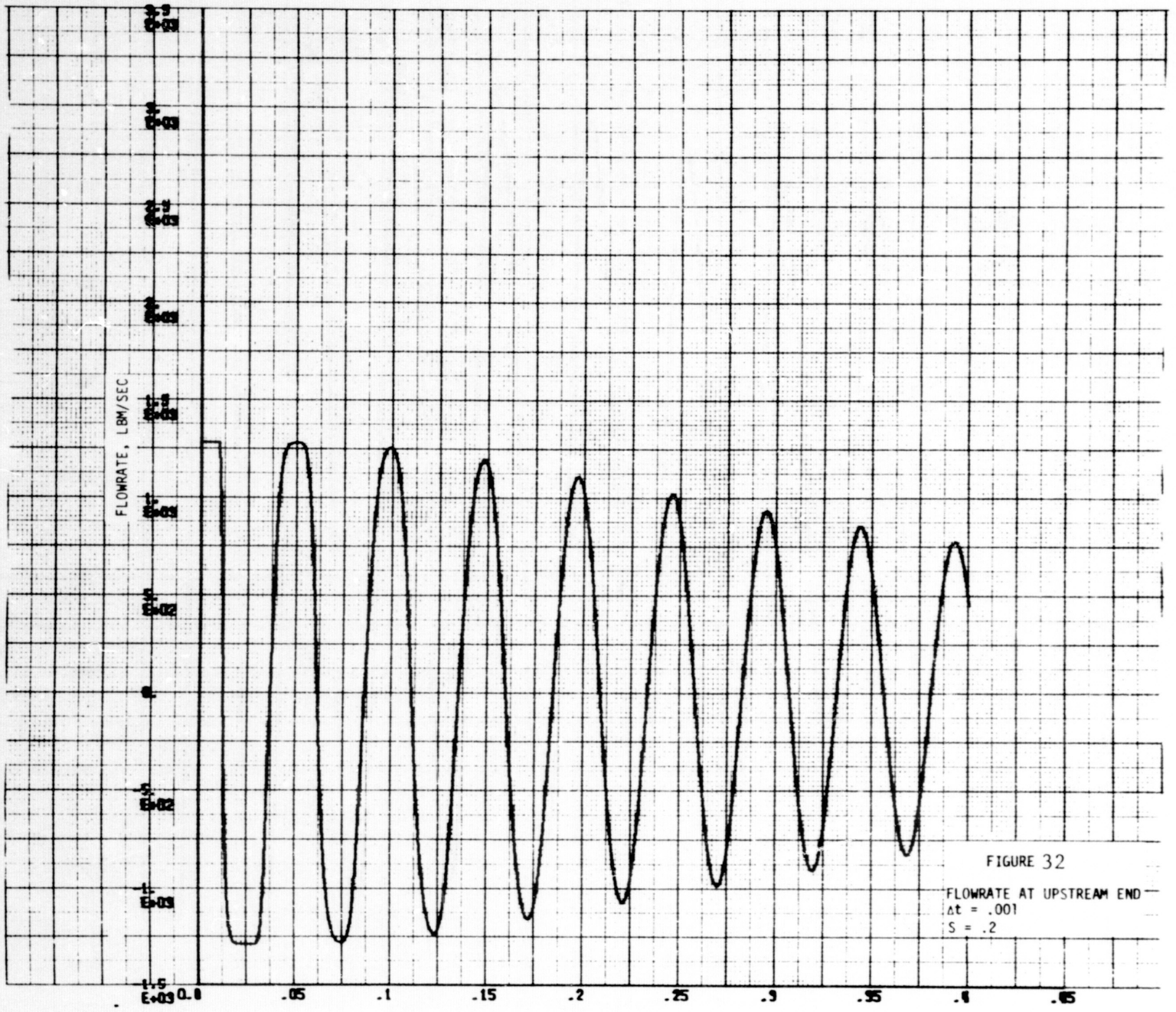

FIGURE 32

FLOWRATE AT UPSTREAM END
Δt = .001
S = .2

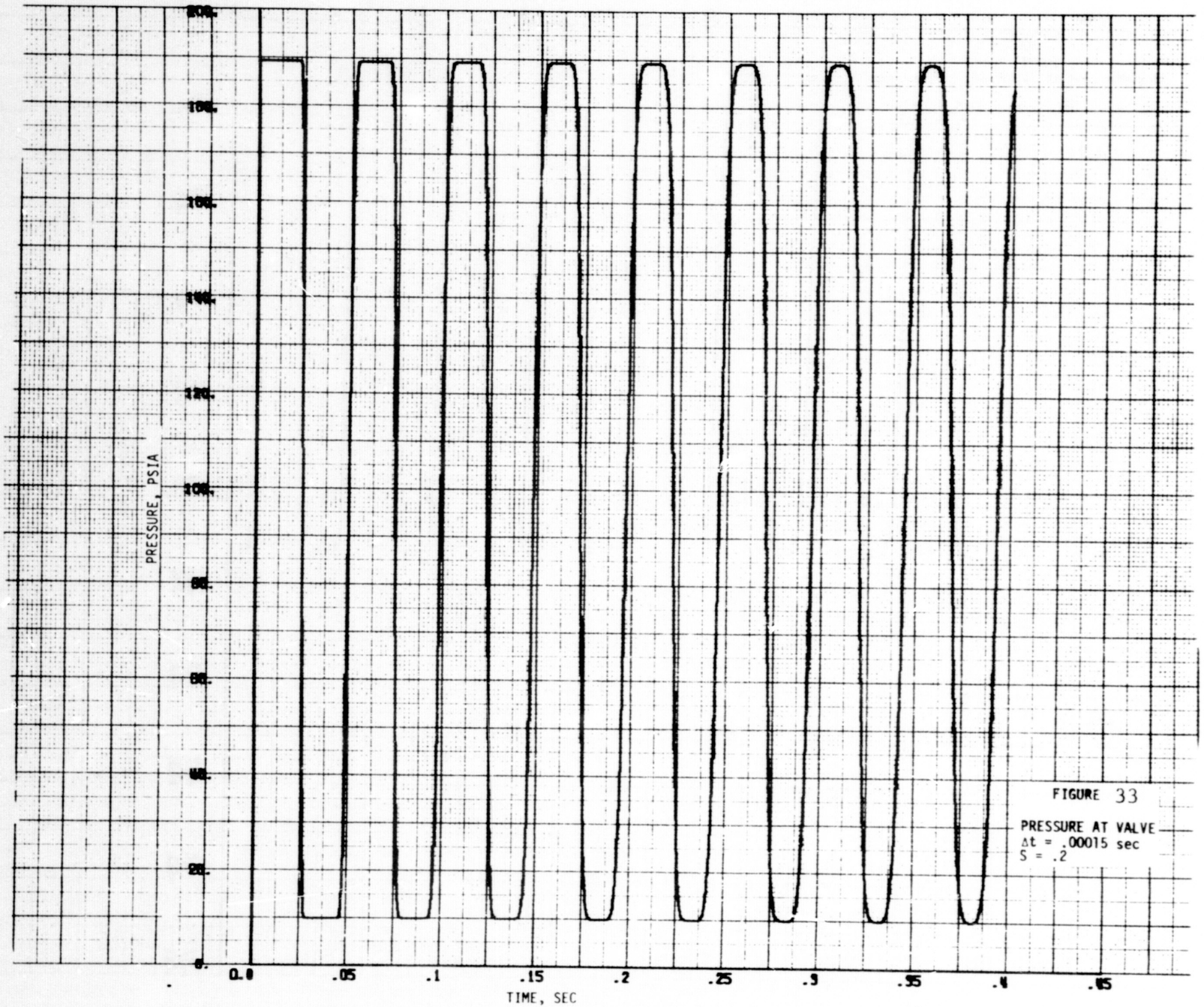

FIGURE 33

PRESSURE AT VALVE
Δt = .00015 sec
S = .2

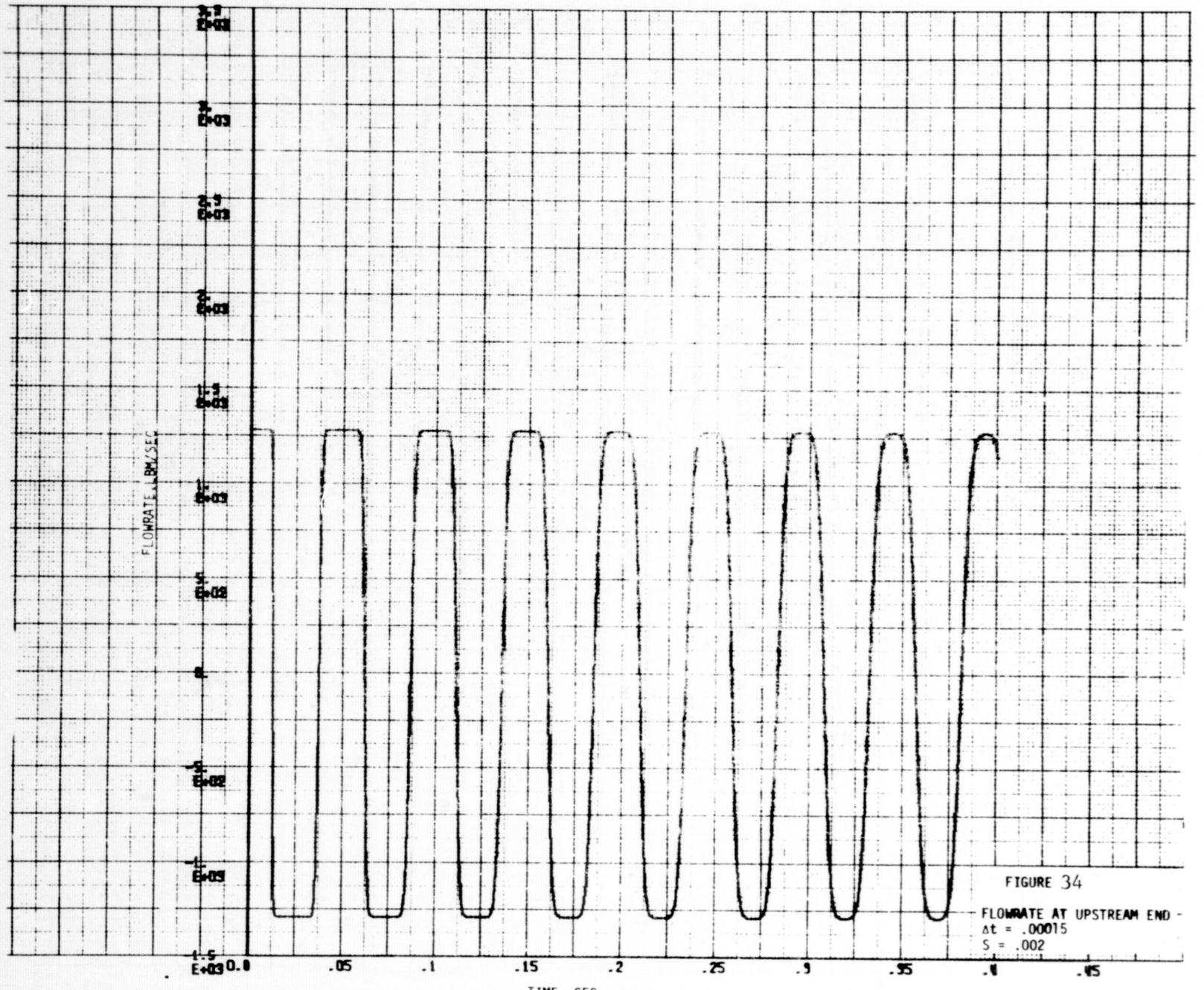

FIGURE 34

FLOWRATE AT UPSTREAM END -
Δt = .00015
S = .002

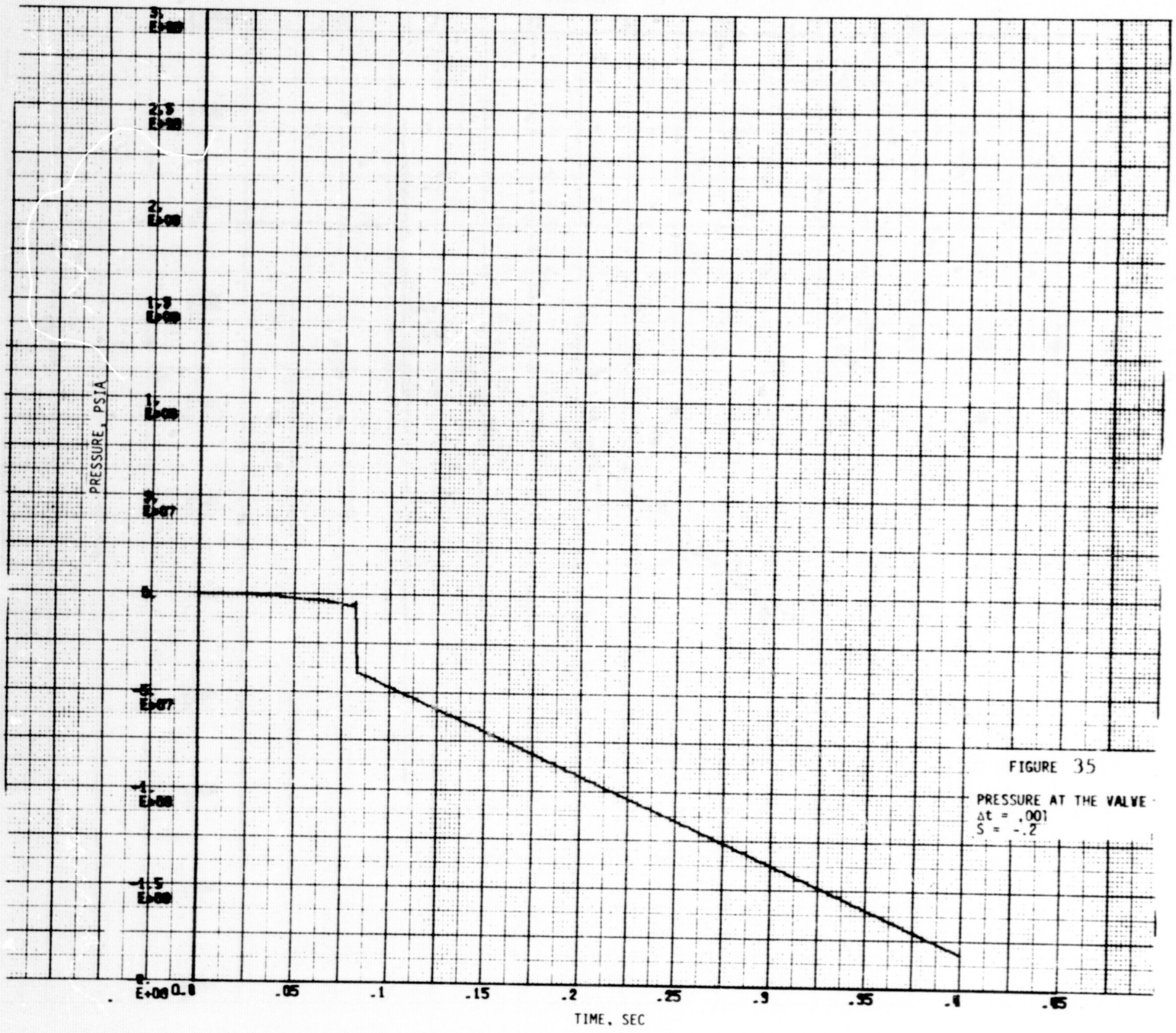
PRESSURE, PSIA
TIME, SEC
0.
.05
.1
.15
.2
.25
.9
.35
.4
.45
PRESSURE AT THE VALVE
Δt = .001
S = -.2

FIGURE 35

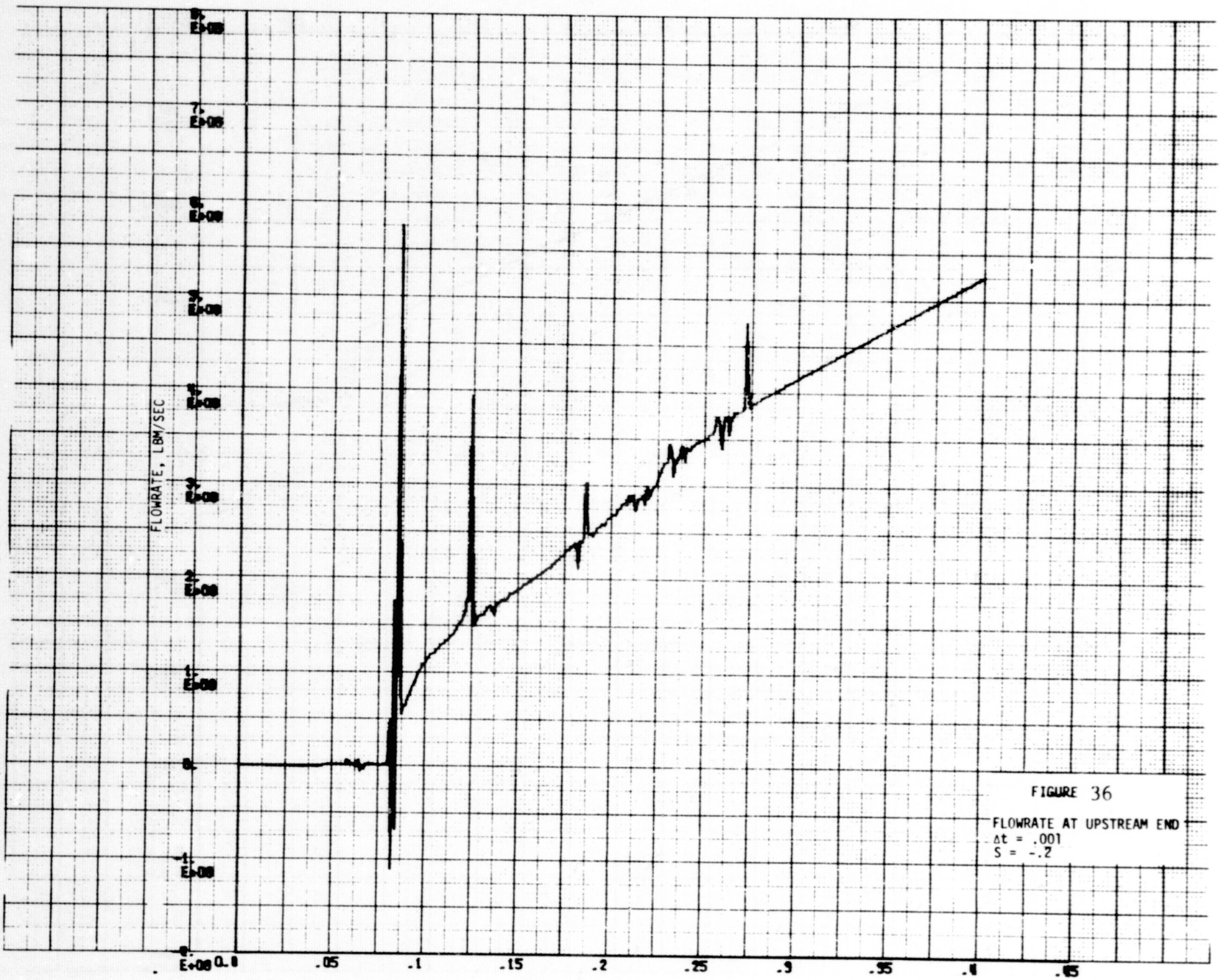
FLOWRATE, LBM/SEC
TIME, SEC
E+08
0.
.05
.1
.15
.2
.25
.9
.95
.1
.05
FIGURE 36
FLOWRATE AT UPSTREAM END
Δt = .001
S = -.2

67

A dynamic model of an ACPS combustor was developed on the time share terminal and implemented on the MSC 1108 computer. This basic model is used as the combustor component of the total ACPS transient program. A study was performed utilizing this preliminary combustor model to determine its numerical stability and running time, and to investigate the advantages of various numerical integration techniques. This model was expanded to include curve fits of combustor performance data for a typical engine thruster.

Based on the study results, the following conclusions were made:

1 - Representation of the ACPS combustors with this type model was satisfactory and, therefore, a more detailed model was constructed with this characterization as the foundation.

2 - Numerical integration of the model equations utilizing Euler's integration scheme is relatively unstable. After thrust build-up and during the period that the engine simulation is in steady-state, the simulated chamber pressure oscillates $\pm$0.3 psia with a 0.01 millisecond (ms) computation interval and $\pm$2 psia with a 0.25 ms computation interval. The solution never stabilizes.

3 - The Runge-Kutta integration scheme operates very well with the model equations. No oscillations were observed during any of the computation intervals. The solution stabilizes after 2.4 ms of calculations and only becomes unstable if a computation interval of 0.5 ms is exceeded. These results are for a step change in pressure. For slow valve opening times, a larger time increment can be used.

The combustor model is defined in Section 3.4.12. The model was set up initially as a "stand alone" model which operates with a constant pressure

boundary upstream of the chamber, thereby eliminating the effects of any feedline perturbations for this study only. This was done to simplify the stability, time step, and integration study.

During the checkout phase of the program development, the combustor model was exercised as a "stand alone" program for simulating a typical engine. For this checkout phase, a test case was employed with the combustor model utilizing gaseous oxygen and gaseous hydrogen as propellants with the following input data: characteristic exhaust velocity = 7500 ft/sec, nozzle throat area = 5.1 in^2, combustor gas temperature = 6000°R, and the specific heat ratio was fixed at 1.4. The propellant feedlines to the combustor were maintained as a constant pressure boundary of 360 psia and a temperature of 530°R. The propellant flow control valves were opened instantaneously and transient profiles of the propellant flow into the combustor and the chamber pressure were calculated.

The model was exercised at various integration step sizes using both the Euler and the Runge-Kutta numerical integration schemes. Arbitrary variations were used for the integration step sizes to evaluate the maximum integration interval which can be effectively utilized, the accuracy of the results and the model's stability. The integration step sizes examined were 0.01, 0.10, 0.25 and 0.4 ms. As noted on Figure 37 the simple Euler integration scheme has a transient response which is somewhat erratic except for the 0.01 ms time step. With a step size of 0.5 ms, the solution diverges. It was also noted that a stable condition never really existed even at 0.01 ms since the chamber pressure was still oscillating at ±0.3 psia. At a step size of 0.25 ms, the oscillations are ±2 psia while for a step size of 0.1 ms, the oscillations are approximately ±5 psia.

In an attempt to decrease the running time and increase the accuracy over that achieved with the Euler technique, the Runge-Kutta integration scheme was evaluated at calculation intervals of 0.01, 0.1, 0.125, and 0.4 ms. Stable solutions were obtained as noted in Figure 37. As the integration interval was increased to 0.5 ms, the transient pressure rise becomes less accurate during the period from 0.8 ms to 4.0 ms of elapsed time as noted from the slow pressure buildup shown in Figure 37. By 4 ms, all solutions reached a steady-state simulation of 310 psia chamber pressure. The integration step size was increased to 0.5 ms and the solution diverged extensively from the true physical system and went unstable because too much propellant was allowed into the chamber, thus driving the model into a reverse flow situation.

From this study, it was concluded that a Runge-Kutta integration scheme was satisfactory. A computational step size of approximately 0.25 ms, which is one-fourth the step size being utilized with the dynamic feedline model, appears to be ideal. This time increment is for step changes in pressure, slower valve opening times allow larger time increments.

COMBUSTOR TRANSIENT MODEL STUDY

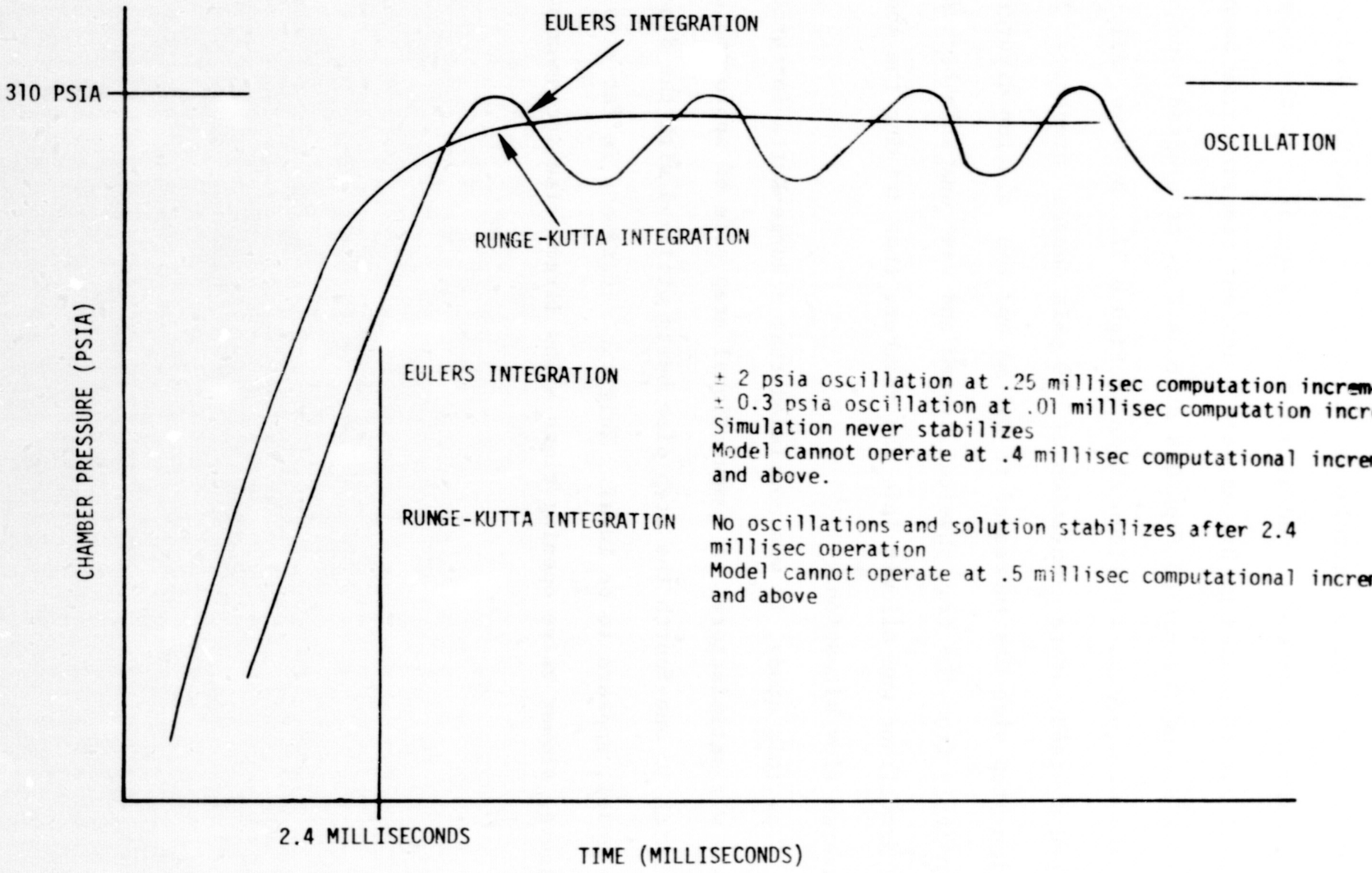

FIGURE 37

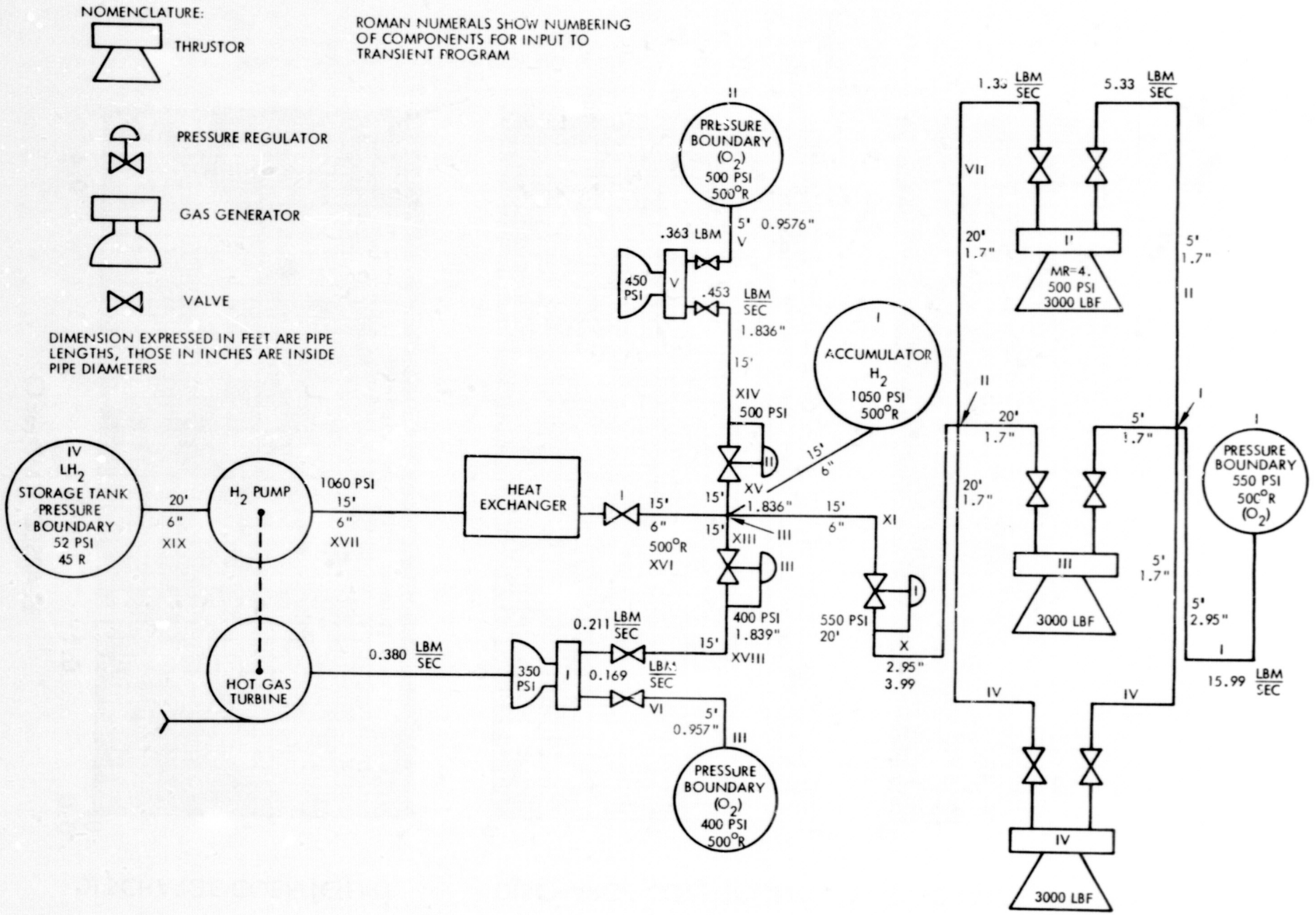

FIGURE 38. ACPS TRANSIENT TEST CASE SCHEMATIC

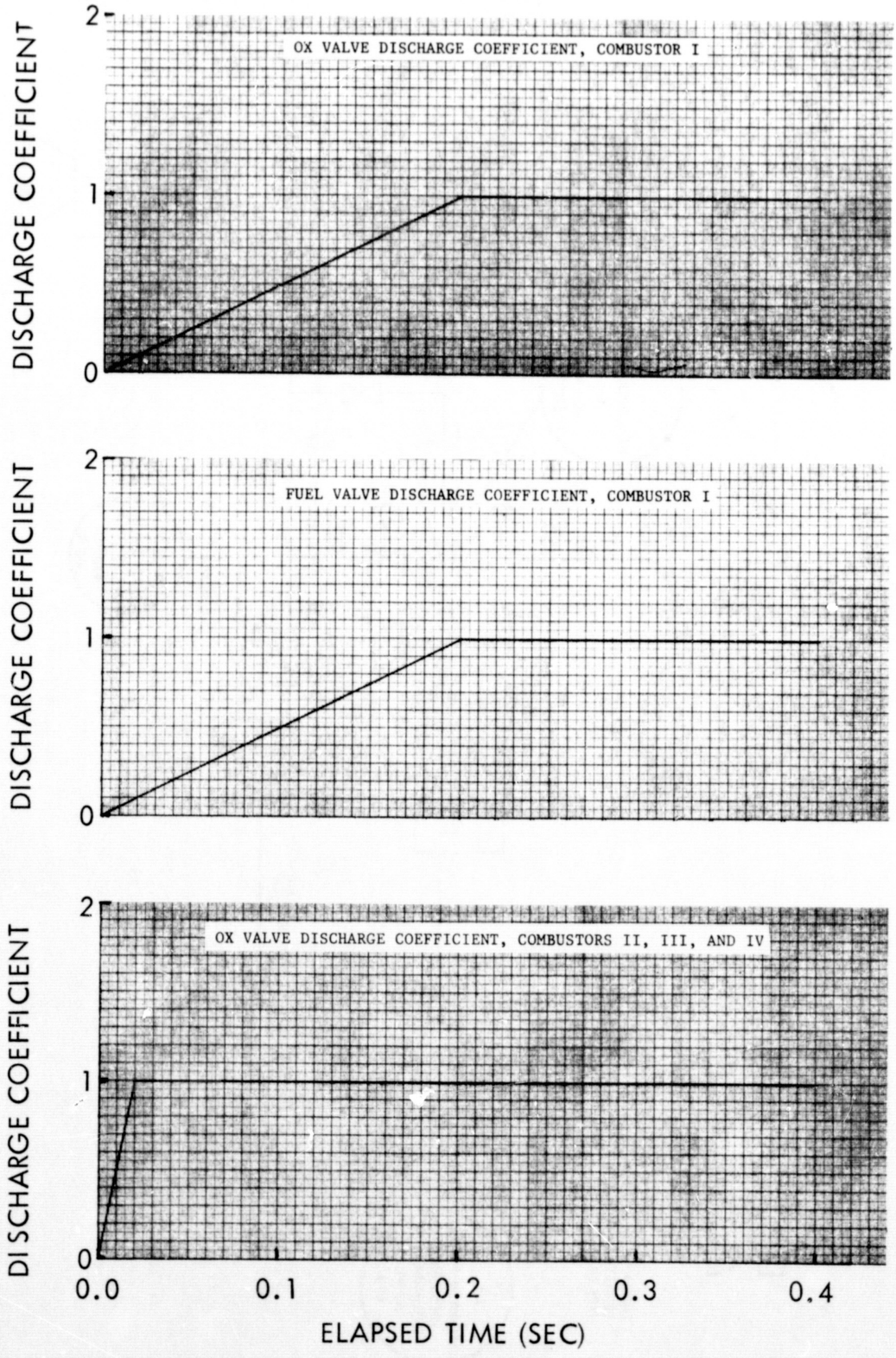

Figure 39a. ACPS Transient Test Case

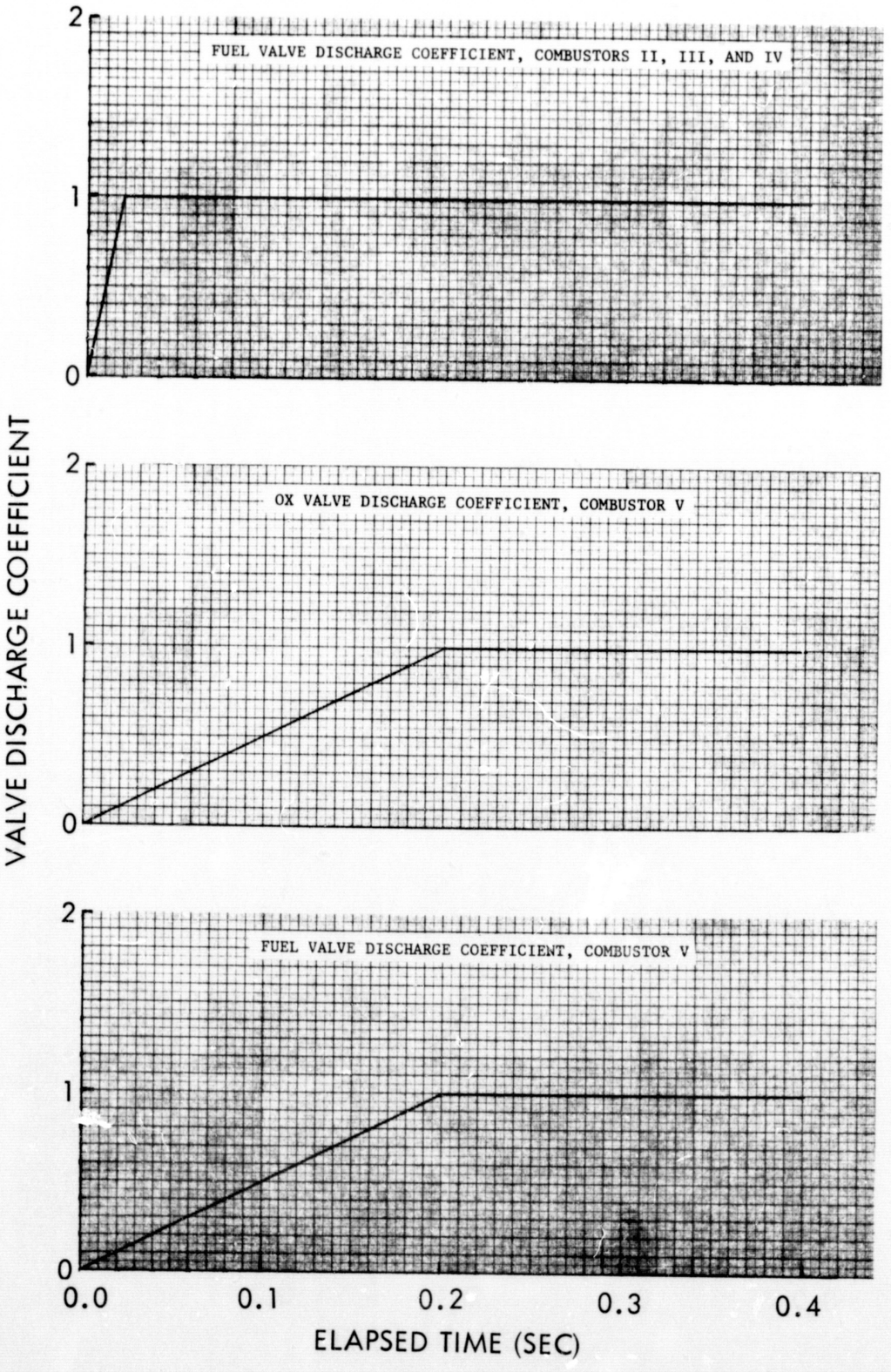

Figure 39b. ACPS Transient Test Case

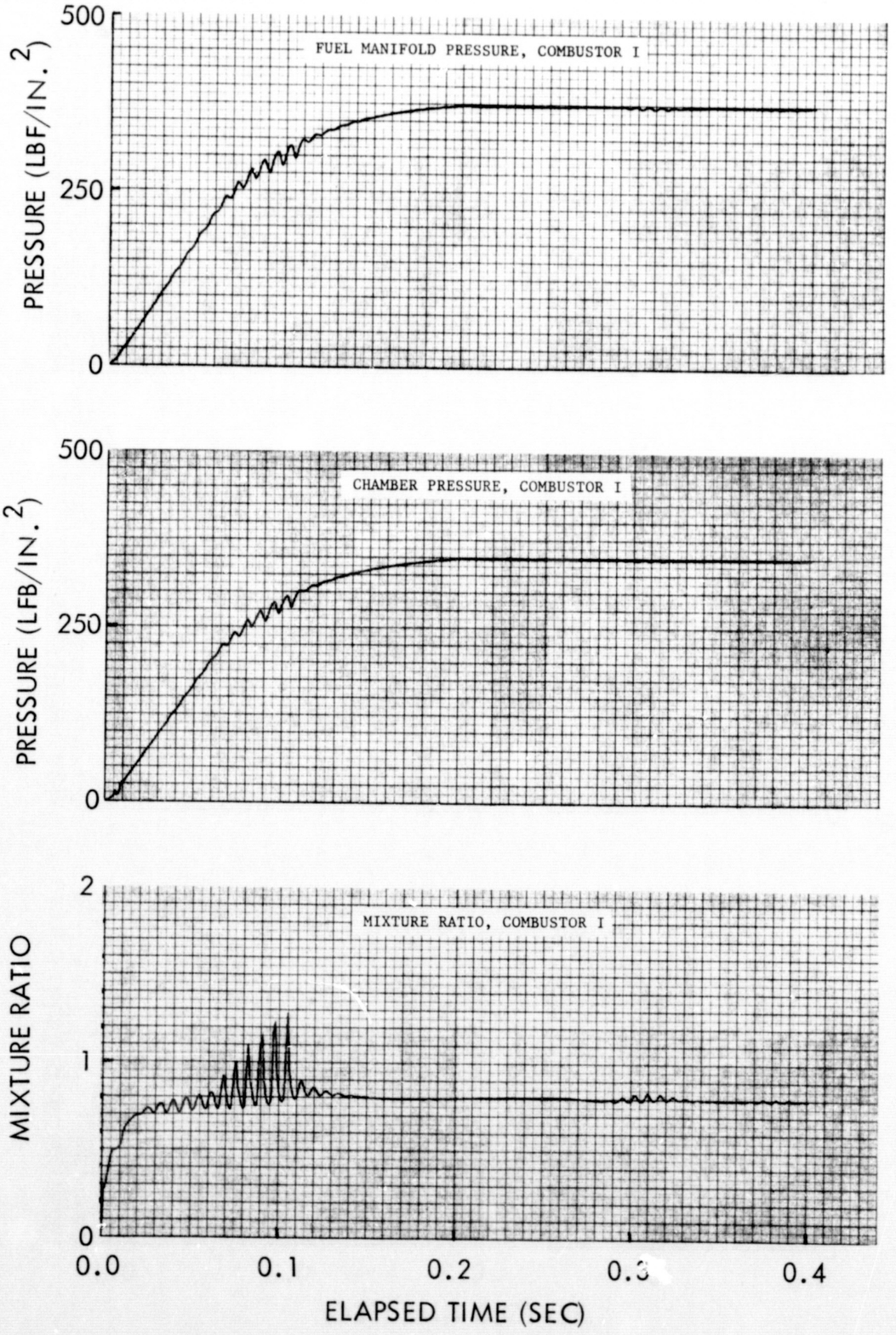

Figure 39c. ACPS Transient Test Case

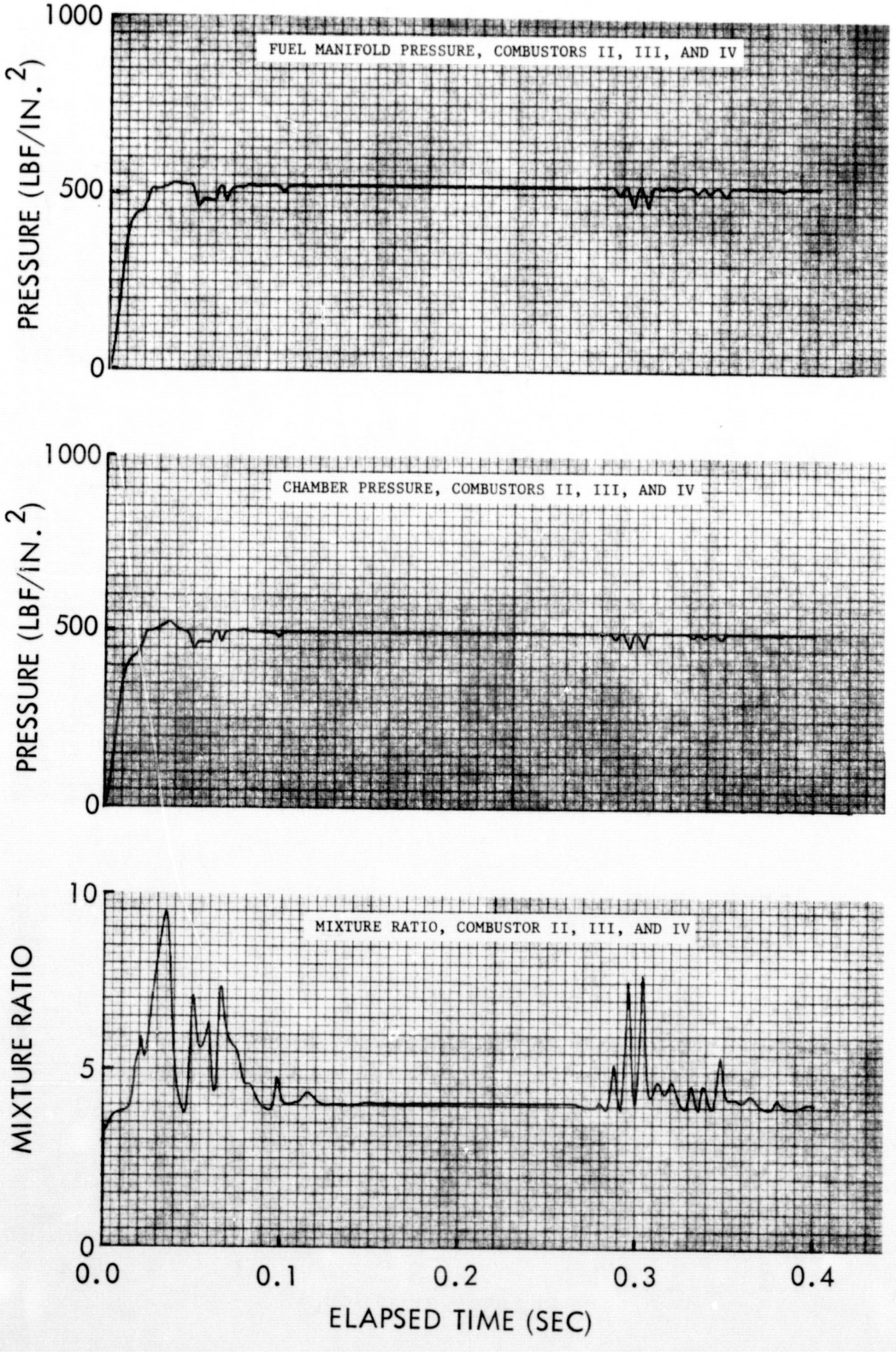

Figure 39d. ACPS Transient Test Case

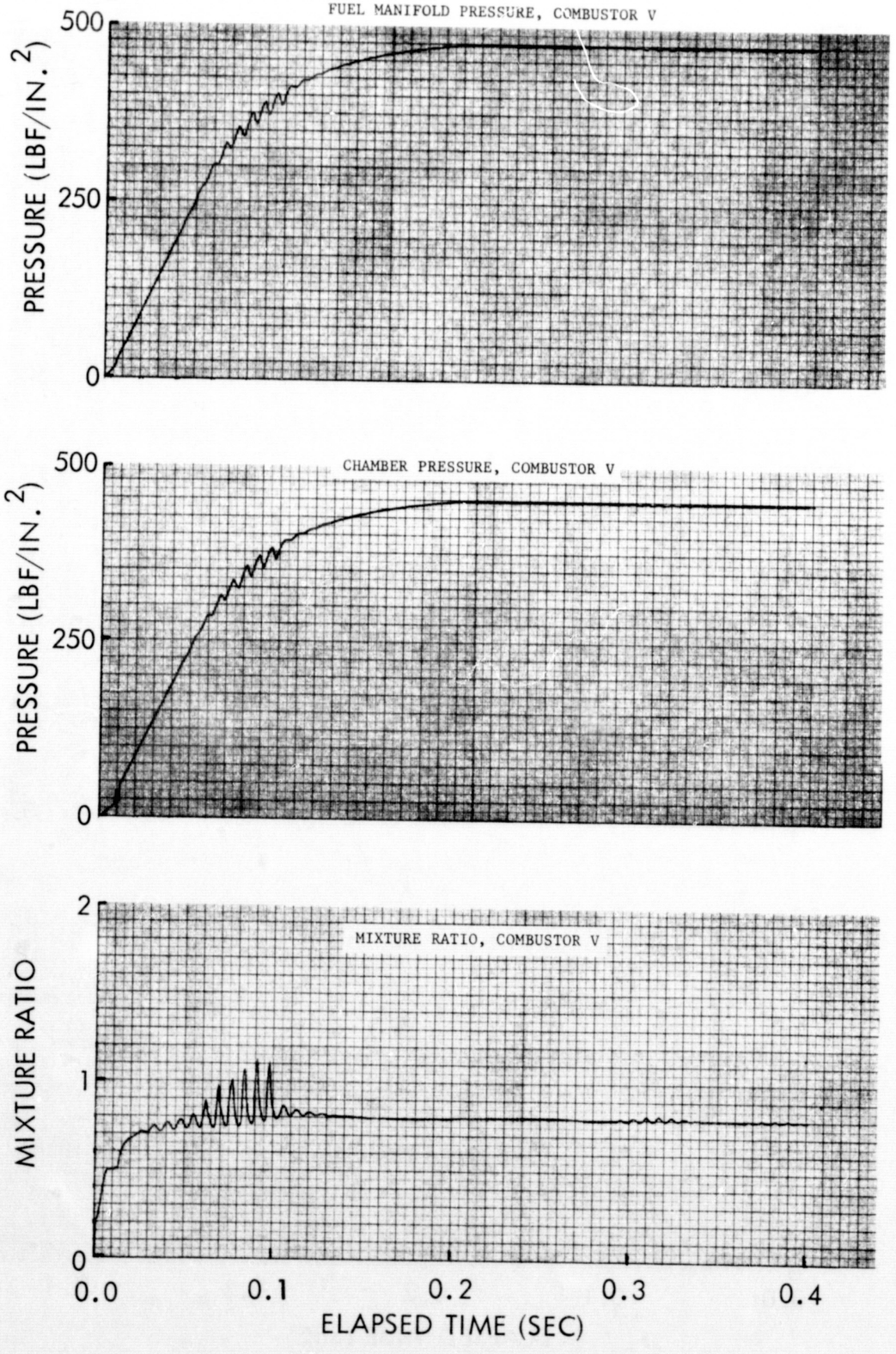

Figure 39e. ACPS Transient Test Case

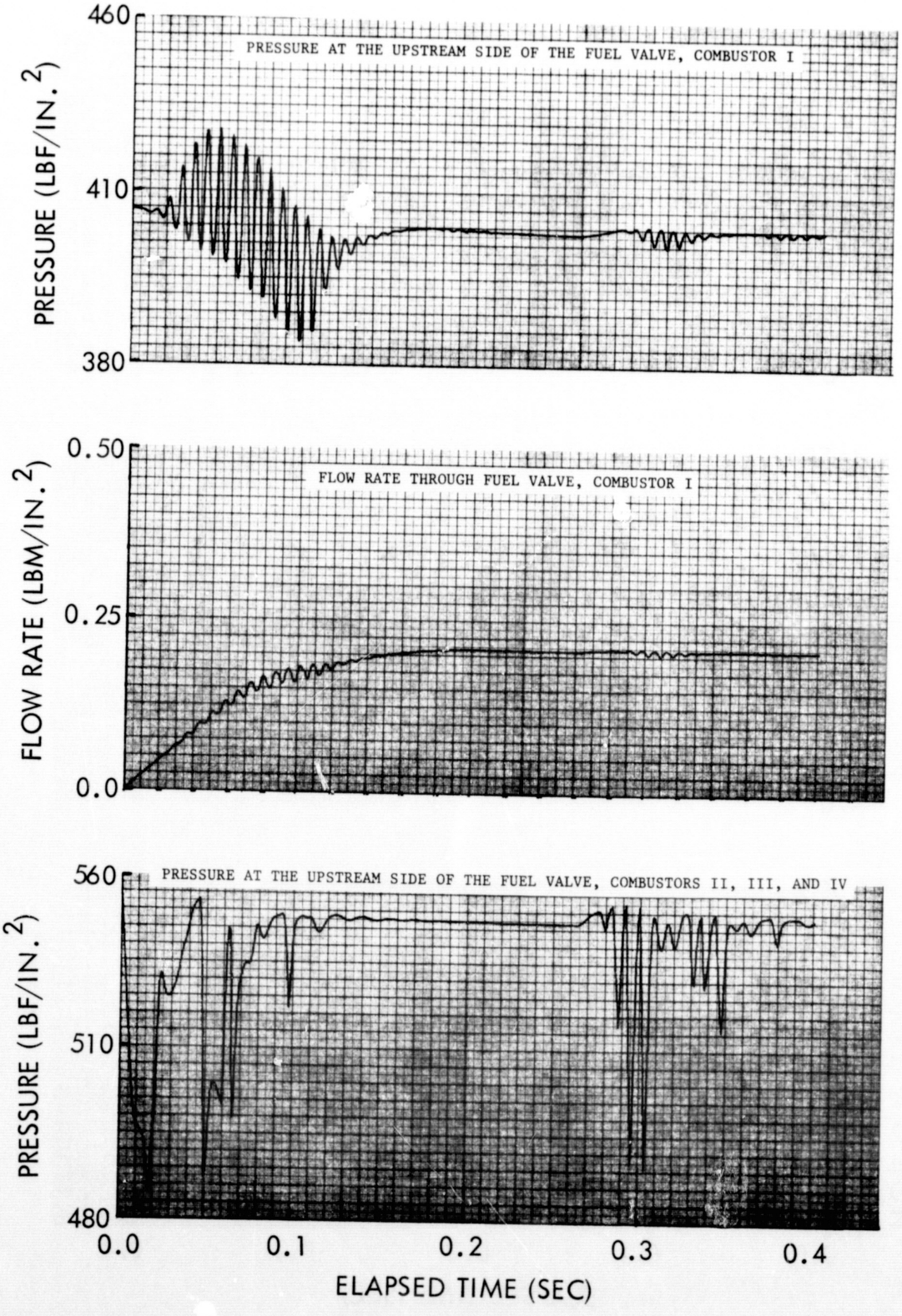

Figure 39f. ACPS Transient Test Case

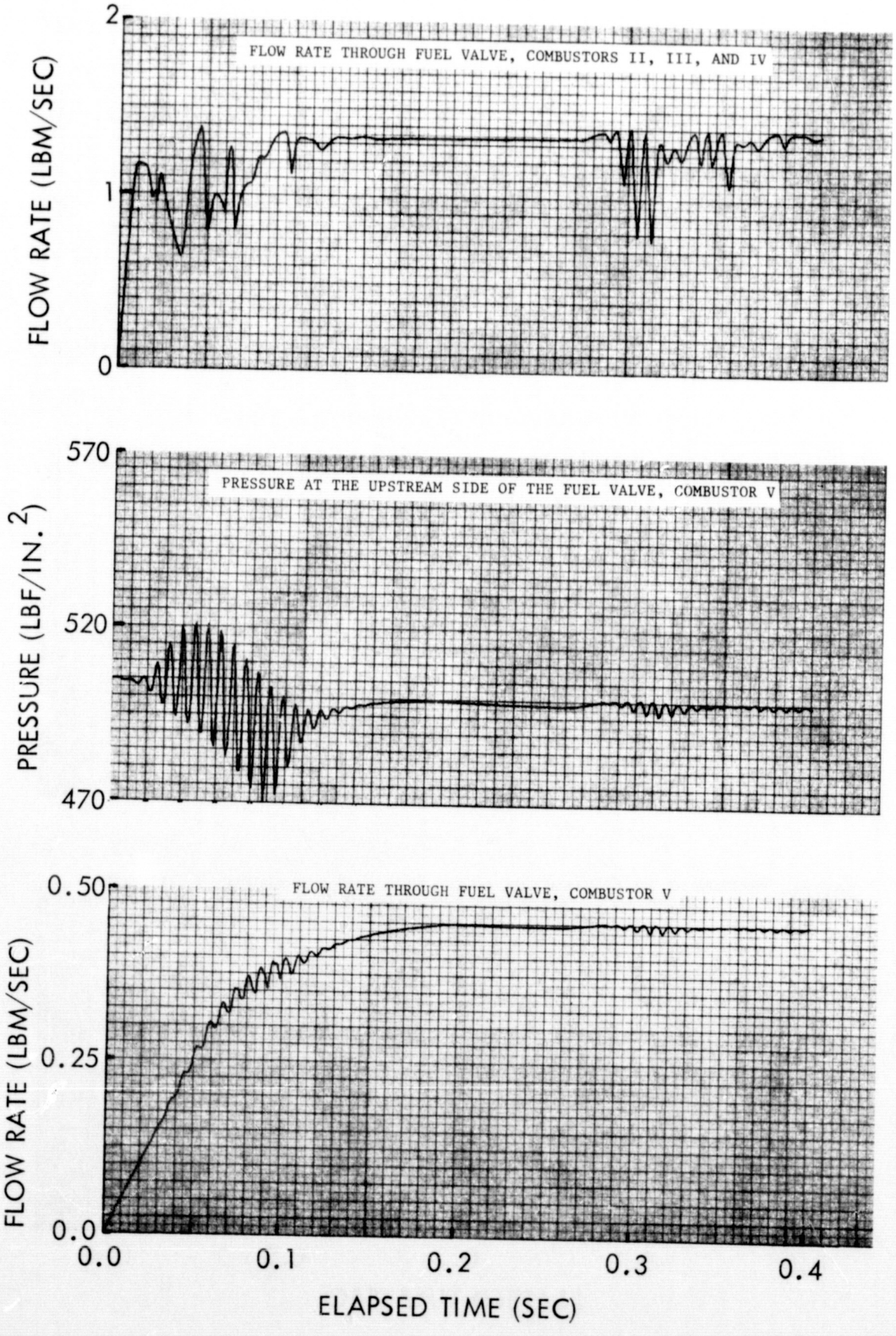

Figure 39g. ACPS Transient Test Case

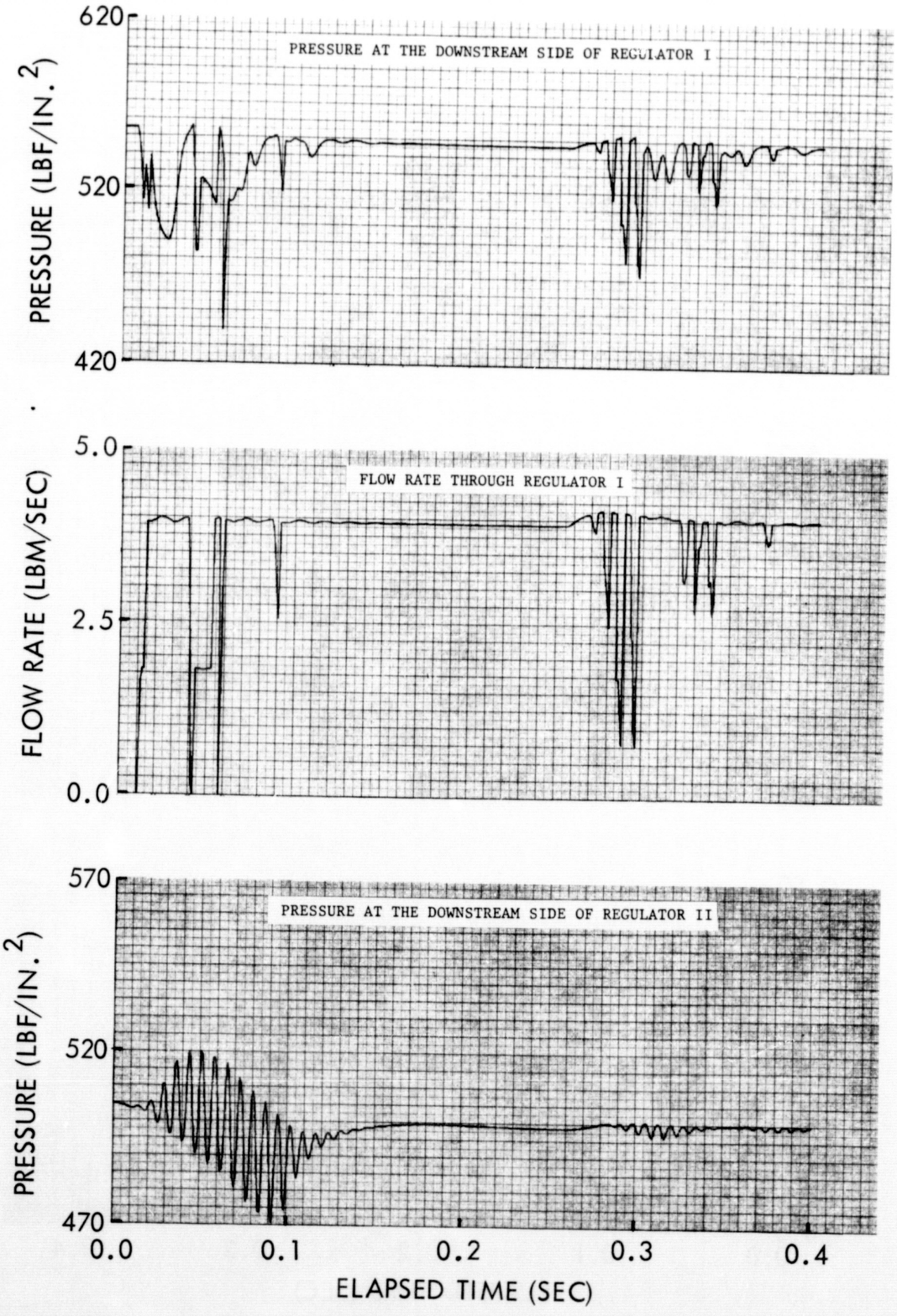

Figure 39h. ACPS Transient Test Case

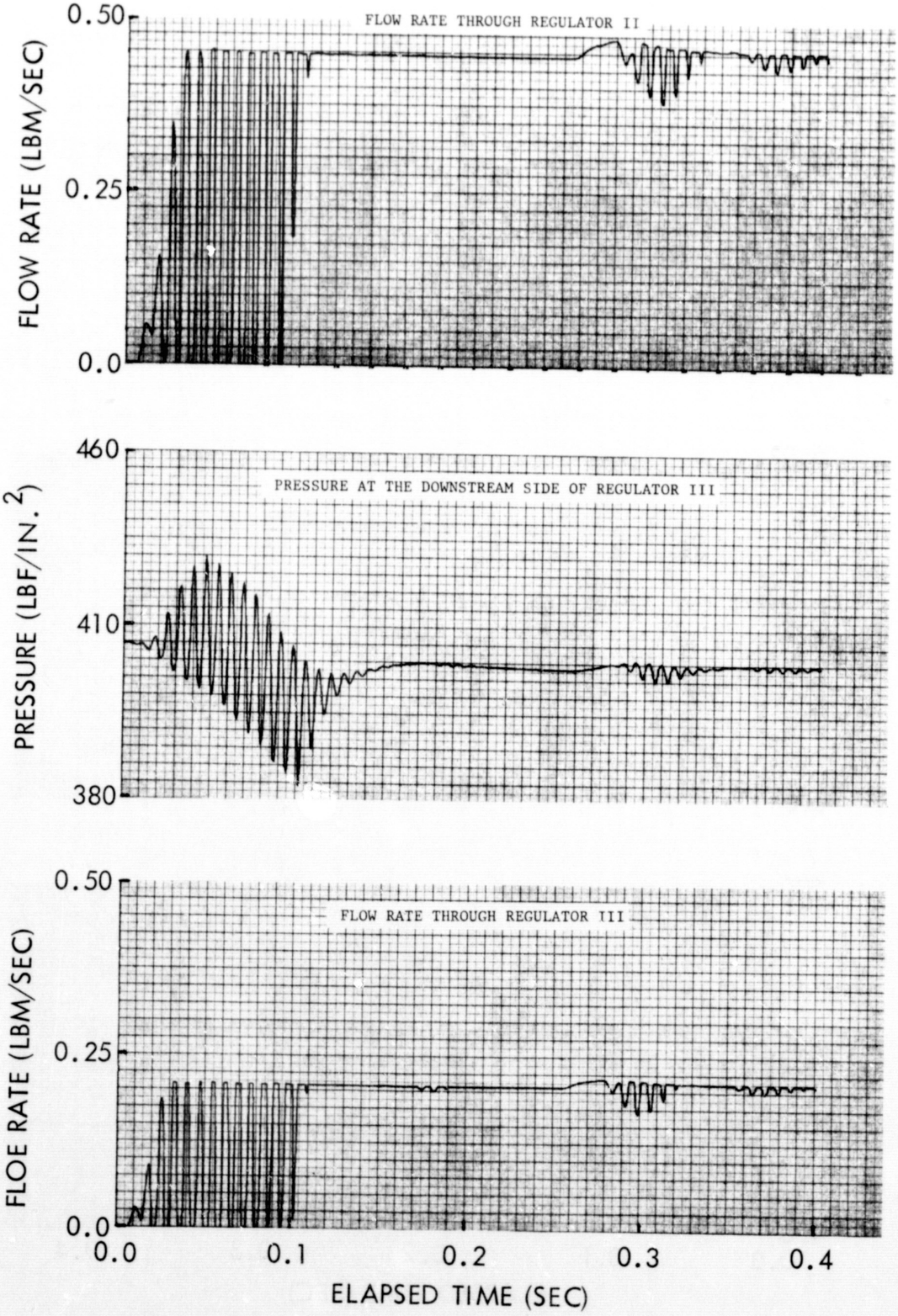

Figure 39i. ACPS Transient Test Case

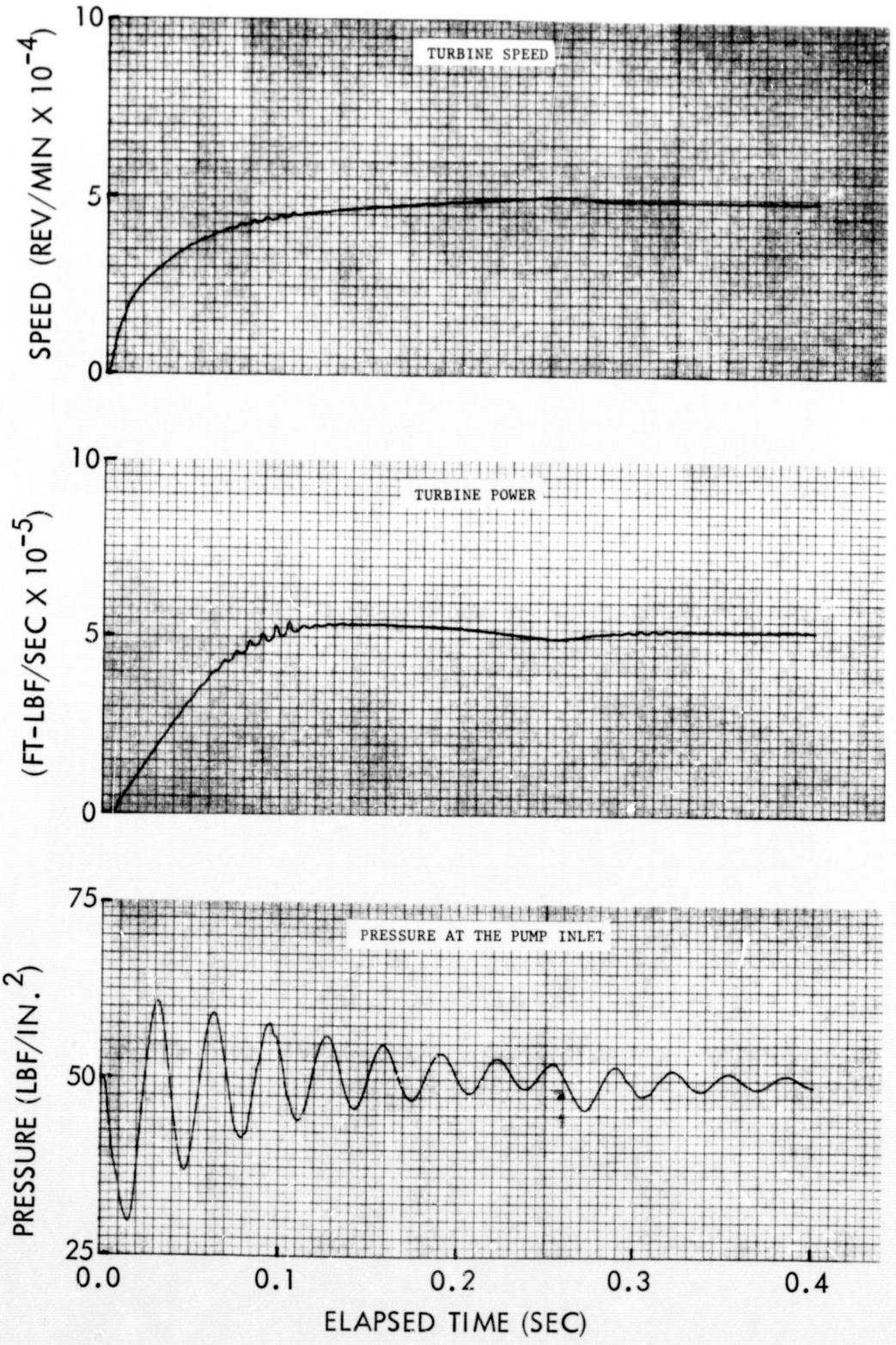

Figure 39j. ACPS Transient Test Case

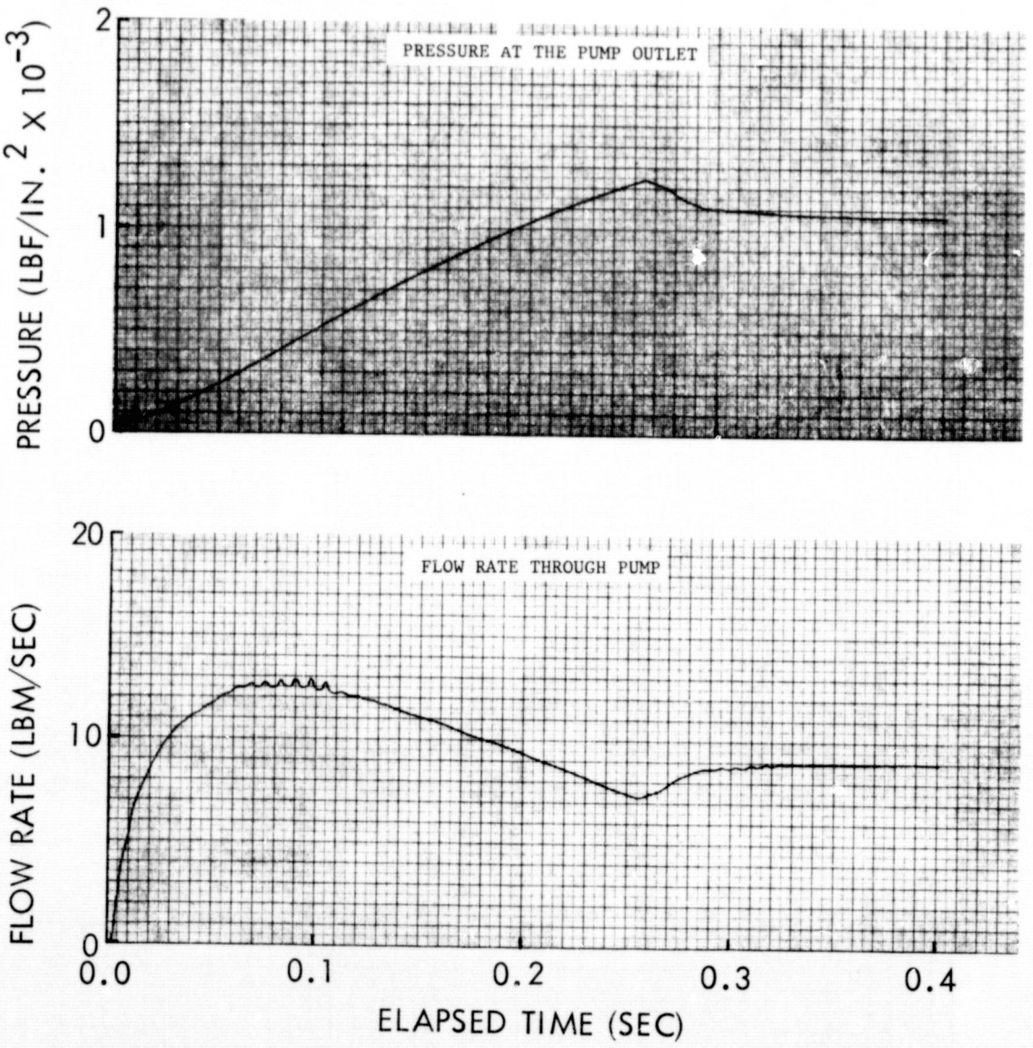

Figure 39k. ACPS Transient Test Case

5.0 REFERENCES

1. "High Pressure Auxiliary Propulsion Subsystem Definition Study," Contract No. NAS 8-26248, McDonnell-Douglas Corporation, 6 October 1970.

2. "Low Pressure APS Study," Contract No. NAS 9-11012, "Conceptual Sub-System Definition Review," McDonnell-Douglas Corporation, 7 October 1970.

3. "Space Shuttle High Pressure Auxiliary Propulsion Subsystem Definition," Contract NAS 9-11013, TRW Systems Group, 8 October 1970.

4. "Space Shuttle Low Pressure Auxiliary Propulsion Subsystem Definition," Contract NAS 8-26249, TRW Systems Group, 5 October 1970.

5. Halbert, P. W., and Lotito, L. A., The Simulation of Gas Flow Dynamics in Pipeline Networks, March, 1970.

6. Matrix Oriented Program Assembly System (MOPAS) User's Manual, Chrysler Space Division, April, 1968.

7. Powers, C. S. and Smith, L. H., "Oracle-Mafia Program (Propulsion Analysis Program, PAP)," Report 05952-6178-T000, 27 September 1967.

8. Krane, R. J. and Reiff, A., "A Method of Characteristics Solution for the Equations Governing the Unsteady Flow of Liquids in Closed Systems," Technical Report No. 388, Operations Research Inc., 30 August 1966.

9. Streeter, Victor L., and Lai, Chintu, "Water-Hammer Analysis Including Fluid Friction," Journal of the Hydraulics Division Proceedings of the American Society of Civil Engineers, May, 1962.

10. Roberts, L., "On the Numerical Solution of the Equations for Spherical Waves of Finite Amplitude," Journal of Math and Physics, Vol. XXXVI, No. 4., January 1958.

11. Streeter, V. L., and Wylie, E. B., Hydraulic Transients, McGraw-Hill Book Company, 1967.

12. One-Dimensional Equilibrium Nozzle Analysis Computer Program Developed by NASA-Lewis Research Center.

13. Turbulent Boundary Layer Nozzle Analysis Computer Program, Developed by Pratt & Whitney Aircraft.

14. Two-Dimensional Equilibrium Nozzle Analysis Computer Program, Developed by Pratt & Whitney Aircraft.

15. ICRPG Two-Dimensional Kinetic Nozzle Analysis Computer Program, July 1968, Interagency Chemical Rocket Propulsion Group, Army-Navy-Air Force-ARPA-NASA Performance Standardization Working Group.

16. ICRPG One-Dimensional Kinetic Nozzle Analysis Computer Program, July 1968, Interagency Chemical Rocket Propulsion Group, Army-Navy-Air Force-ARPA-NASA Performance Standardization Working Group.

17. Ralston, A. and Wilf, H. S., Mathematical Methods for Digital Computers, John Wiley & Sons, Inc., 1960.

18. Forsythe, G. E. and Wasow, W. R., Finite-Difference Methods for Partial Differential Equations, John Wiley & Sons, Inc., 1960.

19. Fox, L., Numerical Solution of Ordinary and Partial Differential Equations, Addison, Wesley Publishing, Inc., 1962.

20. Shapiro, A. H. , The Dynamics and Thermodynamics of Compressible Fluid Flow, Ronald Press Co., 1953, Vol. 1 and 2.

21. Richtmyer, R. D., Difference Methods for Initial-Value Problems, Interscience Publishers, Inc., 1957.

22. London, A. L., Biancardi, F. R., and Mitchell, J. W., The Transient Response of Gas Turbine Plant Heat Exchangers Regenerators, Trans. ASME, Vol. 81, p. 433, 1959.

23. McAdams, W. H., Heat Transmission, McGraw-Hill Book Company, 1954.

24. Knudsen, J. G., and Katz, D. L., Fluid Dynamics and Heat Transfer, McGraw Hill Book Company, 1958.

25. Janak, P. H., "General Propellant Pressurization Program", Brown Engineering Company, Inc., Technical Report No. BSVD-P-67-TR-006, August 4, 1967.

26. Crane Industrial Products Group Technical Paper No. 410, "Flow Fluids Through Valves, Fittings, and Pipe," Engineering Division, 1957.

27. "Heat Transfer to Hydrogen and Helium with Water-to-Fluid Temperature Ratio to 11.09." by McCarthy and Wolf, Rocketdyne RR-60-12, Dec. 1960.

28. "Experimental Heat Transfer and Pressure Drop of Liquid Hydrogen Flowing Through a Heated Tube," by R. C. Hendricks, etal, NASA-TN-D-765, May, 1961.

29. E. P. Demetri and M. Platt, Computer Program for the Prediction of Thermal Transients in Compact Heat Exchangers, Volume I Development of Theory and Solution Procedures, NREC - 1135 - 2, NASA Contract 9-8134, August 1969.

30. A. L. London, A. J. Oberg, and R. M. Cima, "The Transient Response of a Two-Fluid Counter-Flow Heat Exchanger - The Gas Turbine Regenerator", TR-N-32) ME Dept. Stanford University, August, 1957.

31. R. M. Cima and A. L. London, "The Transient Response of a Two-Fluid Counterflow Heat Exchanger - The Gas Turbine Regenerator", Trans. ASME, Vol. 80, 1958, p. 1169.

32. W. M. Kays and A. L. London, Compact Heat Exchangers, McGraw-Hill Book Co., N.Y., N.Y., 1964, Chapter 3, pp 64-85.

33. P. F. Thompson, "Characterization Evaluation of Attitude Control Propulsion System Interim Report," TRW Technical Report 17618-H070-R0-00, December 1970.

34. F. M. Young, "Hydraulic Transient Analysis Program," Report LME-1-71, December 1970.

35. W. J. Hall, R. D. McCarty, and H. M. Roder, "Computer Programs for Thermodynamic and Transport Properties of Hydrogen," NBS Report No. 9288, (NASA-CR88086), August 1967.

36. L. A. Weber, "Thermodynamic and Related Properties of Oxygen from the Triple Point to 300°K at Pressures to 300 Atmospheres," NBS Report 9710A, 29 August 1968.

37. H. M. Roder, "Viscosity and Thermal Conductivity of Oxygen," NBS Letter 275.02 to J. Smithson, EP5, NASA/MSC, 24 September 1970.

38. P. F. Thompson, R. C. Turley, "Steady-State Attitude Control Propulsion System Computer Program Documentation and User's Manual," MSC/TRW Task 705-1, TRW Technical Report No. 17618-H1B1-R0-00, Volume I & II, June 1971.

39. T. A. Walsh, R. W. Pringle, "Transient Analysis Attitude Control Propulsion Systems Computer Program Documentation and User's Manual, MSC/TRW Task 705-1," TRW Technical Report 17618-H1B1-R0-00, June 1971.

PRECEDING PAGE BLANK NOT FILMED

6.0 BIBLIOGRAPHY

1. Saito, T., "Self-Excited Vibrations of Hydraulic Control Valve Pipelines," Bulletin of JSME, Vol. 5, No. 19, 1962.

2. Ezekiel, F. D., "The Effect of Conduit Dynamics on Control-Valve Stability," Transactions of the ASME, May, 1958.

3. Jaeger, C., "The Theory of Resonance in Hydropower Systems. Discussions of Incidents and Accidents Occurring in Pressure Systems," Journal of Basic Engineering, December 1963/631.

4. Jaeger, C., "A Review of Surge Tank Stability Criteria," Journal of Basic Engineering, December 1960/765.

5. Rudinger, George, Wave Diagrams for Nonsteady Flow in Ducts, D. VanNostrand Company, Inc., 1955.

6. Parmakian, John, Waterhammer Analysis, Prentice-Hall Civil Engineering and Engineering Mechanics Series, 1955.

7. Rich, George R., Hydraulic Transients, Dover Publications, Inc., 1963.

8. Carnahan, Brice, H. A. Luther, and James O. Wilkes, Applied Numerical Methods, John Wiley & Sons, 1969.

9. Zucrow, J. J., Aircraft and Missile Propulsion, Volume I and II, John Wiley & Sons, Inc., 1958.

10. "Thermal Design of Cryogenic Heat Exchangers for Space Vehicle Pressurization Systems," by J. H. Hargis and H. A. Stokes, George C. Marshall Space Flight Center, 1965.

11. Heat Transfer (Vol I and Vol II), by Jakob; Wiley, 1957.